UNLIMITED
UNCLASSIFIED

Canada

AN EXPERIMENTAL STUDY OF TRANSONIC BUFFET OF A SUPERCRITICAL AIRFOIL WITH TRAILING EDGE FLAP

by

B.H.K. Lee and F.C. Tang

National Aeronautical Establishment

OTTAWA
SEPTEMBER 1988

AERONAUTICAL NOTE
NAE-AN-54
NRC NO. 29542

National Research Council Canada
Conseil national de recherches Canada

UNLIMITED
UNCLASSIFIED

AN EXPERIMENTAL STUDY OF TRANSONIC BUFFET OF A SUPERCRITICAL AIRFOIL WITH TRAILING EDGE FLAP

ÉTUDE EXPÉRIMENTALE DU BUFFET TRANSSONIQUE D'UN PROFIL AÉRODYNAMIQUE SUPERCRITIQUE MUNI DE VOLETS DE BORD DE FUITE

by/par

B.H.K. Lee and F.C. Tang

National Aeronautical Establishment

AERONAUTICAL NOTE
NAE-AN-54
NRC NO. 29542

OTTAWA
SEPTEMBER 1988

L.H. Ohman, Head/Chef
High Speed Aerodynamics Laboratory/
Laboratoire d'aérodynamique à hautes vitesses

G.F. Marsters
Director/Directeur

SUMMARY

A supercritical airfoil with a trailing edge flap has been the subject of aerodynamic investigation in the National Aeronautical Establishment's High Reynolds Number 2-D Test Facility. The effects of flap deflection on buffet intensities and delay of buffet onset at transonic speeds were studied. Buffet boundaries for various flap angles were determined from the divergence of the fluctuating balance normal force measurements (C'_N). The onset of buffet was obtained from plots of C'_N versus C_L at values of C_L where the slope was 0.1. This value for the slope was arbitrarily chosen, but was found to give consistent results which agreed well with values computed from the criterion using the trailing edge pressure divergence for those cases where buffet onset is primarily due to trailing edge separation.

For given flow conditions the deflection of the trailing edge flap altered the circulation and hence the position of the shock wave and its strength. The variations of these two quantities with flap angles were determined from pressure measurements carried out on the airfoil surface. The test was performed quite deep inside the buffet régime and shock wave oscillations were investigated from spectral analyses of the balance outputs. Fluctuations in the shock motion of approximately 70 Hz were detected.

The drag of the airfoil was computed from the wake stagnation pressure deficit and the drag penalties for large flap angles were quite significant. Analysis of the wake profiles with flap settings was carried out to study the changes in wake characteristics.

This investigation shows that trailing edge flap is a useful device for passive buffet alleviation of supercritical airfoils. For Mach numbers less than the design values, the lift coefficients at buffet onset are very close to and in some cases correspond to $C_{L_{max}}$. This is quite unlike conventional airfoils when regions of mild, moderate and heavy buffet can be detected before $C_{L_{max}}$ is reached.

RÉSUMÉ

Un profil aérodynamique supercritique muni de volets de bord de fuite a fait l'objet d'une étude aérodynamique à l'installation d'essais bidimensionnels avec nombre de Reynolds élevé de l'Établissement national aéronautique. Les effets de la sortie des volets sur l'intensité du buffet et le retard de ces vibrations aux vitesses transsoniques ont été étudiés. Les limites du buffet pour différents angles des volets ont été déterminées à partir de la divergence des fluctuations de la force normale de la balance (C'_N). L'apparition du buffet a été déterminée à partir des courbes de C'_N en fonction de C_L aux valeurs de C_L où la pente est égale à 0,1. Cette valeur de la pente a été choisie arbitrairement, mais s'est avérée la valeur qui donne des résultats qui sont systématiquement conformes aux calculs découlant du critère basé sur la divergence de pression au bord de fuite, lorsque les vibrations tiennent principalement à la séparation du bord de fuite.

Dans des conditions d'écoulement données, la sortie des volets du bord de fuite ont modifié la circulation et, partant, la position et l'amplitude de l'onde de choc. Les variations de ces deux paramètres en fonction de l'angle des volets ont été déterminées à partir de mesures de pression effectuées sur la surface du profil. L'essai a été mené en plein régime des vibrations, et les oscillations de l'onde de choc ont été étudiées à partir d'analyses spectrales de la réponse d'équilibre. Des fluctuations d'environ 70 Hz ont été décelées dans le mouvement de choc.

La traînée du profil a été c alculée à partir de la dépression dans la zone de stagnation du sillage, et une pénalité importante de la traînée est notée aux grands angles de sortie des volets. L'analyse des profils du sillage en fonction de différents réglages des volets visait à étudier les changements dans les caractéristiques du sillage.

Cette recherche montre que les volets du bord de fuite est un dispositif utile pour atténuer passivement l'intensité du buffet des profils supercritiques. Pour les nombres de Mach inférieurs à la valeur du calcul, les coefficients de portance à l'apparition du buffet approchent et égalent parfois $C_{L_{max}}$. Ces profils diffèrent beaucoup des profils classsiques pour lesquels on peut déceler le buffet faible, moyen et intense avant que C_L ne soit maximal.

Table of Contents

List of Symbols

b	model span
c	chord length
C_D	drag coefficient from wake integration
C_L	lift coefficient from balance measurement
C_{L_P}	lift coefficient from pressure integration
$C_{L_{max}}$	maximum lift coefficient from balance measurement
C_N	normal force coefficient from balance measurement
C'_N	rms value of fluctuating normal force coefficient defined in Eq. 1
C'_{N_B}	rms value of fluctuating normal force coefficent at buffet onset
C_P	pressure coefficient
C^*_P	pressure coefficient at M = 1
ΔC_{P_S}	shock strength
$C_{P_{TE}}$	pressure coefficient at trailing edge
$\Delta C_{P_{TE}}$	defined in Eq. (2)
$C_{P_{TEdiv}}$	divergence trailing edge pressure coefficient
M	Mach number
M_D	drag rise Mach number
M_{DES}	design Mach number
N_{rms}	rms value of normal force from balance measurement

List of Symbols

q_∞	free stream dynamic pressure
R_c	Reynolds number based on chord length
t	maximum thickness of airfoil
w	thickness of wake
x	distance measured in the flow direction from the airfoil leading edge
x_s	shock position
y	distance traversed by wake probe, perpendicular to flow direction
α	angle of incidence
α_{div}	angle of incidence when trailing edge pressure divergence occurs
$\Delta\alpha$	defined in Eq. (3)
δ	flap angle

Illustrations

interesting to note from this figure that some of the curves show that C_N' reaches a maximum and then decreases. For M = 0.772 and 0.792, a very rapid increase in C_N' is not detected and the slopes of the curves do not become negative since there is no $C_{L_{max}}$, as illustrated in Figure 2.

The buffet boundaries for various flap settings are shown in Figures 10 and 11. Figure 10 shows C_L plotted against M and it is seen that the boundaries can be raised appreciably and there is a large increment in lift with positive changes in δ. Characteristic of supercritical airfoils, the buffet boundary decreases rapidly for $M > M_{DES}$. At M = 0.75 which corresponds to the drag rise Mach number M_D at design C_L, this airfoil shows only small improvements in alleviating buffet by the use of flaps. Further increase in Mach number again show an increase in the lift before encountering buffet. Figure 11 gives the buffet boundaries plotted as α versus Mach number. The angle of incidence at which buffet occurs is obtained from the C_L versus α curves using the buffet onset value of C_L given in Figure 10. For $M > M_{DES}$, it is difficult to determine α accurately since C_L at buffet is very close to and in some cases correspond to $C_{L_{max}}$, and small errors in C_L magnifies considerably in terms of α.

For conventional airfoils, it is often possible to designate regions of mild, moderate or heavy buffeting. Because buffet onset occurs so close to $C_{L_{max}}$ for M near or less than M_{DES}, it is not too meaningful to assign a degree of severity except when M is greater than some value, for example, M_D for this particular airfoil. Figures 12-17 show the buffet onset boundaries and curves with given buffet intensities for various flap angles. Also shown in the figures are the values of $C_{L_{max}}$ for those values of M where a maximum in C_L can be detected.

3.3 Pressure Distributions on Airfoil Surface

Static pressure measurements were obtained from 50 and 30 pressure ports on the upper and lower surface of the model respectively. The C_p distributions for the airfoil near the design Mach

Number for zero flap setting are shown in Figure 18 for various angles of attack. According to Figure 11, at the Mach number of interest (0.722), buffet occurs at $\alpha = 3.4°$. It can be seen that the shock waves for the larger α are not as sharply defined as those for $\alpha < 3.4°$.

The effects of varying δ are shown in Figures 19-22 for four Mach numbers. At Mach number close to M_{DES}, Figure 19 shows the pressure distributions at α about 4.5°. It was difficult in the tests to keep both α and M constant. The values of α for $\delta \geq 0°$ are well into buffet régime (pronounced TE separation) while that for $\delta = -4°$ is slightly greater than the buffet onset value. For $\delta = -8°$, α is just below the buffet boundary.

Figure 20 shows the C_p distributions at M about 0.612 for α about 6.5°. Except for the $\delta = -8°$ curve, all the other curves are for α values larger than the buffet onset value. The pressure distribution behind the shock shows a shock induced separation bubble. Quite deep inside the buffet régime, Figure 21 shows that a well defined shock wave is not observed. In Figure 22 which is at a higher Mach number (M about 0.791), the shock wave becomes less unsteady even though the values of α exceeded those at buffet onset given in Figure 11 by a fair amount.

3.4 Power Spectra of Balance Normal Force

The IEEE computer program (Ref. 16) for computing power spectra was used in spectral analyses of the normal force outputs from the balance. Figure 23 shows the results using a FFT block size of 256 and a signal length of 2 seconds. The sampling frequency was 1.6 KHz. The conditions of this figure correspond to those in Figure 19. For $\delta \geq 0°$, the spectra show distinct peaks at approximately 70 Hz. Similar results were obtained in a previous investigation of the BGK No. 1 airfoil (Ref. 3) and they were identified as due to oscillations of the shock wave. Higher frequency peaks are present when the flap angle is increased. For $\delta = -4°$, the airfoil is operating slightly inside the buffet régime while for $\delta = -8°$ it is outside the buffet boundary. No distinct 70 Hz peaks are detected for these two flap

angles because the shock waves are quite steady as can be seen from the C_p distributions in Figure 19.

In Figure 24, the values of M and α are the same as those in Figure 20. Except for $\delta = -8°$, the airfoil is experiencing buffeting. The intensities of C_N' are not as large as those in the previous figure and the higher frequency peaks are also not so pronounced. Figures 25 and 26 are for the same conditions as Figures 21 and 22 and the airfoil is quite deep into the buffet régime. The poorly defined shock waves in Figure 21 indicate that they are very unsteady and are shown in Figure 25 as very large and distinct peaks of approximately 70 Hz. As the Mach Number increases, the magnitudes of C_N' decrease and Figure 22 shows the shock waves to be more steady. The spectra in Figure 26 clearly indicate the shock oscillations to be much weaker than those in the previous figure.

3.5 Shock Positions and Strengths

When the shock wave is oscillating, its location determined from the C_p plots falls within the range of positions that may occur during one pressure scan cycle of approximately $2\frac{1}{2}$ seconds. When buffet is severe or C_N' is large, locating the shock position is difficult. In this report, the position and strength of the shock wave are defined in a manner similar to the definition used in Reference 18 (Figure 27). There is certain arbitrariness in this definition, but for large oscillating shock motion, this gives more easily measured and consistent results.

The effects of Mach number on shock location x_s/c is shown in Figure 28 for trailing edge flap angle $\delta = 0°$. Except for the two higher Mach numbers (M = .772, M = .792) which show x_s/c to decrease with α, it is seen from the other cases that x_s/c increases with α and reaches a maximum before decreases slowly. Figure 29 gives the shock locations for various flap angles at a Mach number of 0.723. The following two figures (Figures 30, 31) show x_s/c at Mach numbers below and above the design value. The motion of the shock wave with α is quite different for these two cases. The variation of x_s/c with Mach number is illustrated in Figure 32 for an angle of incidence $\alpha = 3°$.

The curves show the shock position to move downstream with increasing Mach number until a maximum x_s/c is reached. From then onwards it moves gradually upstream or in some instances remains more or less stationary. Similar trends are observed when the shock locations at buffet onset are plotted against Mach number for various flap angles (Fig. 33).

The shock strengths ΔC_{P_S} corresponding to the conditions in Figures 28-31 are given in Figures 34-37. They increase with α irrespective of whether the shock moves upstream or downstream. At a constant angle of incidence $\alpha = 3^\circ$ (Figure 38), ΔC_{P_S} varies slightly with Mach number for $M < 0.72$ even though the change in shock position is very large (Figure 32). For $M > 0.72$ (corresponding to its design value), changes in x_s/c and ΔC_{P_S} are small compared to their variations with Mach Number for $M < 0.72$. Figure 39 shows a plot of the shock strengths at buffet onset against Mach number for various flap angles. The shock strength decreases almost linearly with increasing Mach number up to the design value.

3.6 Trailing Edge Pressure Measurements

In this study on buffet characteristics of a supercritical airfoil, the trailing edge pressure was measured as the airfoil operating condition moved into the buffet régime. From the pressure coefficient versus α plots, the value of the trailing edge pressure $C_{P_{TE}}$ when divergence occurred (onset of buffet) was noted together with the value of α. The severity of buffet is denoted in terms of $C_{P_{TE}}$ as

$$\Delta C_{P_{TE}} = C_{P_{TE}} - C_{P_{TEdiv}} \qquad (2)$$

where the subscript 'div' denotes the value of $C_{P_{TE}}$ at divergence (Ref. 1). The intrusion into the buffet régime is expressed in terms of the angle of incidence as

$$\Delta\alpha = \alpha - \alpha_{div} \qquad (3)$$

Figure 40 shows the change in trailing edge pressure coefficient with $\Delta\alpha$ for M = 0.723. It is seen that $\Delta C_{P_{TE}}$ decreases monotonically with $\Delta\alpha$. For the range of Mach numbers tested, it is observed that for M < 0.72, $C_{P_{TE}}$ at $\delta = 8°$ and 14° shows smaller drop with $\Delta\alpha$ than for the other values of δ. For higher Mach numbers (Figure 41), the curves for the smaller values of δ do not cross each other as in low Mach numbers (Figure 42), and show quite distinctly that as δ increases, smaller decreases in trailing edge pressure will result.

To study the change of normal force fluctuations with trailing edge pressure, define

$$\Delta C'_N = C'_N - C'_{N_B} \tag{4}$$

where C'_{N_B} denotes the value at buffet onset. The two quantities $\Delta C'_N$ and $\Delta C_{P_{TE}}$ are plotted in Figure 43 for M = 0.723. Figures 44 and 45 show the effects of Mach numbers for M = 0.673 and 0.772. Based on results for other Mach numbers tested, it can be concluded that in the neighbourhood of M_{DES}, much larger changes in $\Delta C'_N$ with $\Delta C_{P_{TE}}$ occur than at M lower or higher than M_{DES}. In the range of Mach Number near M_{DES} the effects of flaps show consistently that increasing δ results in larger $\Delta C'_N$ changes with $\Delta C_{P_{TE}}$. This range of Mach numbers is near the "elbow" of the buffet onset boundaries (Figure 10) and force measurements have shown large fluctuations because of the strong shock oscillations.

3.7 Drag Measurements

The drag polar determined from wake measurements is shown in Figure 46 for flap angle $\delta = 0°$. Included in this figure are the drag values at buffet onset. It can be seen that the drag rise from its value at design conditions ($C_D \simeq 0.01$) is quite appreciable at buffet.

The effect of flap angles on C_D is demonstrated in Figures 47-49. Near the design Mach number, the drag is the lowest for the zero flap setting at the design C_L. The effects of Mach number are given in Figures 48 and 49 for M equal to 0.673 and 0.772 respectively.

Using the results from the drag polars, C_D can be plotted versus M for various C_L. Figure 50 shows results presented for $\delta = 0°$. At design conditions the drag rise Mach number, using the criterion based on a slope of $dC_D/dM = 0.1$ is determined to be 0.75.

At the design $C_L = 0.6$, C_D versus M are plotted in Figure 51 for various flap angle settings. Small flap angles ($\delta = \pm 4°$) do not increase the drag significantly, however, the 8° and 14° flaps appear to have quite a large effect. For off design conditions ($C_L = 0.4$ and 0.8), Figures 52 and 53 show the drag increase for negative flap angles is much larger than that for positive flap angles.

For a given flap setting and C_L, curves such as those given in Figures 50-53 can be used to determine the drag rise Mach number and the corresponding value of drag coefficient C_D. Curves of C_L corresponding to the evaluated M_D can be plotted as shown in Figure 54 for various flap settings. Positive flap angles help to delay the drag rise Mach number for off design conditions at values of C_L approximately greater than 0.75 for this particular airfoil.

The drag coefficient corresponding to the C_L at the drag rise Mach number is plotted in Figure 55. At the design $C_L = 0.6$, the zero flap airfoil gives the lowest drag at the drag rise Mach number of 0.75.

3.8 Wake Profiles

Some representative results for the wake profiles are given in Figures 56-58. The growth of the wake at $M = 0.723$ and $\delta = 0°$ is shown in Figure 56 for probe #2 of the traversing rake, and its location is 1.75 inches from the tunnel centre line. The distance y traversed by the wake probe is normalized with respect to the airfoil chord and C_D' on the horizontal scale is proportional to the total pressure drop. The integral of C_D' over the width of the wake gives the total drag. Beyond buffet onset, which occurs approximately at $\alpha = 3.4°$ in this case, the profiles become very unsteady and C_D' shown are values that occur in one pressure scan. The duration of a scan depends on the width of the wake and the traversing speed, but will not exceed a maximum value of $2\frac{1}{2}$ seconds.

The changes in wake profiles at M = 0.723 with δ for two values of the incidence α are shown in Figures 57 and 58. At α about 2.75°, the airfoil is slightly inside the buffet régime for δ = 4° and moderately deep into buffet at δ = 14° while for $\delta \leq 0°$, the airfoil is not experiencing buffet. At α in the neighbourhood of 4.5° the airfoil is buffeting except for δ = -8° which is very close to the onset boundary.

As an indication of the growth of the wake, its width w is measured and normalized with respect to the airfoil maximum thickness t. The value of w is determined from the wake profile at a value of C_D' equal to one percent of its maximum. Figure 59 shows the effect of Mach number at zero flap deflection. The buffet onset value of α is also included in the figure for reference. It is seen that w/t grows with α and there is no special change in the growth rate at the onset of buffet. The higher Mach numbers results in a thicker wake.

The effect of flap settings is shown in Figure 60 for M = 0.723. Positive flap angle increases w/t while negative flap angle gives a smaller value of w/t. At this Mach number, the wake thickness increases quite uniformly over the range of angle of incidence covered in the test. At off design Mach numbers, Figures 61 and 62 show the variation of w/t with α for M = 0.673 and 0.772.

4.0 Conclusions

A 16% thick supercritical airfoil with a trailing edge flap was tested in the NAE Two Dimensional Test Facility at a chord Reynolds number of 20 million. The investigation was carried out quite deep into the buffet régime and the effects of flaps on lift increments and buffet severity were analyzed. The results can be summarized as follows:

a) The onset of buffet can be determined quite accurately from plots of C_N' versus C_L at values of C_L where the slope of the curves is 0.1. For those conditions where buffet onset is primarily due to trailing edge separation, this value for the slope is found to

give consistent results which agree quite well with values computed from the criterion using the trailing edge pressure divergence.

Buffet boundaries can be raised appreciably for positive trailing edge flap deflections. Unlike conventional airfoils where regions of mild, moderate or heavy buffeting can be classified, the buffet onset boundaries for supercritical airfoils for $M < M_{DES}$ occur very close to and in some cases correspond to $C_{L_{max}}$. To identify regions of different degree of severity is often not possible. This suggests that the design condition for supercritical airfoils should be further away from the buffet boundary than the usual criteria used for conventional airfoils would indicate.

b) The shock positions and strengths are determined from the C_p measurements. For Mach numbers near or less than the design value the shock initially moves downstream with increasing angle of incidence to a maximum downstream position before moving slowly back upstream or, in some cases, remains more or less stationary. For higher Mach numbers, only upstream motion of the shock is detected and the flap settings do not have much influence on the shock location. For the lower Mach numbers, positive flap angles cause the shock to move further downstream, while the opposite is true for negative flap deflections.

The shock strength increases with incidence irrespective of whether the shock moves upstream or downstream. Positive flap angles increase the strength but the effect is small at higher Mach numbers.

Spectral analyses of the balance normal force outputs show shock oscillations at about 70 Hz for this airfoil. The fluctuations are largest at values of Mach numbers near the design value, beyond which a sharp drop in the buffet boundaries occurs. Slightly inside the buffet régime, the magnitudes of the fluctuating normal force have quite large values near the "elbow" of the

buffet onset curve. As the Mach number increases to higher values, the fluctuations in normal force decreases and the shock waves become more steady.

c) Intrusion into the buffet régime and the resulting buffet severity can be indicated either by the decrease in trailing edge pressure $\Delta C_{P_{TE}}$ or increase in magnitude of the fluctuating normal force $\Delta C_N'$. For Mach numbers near the design value, much larger changes in $\Delta C_N'$ with $\Delta C_{P_{TE}}$ are observed than for other values of M.

d) At the design $C_L = 0.6$, small flap angles do not increase the drag significantly. For off design conditions the drag rise is much larger for negative flap angles than for positive angles of the same magnitude. The wake profiles show large unsteady fluctuations at conditions beyond the buffet onset boundary. Near the design Mach number, positive flap angles increase the wake thickness while negative angles have the opposite effect. The growth of the width of the wake is quite uniform over the range of angle of incidence covered in the test. In most cases drag increases significantly before buffet onset.

5.0 References

1. Pearcey, H.H., Osborne, J., and Haines, A.B. "The Interaction between Local Effects at the Shock and Rear Separation - a Source of Significant Scale Effects in Wind-Tunnel Tests on Aerofoils and Wings", Paper 11, AGARD CP 35, Transonic Aerodynamics, 1968.

2. Roos, F.W. "Some Features of the Unsteady Pressure Field in Transonic Airfoil Buffeting", J. Aircraft, Vol. 17, No. 11, November 1980, pp. 781-788.

References (cont'd)

3. Lee, B.H.K. and Ohman, L.H. "Unsteady Pressures and Forces During Transonic Buffeting of a Supercritical Airfoil", J. Aircraft, Vol. 21, No. 6, June 1986, pp. 439-441.

4. Benoit, B. and Legrain, I. "Buffeting Prediction for Transport Aircraft Applications Based on Unsteady Pressure Measurements", AIAA Paper No. 87-2356, AIAA 5th Applied Aerodynamics Conference, Montery, CA, Aug. 17-19, 1987.

5. Cunningham, A.M., Jr., Waner, P.G., Jr., Watts, J.D., Benepe, D.B., and Riddle, D.W. "Development and Evaluation of a New Method for Predicting Aircraft Buffet Response", AIAA Paper No. 75-69, AIAA 13th Aerospace Sciences Meetings, Pasadena, Calif. Jan 20-22, 1975.

6. Lee, B.H.K. "A Method for Predicting Wing Response to Buffet Loads", J. Aircraft, Vol. 21, No. 1, Jan. 1984. pp. 85-87.

7. Lemley, C.E. and Mullans, R.E. "Buffeting Pressures on a Swept Wing in Transonic Flight - Comparison of Model and Full Scale Measurements", AIAA Paper No. 73-311, AIAA Dynamics Specialists Conference, Williamsburg, Virginia, March 19-20, 1973.

References (cont'd)

8. Butler, G.F. and Spavins, G.R. "Preliminary Evaluation of a Technique for Predicting Buffet Loads in Flight from Wind-Tunnel Measurements on Models of Conventional Construction", Paper No. 23, AGARD CP-204, Prediction of Aerodynamic Loading, 1976.

9. Mabey, D.G. "Prediction of the Severity of Buffeting", Paper No. 7, AGARD-LS-94, Three Dimensional and Unsteady Separation at High Reynolds Numbers, 1978.

10. Redeker, G. and Proksch, H.J. "The Prediction of Buffet Onset and Light Buffet by Means of Computational Methods", Paper No. 24, AGARD CP-204, Prediction of Aeodynamics Loading, 1977.

11. Thomas, F. and Redeker, G. "A Method for Calculating the Transonic Buffet Boundary Including the Influence of Reynolds Number", Paper No. 3, AGARD CP-83, Facilities and Techniques for Aerodynamic Testing at Transonic Speeds and High Reynolds Number, 1971.

12. Friend, E.L. and Sefic, W.J. "Flight Measurements of Buffet Characteristics of the F-104 Airplane for Selected Wing-Flap Deflections", NASA TN D-6943, August 1972.

References (cont'd)

13. Monaghan, R.C. and Friend, E.L. "Effects of Flaps on Buffet Characteristics and Wing-Rock Onset of an F-8C Airplane at Subsonic and Transonic Speeds", NASA TM X-2873, August 1973.

14. Ohman, L.H. "The NAE High Reynolds Number 15" × 60" Two-Dimensional Test Facility", National Research Council, NAE LTR-HA-4, Part 1, April 1970.

15. Eggleston, B., Poole, R.J.D., Jones, D.J. and Khalid, M. "Thick Supercritical Airfoils with Low Drag and Natural Laminar Flow", J. Aircraft, Vol. 24, No. 6, June 1987, pp. 405-41?

16. Rabiner, L.R., Schafer, R.W., and Dlugos, D. "Periodgram Method for Power Spectrum Analysis", Programs for Digital Signal Processing Ed. by the Digital Signal Processing Committee, IEEE Acoustics, Speech, and Signal Processing Society, IEEE Press, 1979.

17. Tang. F.C. and Lee, B.H.K. "Wind Tunnel Investigation of the Buffet Characteristics of a Supercritical Airfoil with Flap at a Reynolds Number of 20 million", NAE LTR-HA-5X5/0179, National Research Council of Canada, August 1988.

References (cont')

18. Blackerby, W.T. and Cahill, J.F. "High Reynolds Number Tests of a C-141A Aircraft Semispan Model to Investigate Shock-Induced Separation", NASA CR-2604, October 1975.

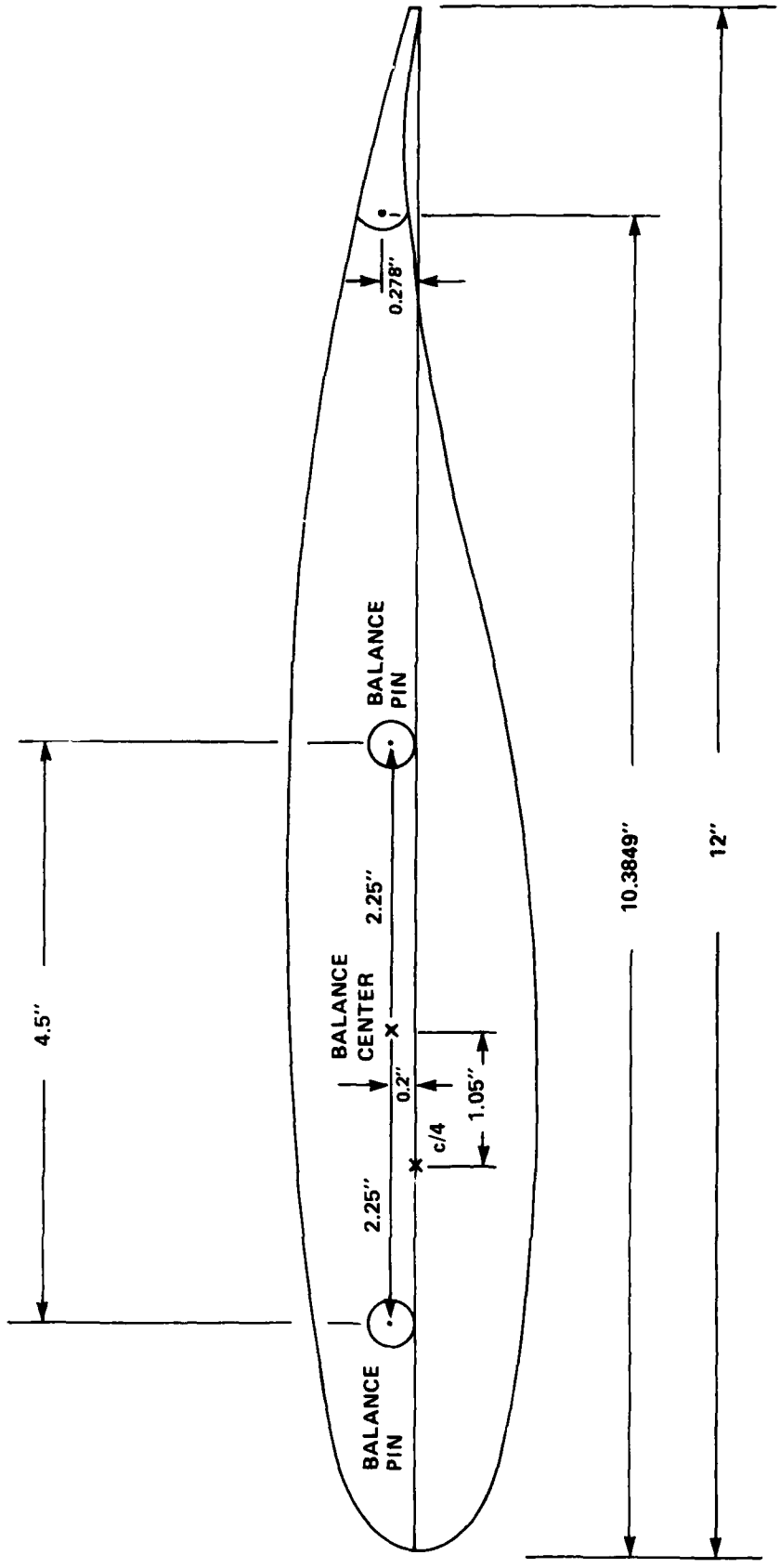

FIG. 1: SCHEMATIC OF SUPERCRITICAL AIRFOIL WITH 16% THICKNESS TO CHORD RATIO

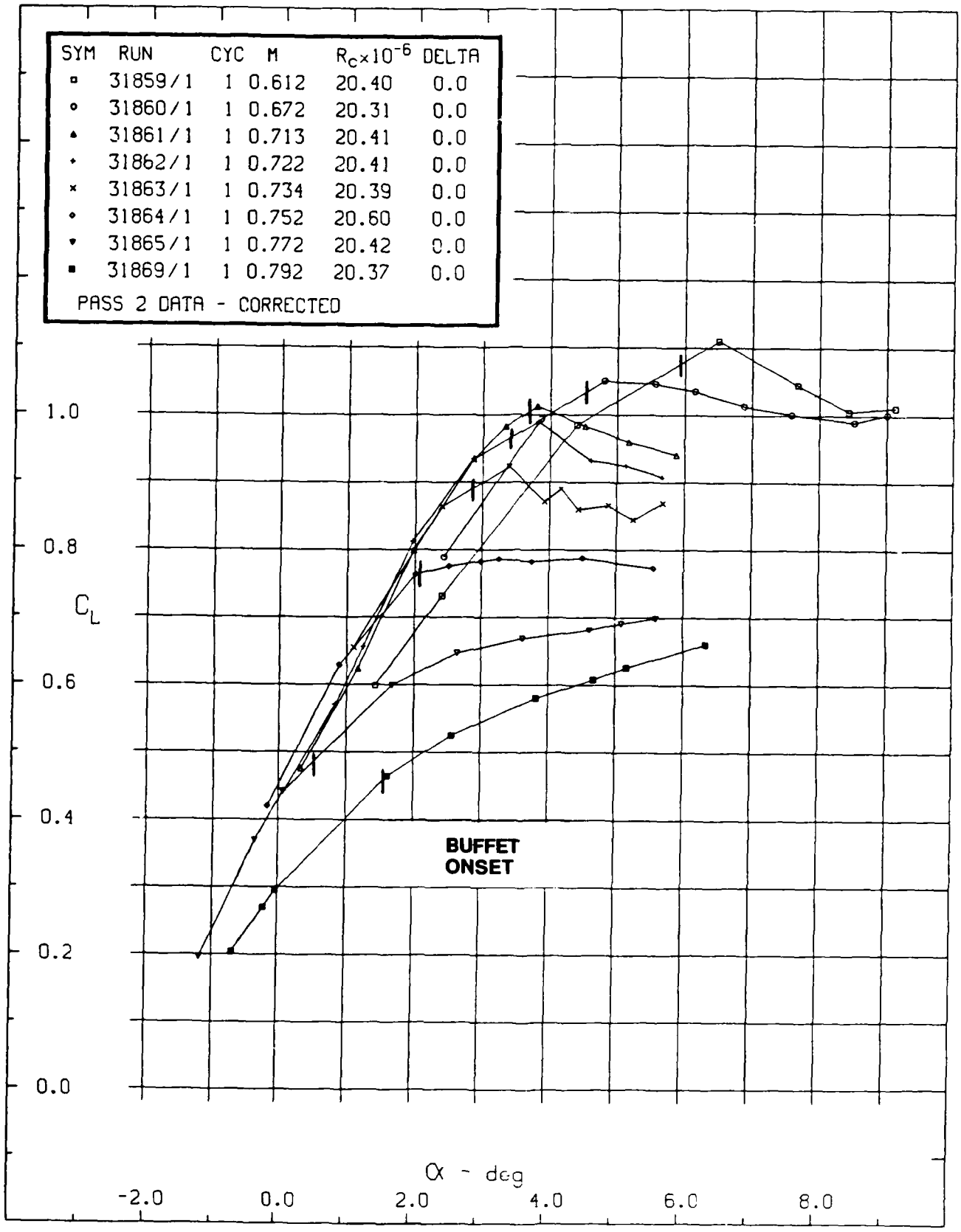

FIG. 2: LIFT VERSUS ANGLE OF INCIDENCE AT VARIOUS MACH NUMBERS FOR FLAP ANGLE $\delta = 0°$

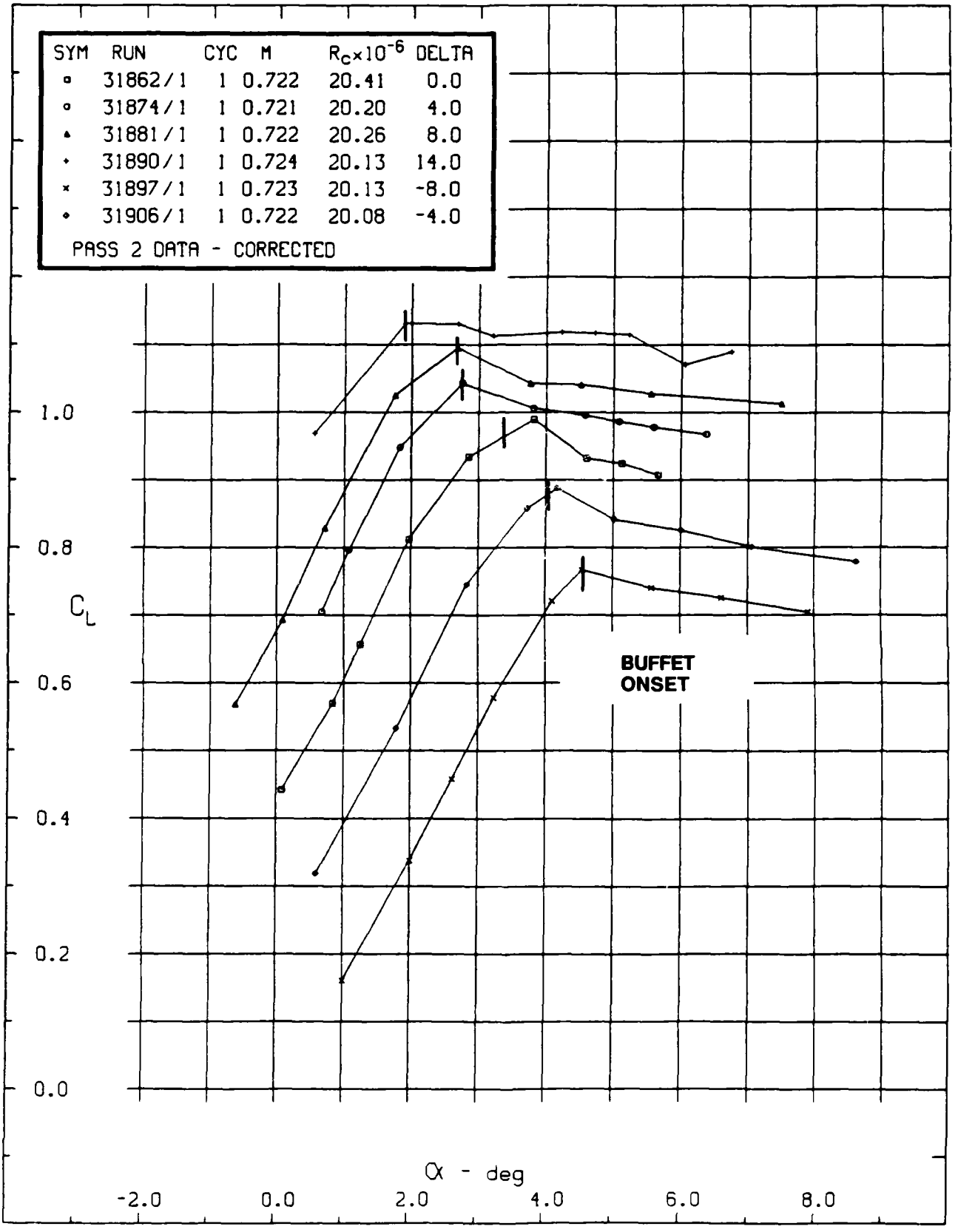

FIG. 3: LIFT VERSUS ANGLE OF INCIDENCE AT M ABOUT 0.723 FOR VARIOUS FLAP ANGLES

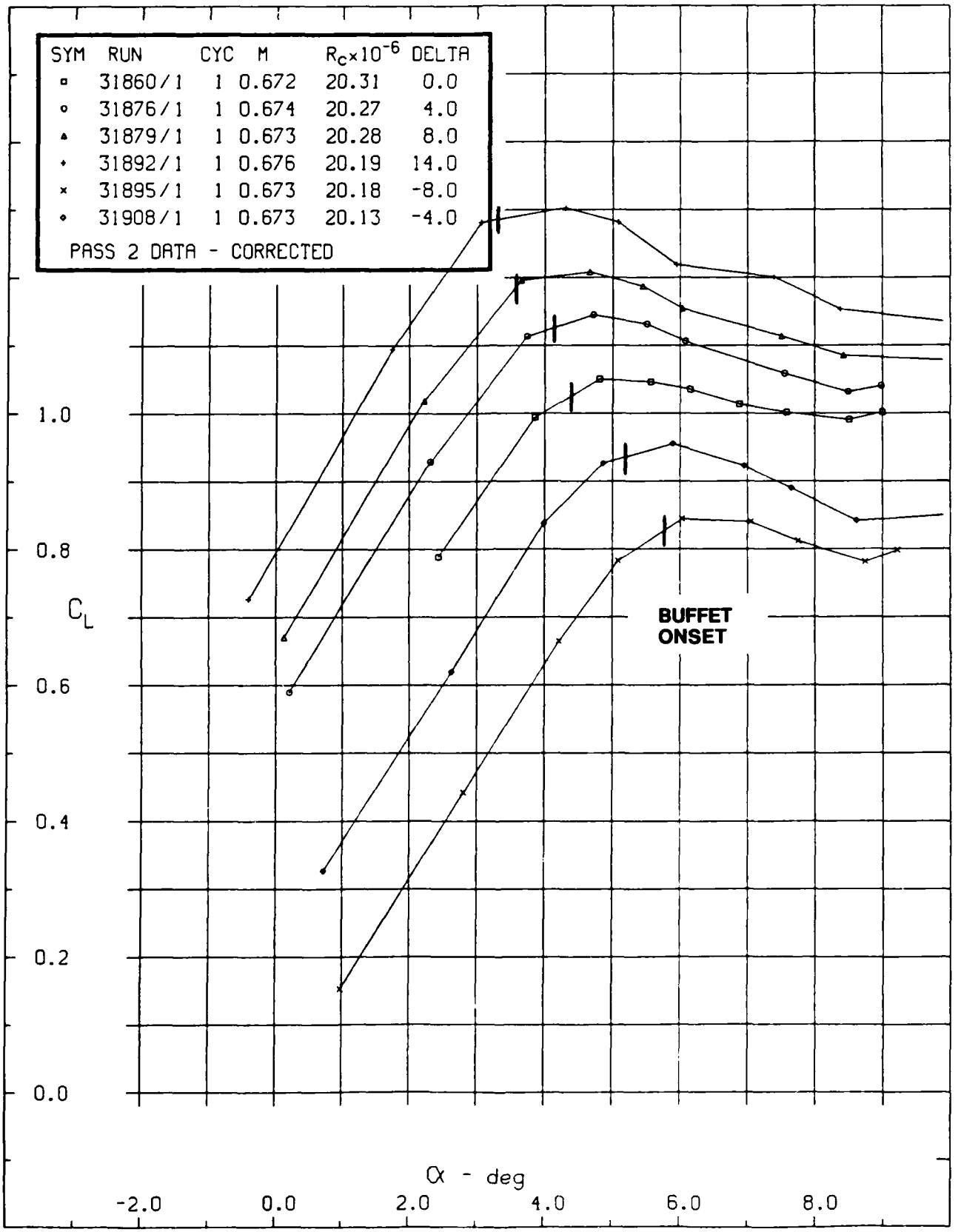

FIG. 4: LIFT VERSUS ANGLE OF INCIDENCE AT M ABOUT 0.673 FOR VARIOUS FLAP ANGLES

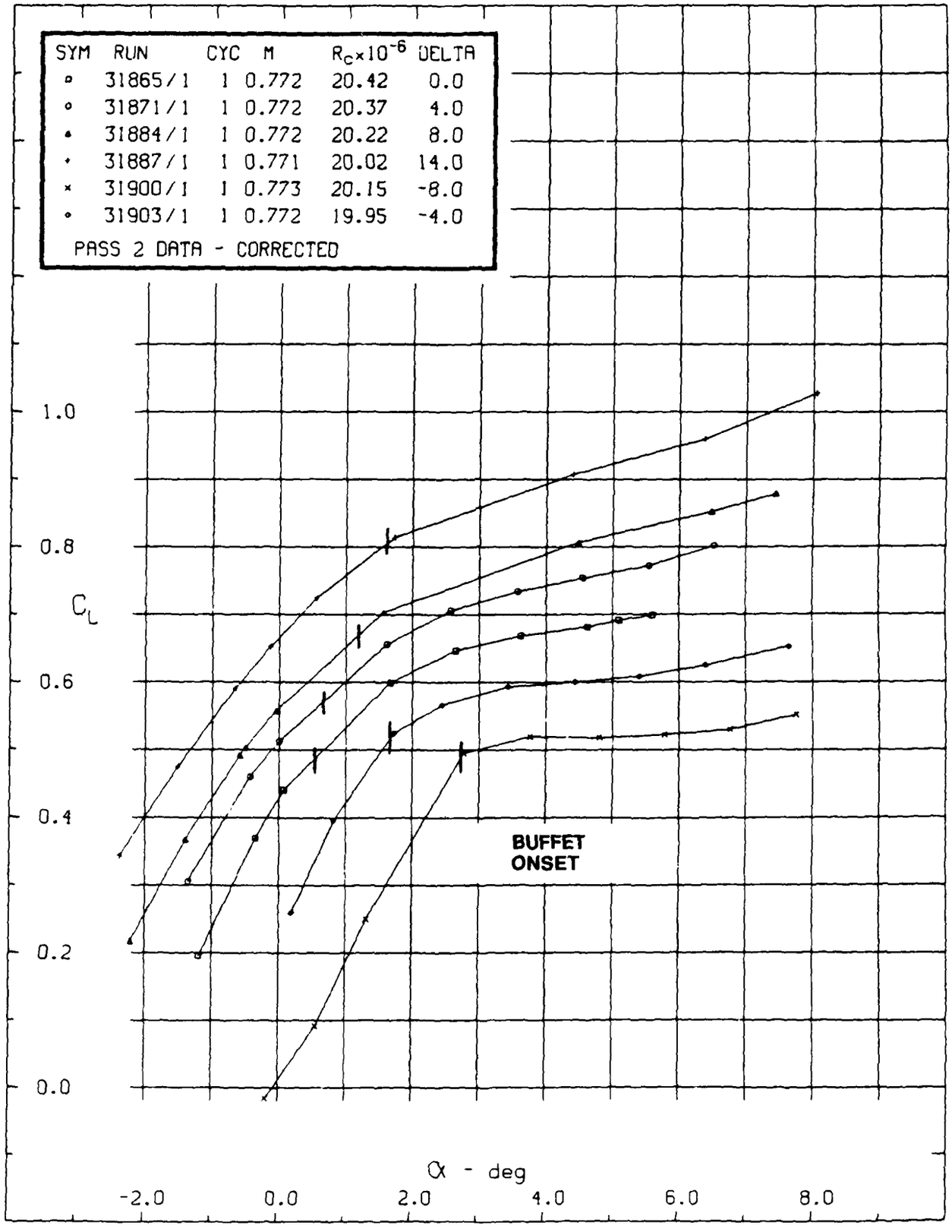

FIG. 5: LIFT VERSUS ANGLE OF INCIDENCE AT M ABOUT 0.772 FOR VARIOUS FLAP ANGLES

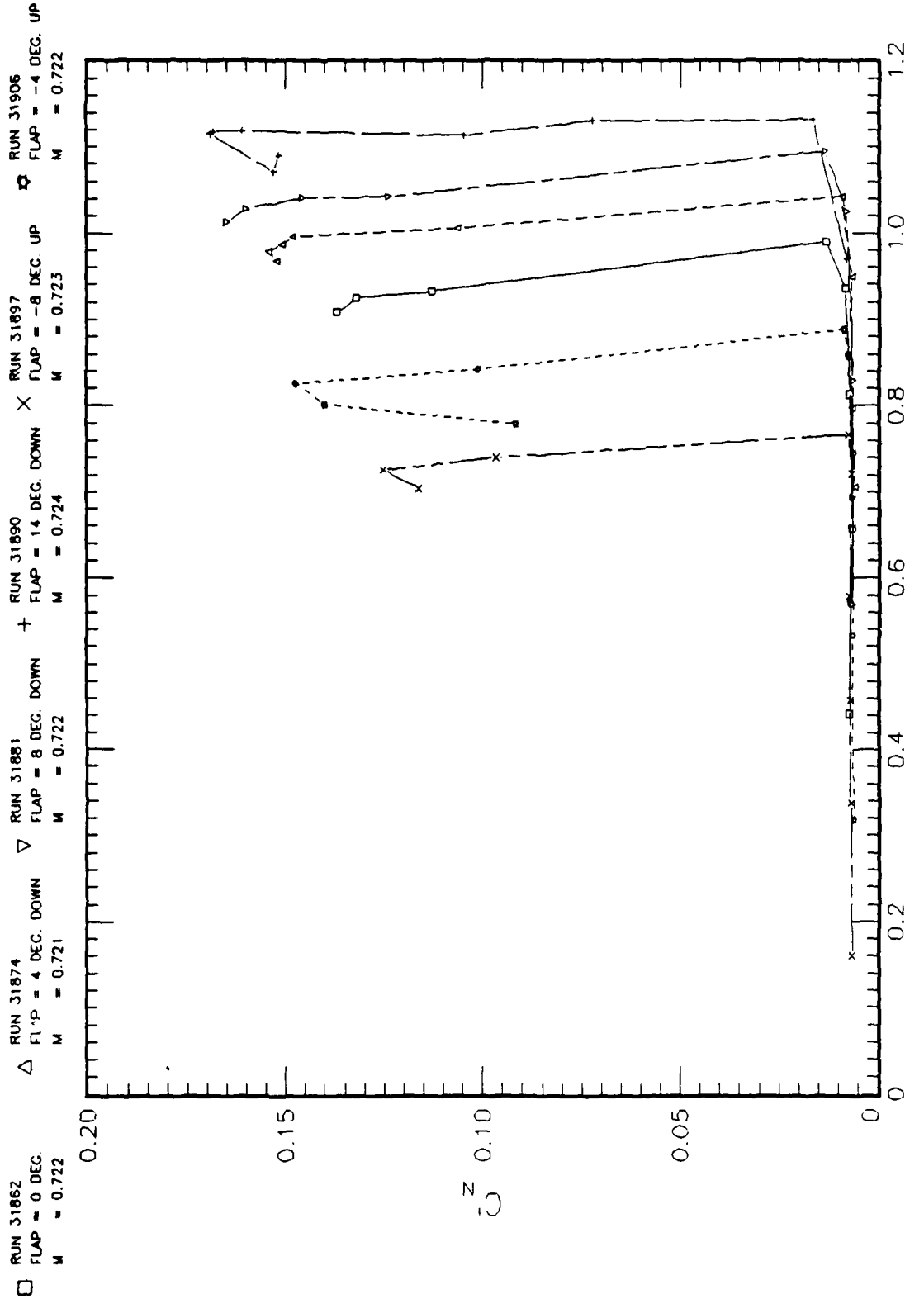

FIG. 6: NORMAL FORCE FLUCTUATIONS VERSUS LIFT AT M ABOUT 0.723 FOR VARIOUS FLAP ANGLES

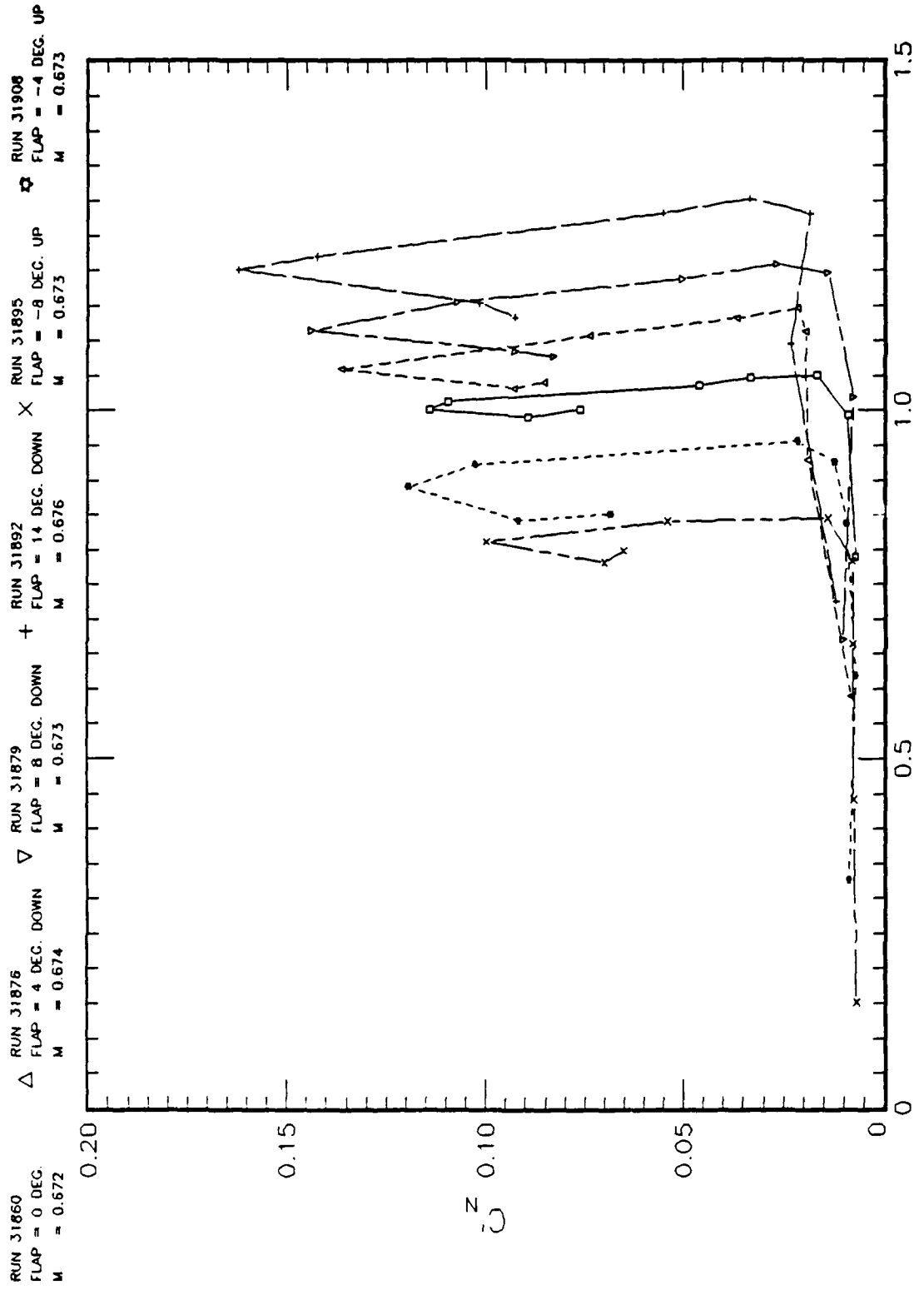

FIG. 7: NORMAL FORCE FLUCTUATIONS VERSUS LIFT AT M ABOUT 0.673 FOR VARIOUS FLAP ANGLES

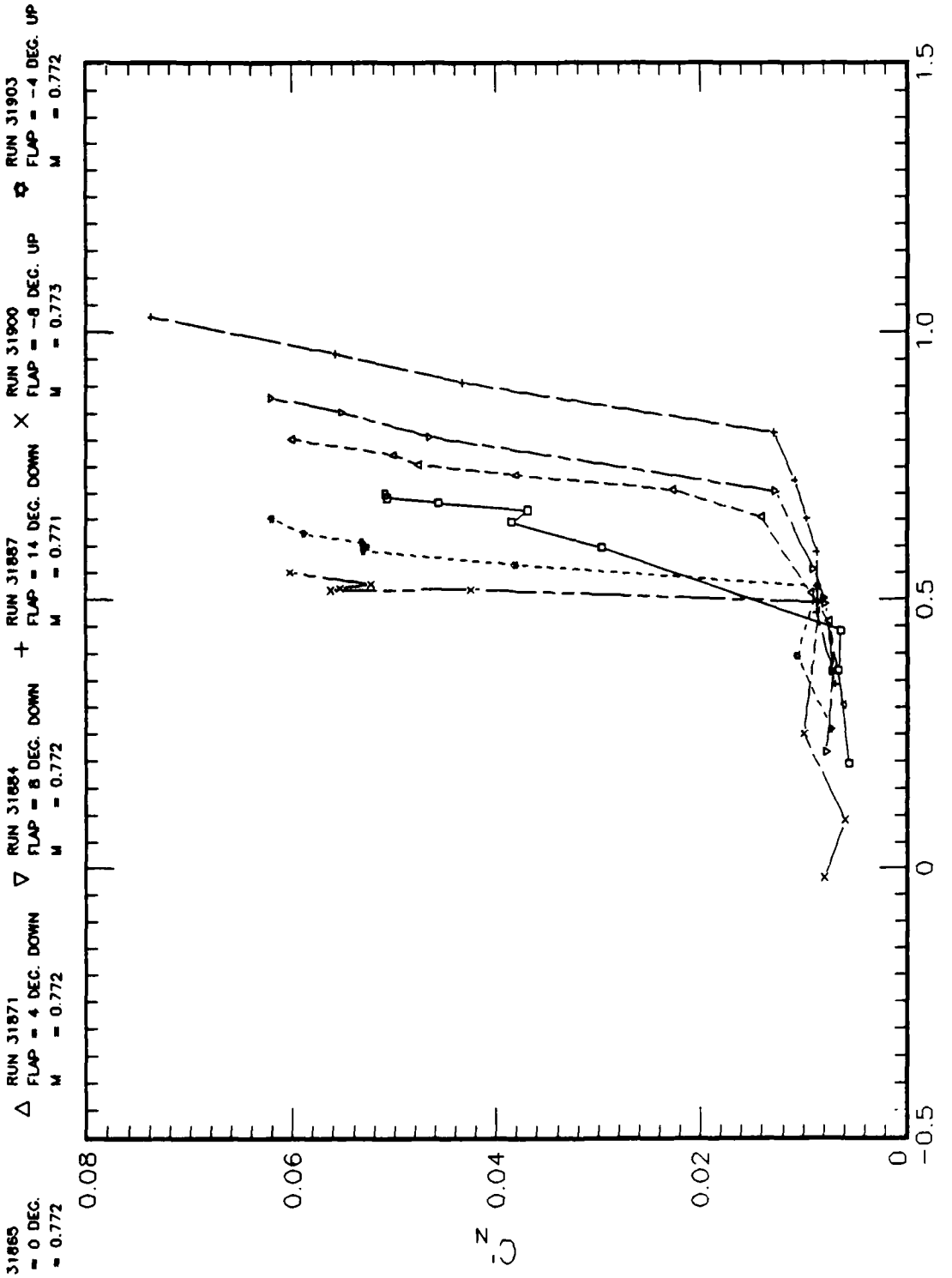

FIG. 8: NORMAL FORCE FLUCTUATIONS VERSUS LIFT AT M ABOUT 0.772 FOR VARIOUS FLAP ANGLES

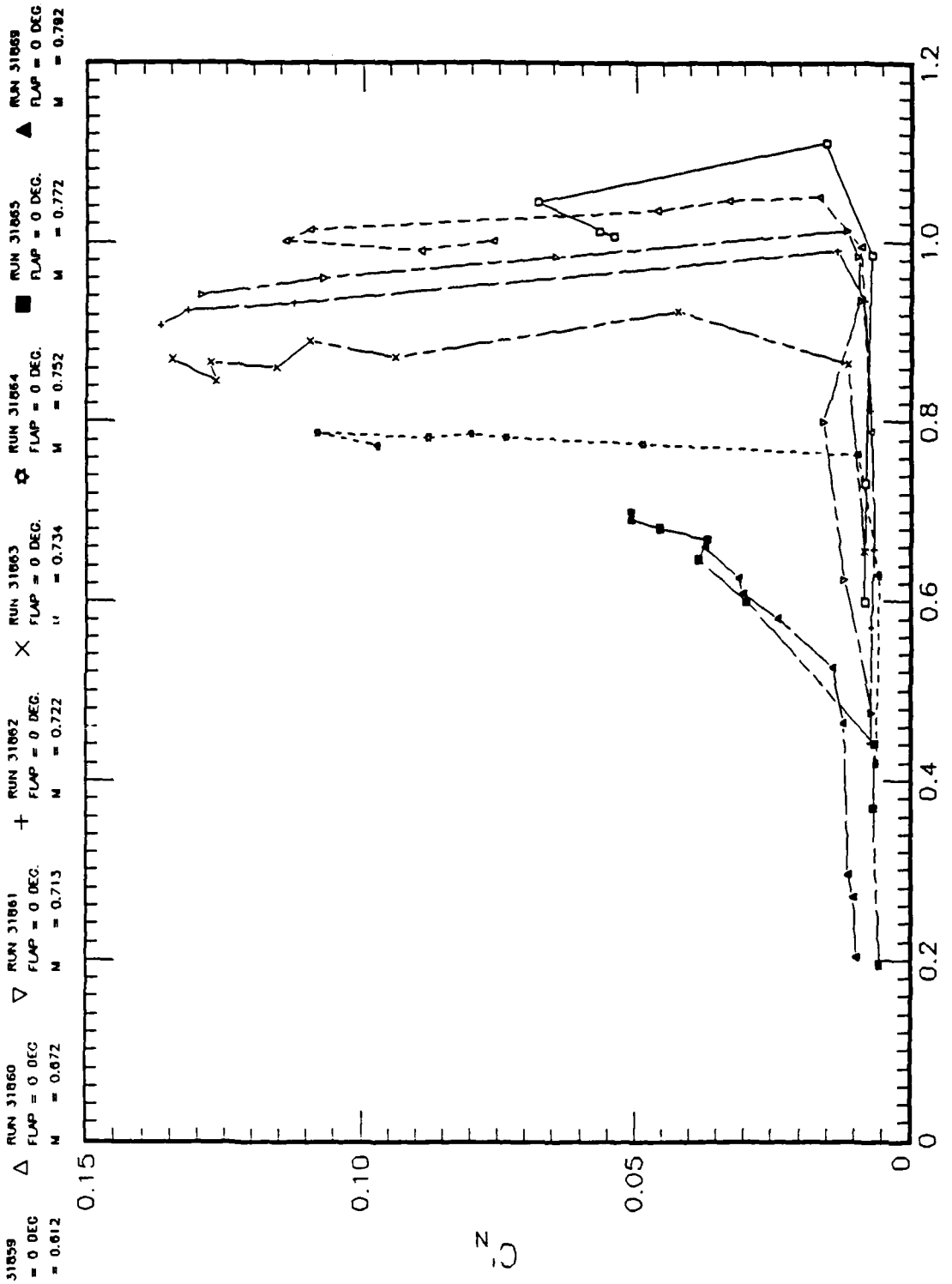

FIG. 9: NORMAL FORCE FLUCTUATIONS VERSUS LIFT AT VARIOUS MACH NUMBERS FOR FLAP ANGLE δ = 0°

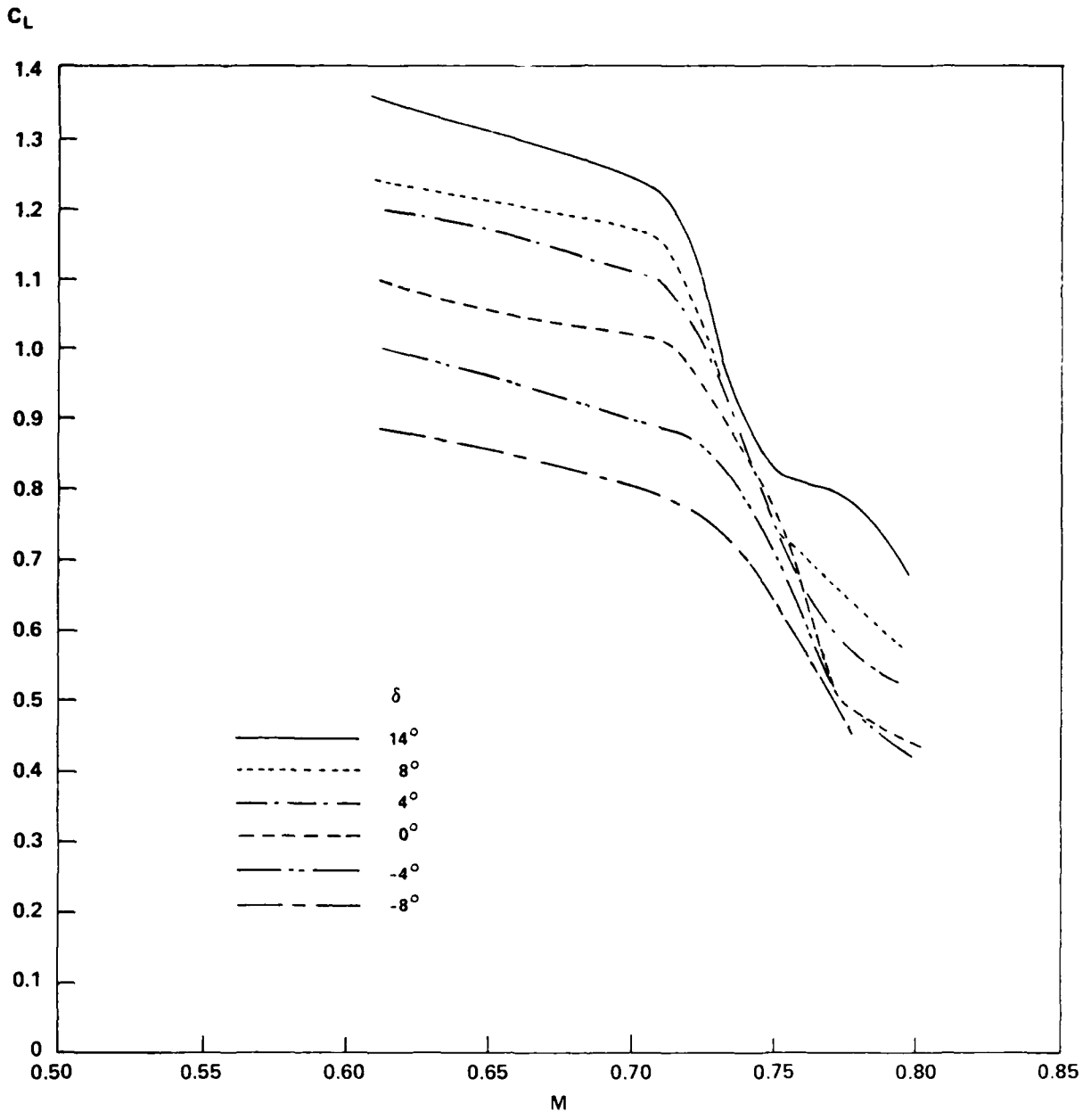

FIG. 10: LIFT VERSUS MACH NUMBER BUFFET BOUNDARIES FOR VARIOUS FLAP ANGLES

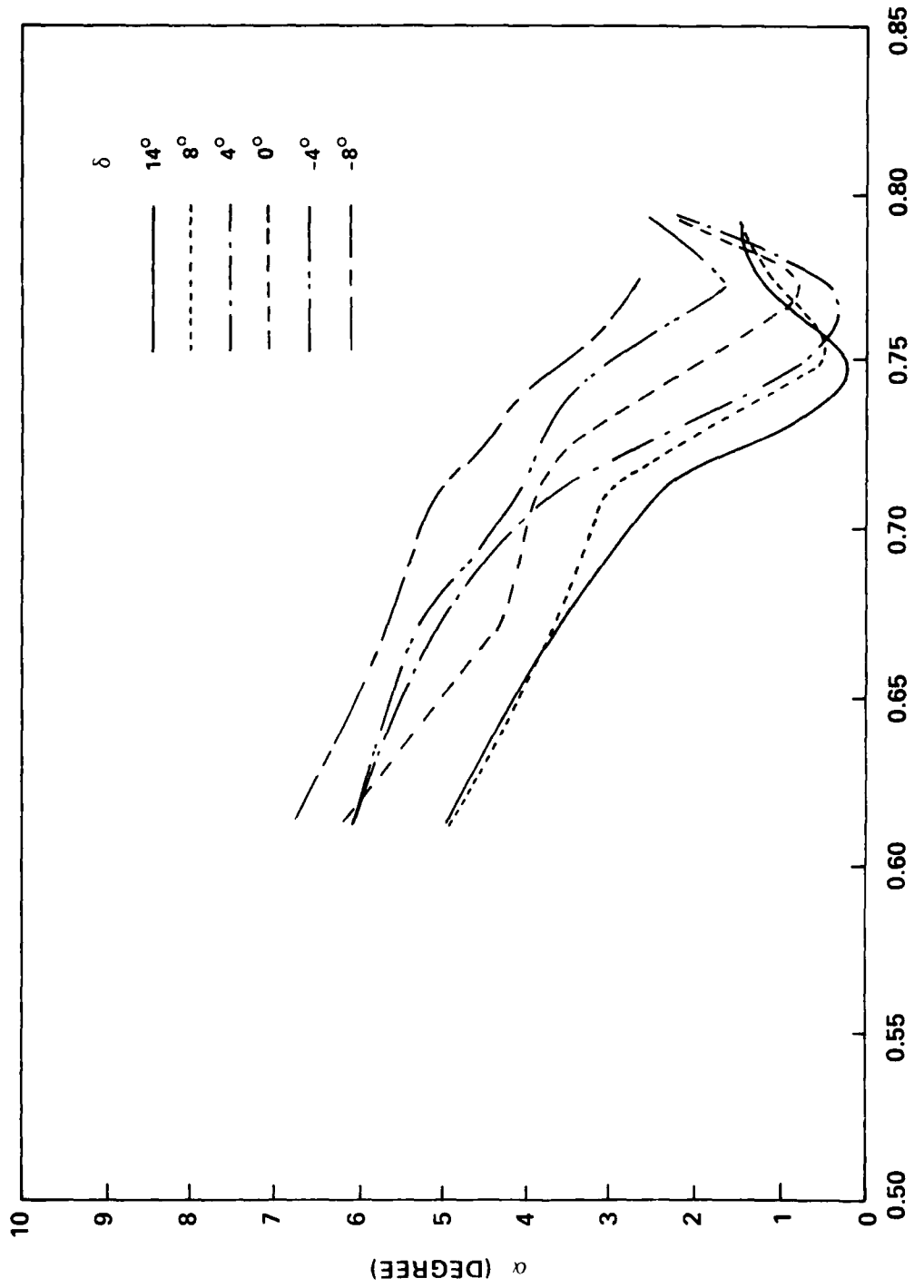

FIG. 11: ANGLE OF INCIDENCE VERSUS MACH NUMBER BUFFET BOUNDARIES FOR VARIOUS FLAP ANGLES

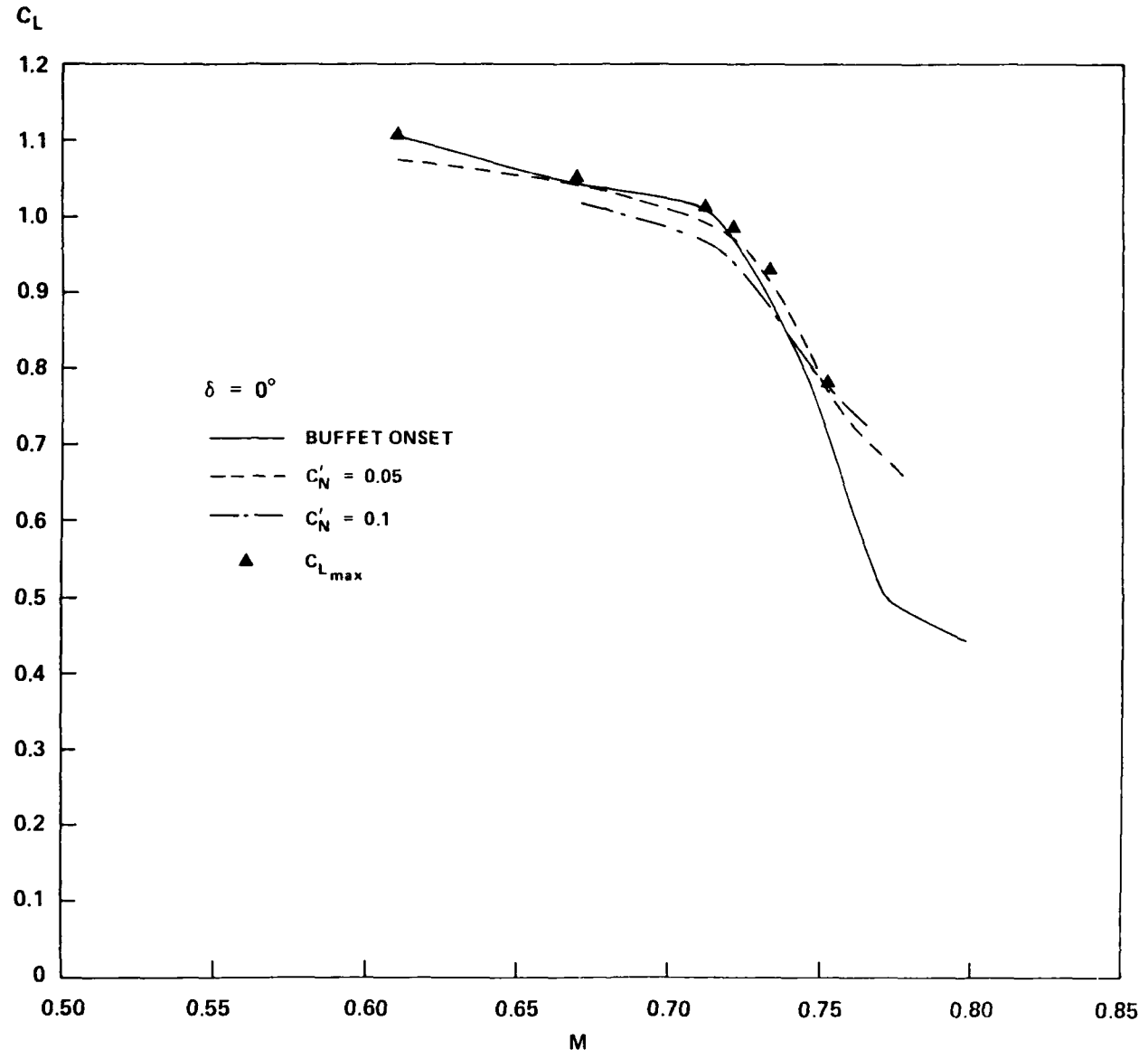

FIG. 12: LIFT VERSUS MACH NUMBER BUFFET BOUNDARIES WITH FLAP ANGLE δ = 0°

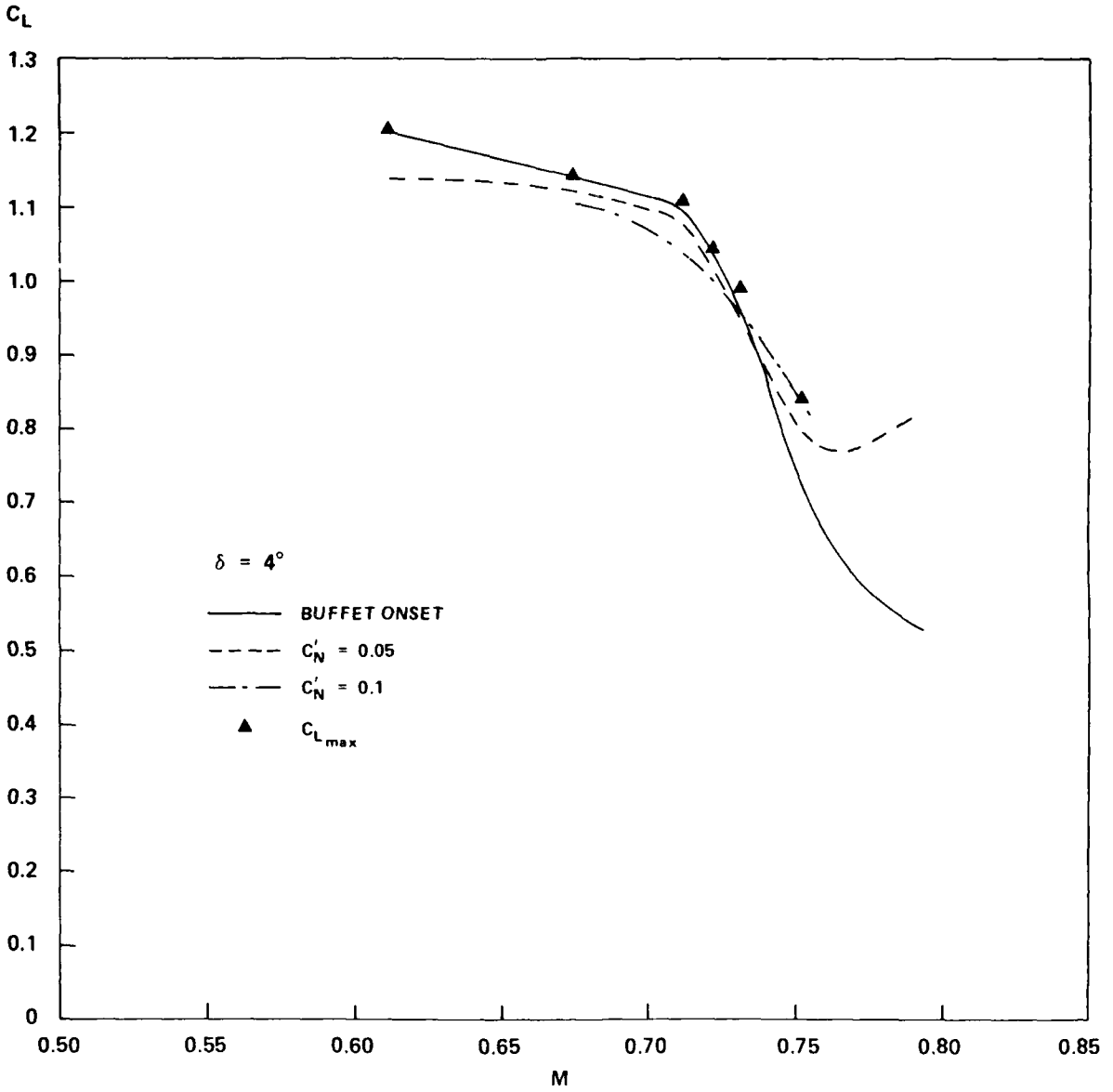

FIG. 13: LIFT VERSUS MACH NUMBER BUFFET BOUNDARIES WITH FLAP ANGLE δ = 4°

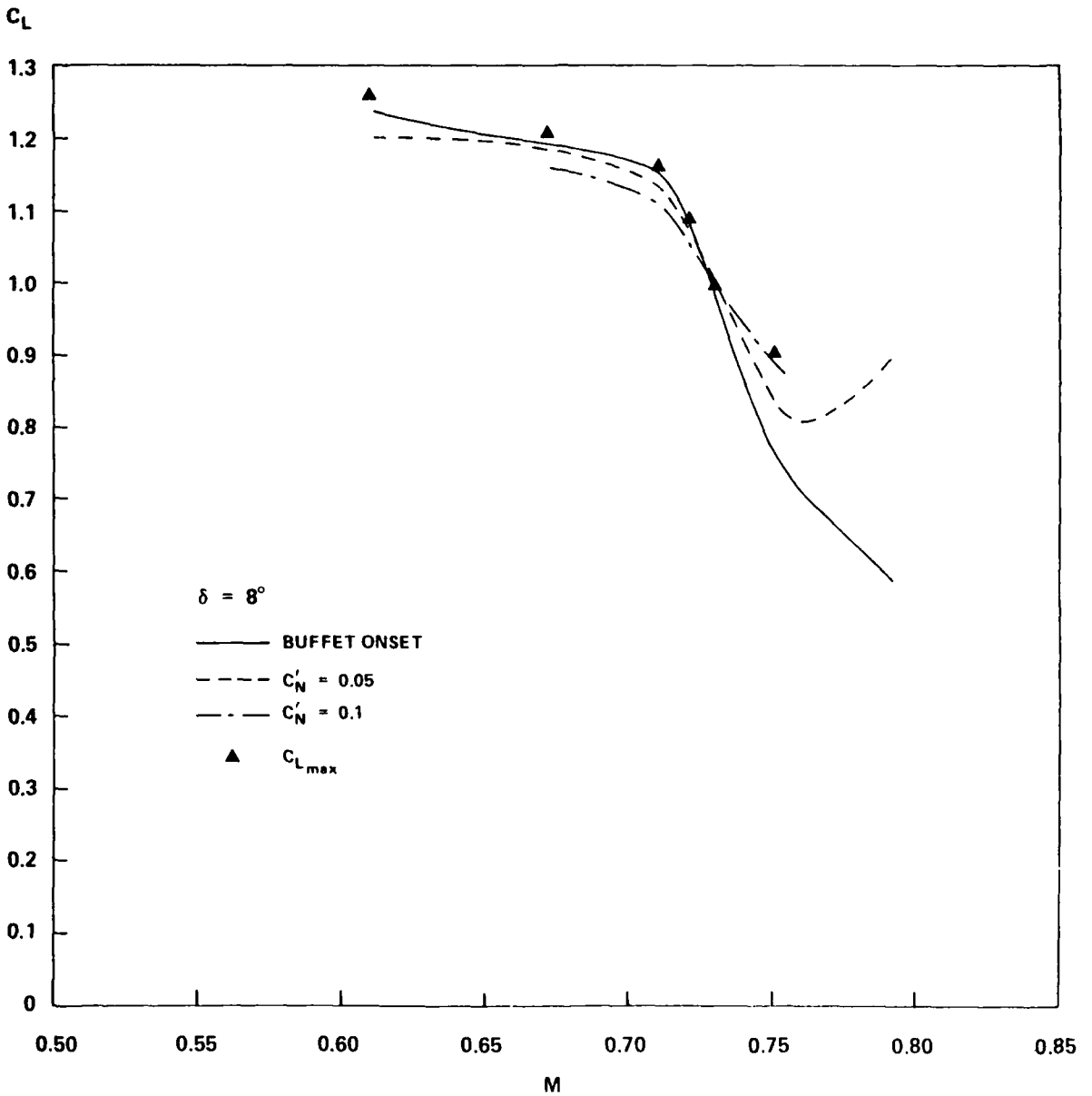

FIG. 14: LIFT VERSUS MACH NUMBER BUFFET BOUNDARIES WITH FLAP ANGLE δ = 8°

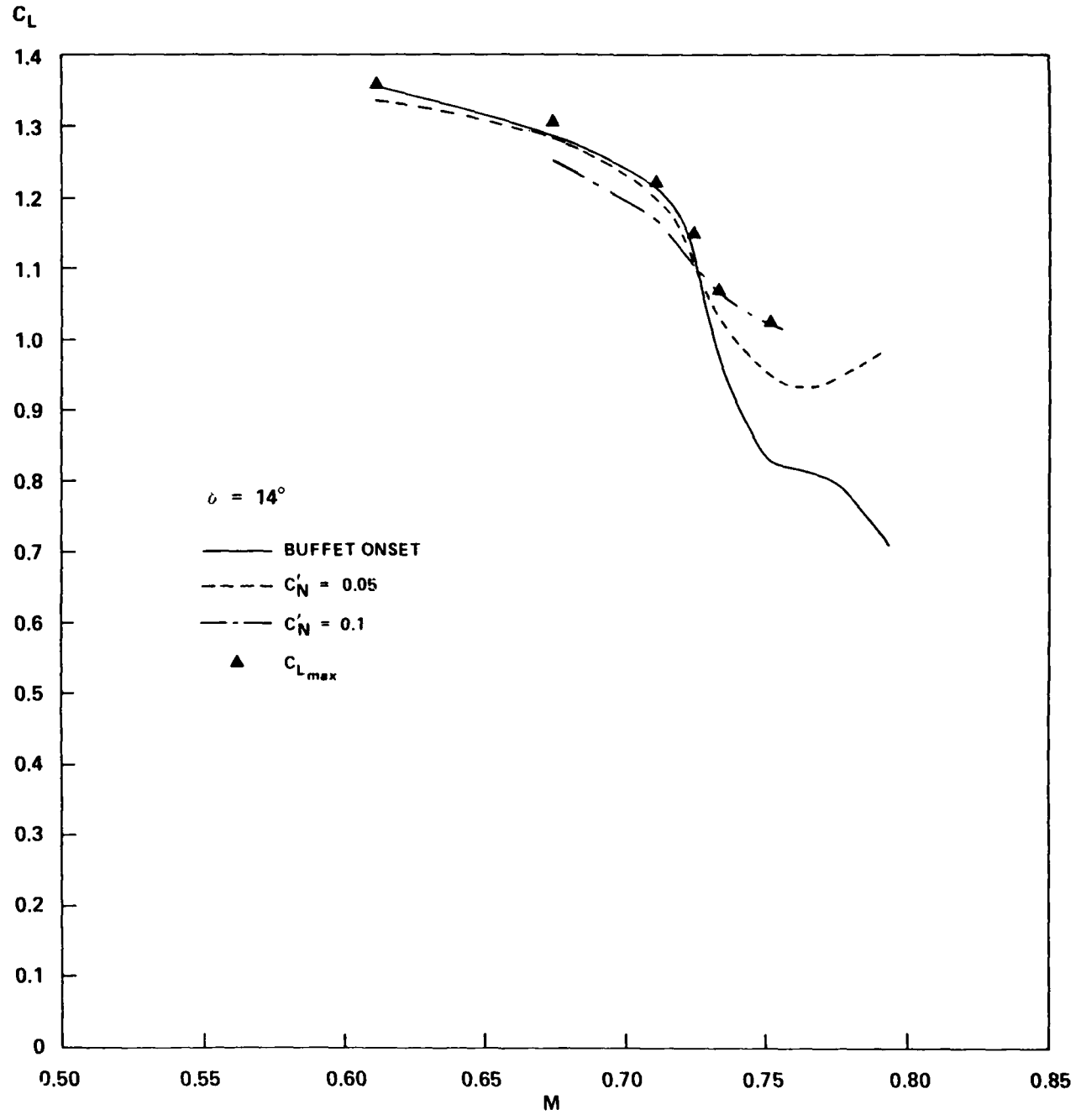

FIG. 15: LIFT VERSUS MACH NUMBER BUFFET BOUNDARIES WITH FLAP ANGLE δ = 14°

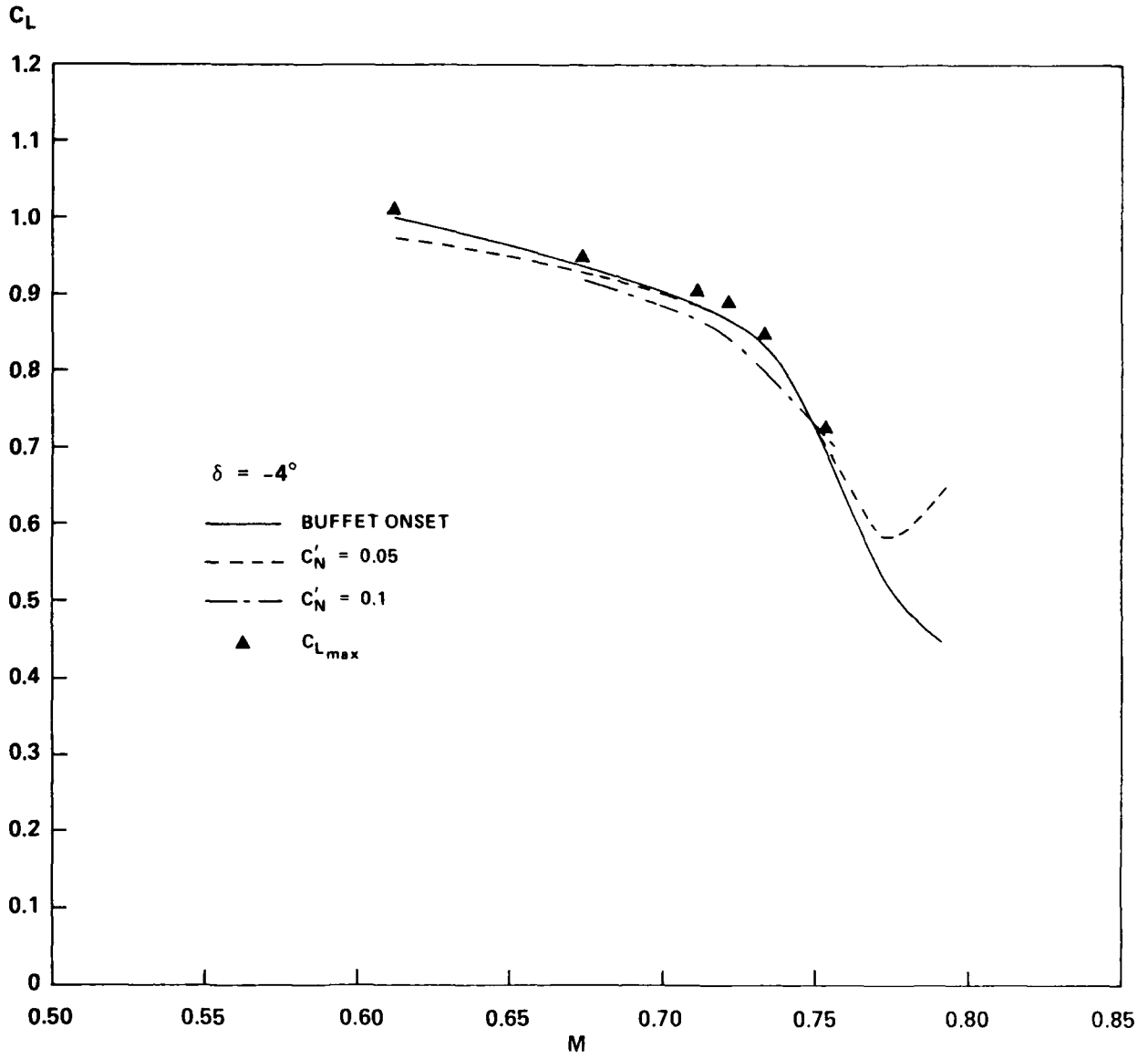

FIG. 16: LIFT VERSUS MACH NUMBER BUFFET BOUNDARIES WITH FLAP ANGLE δ = -4°

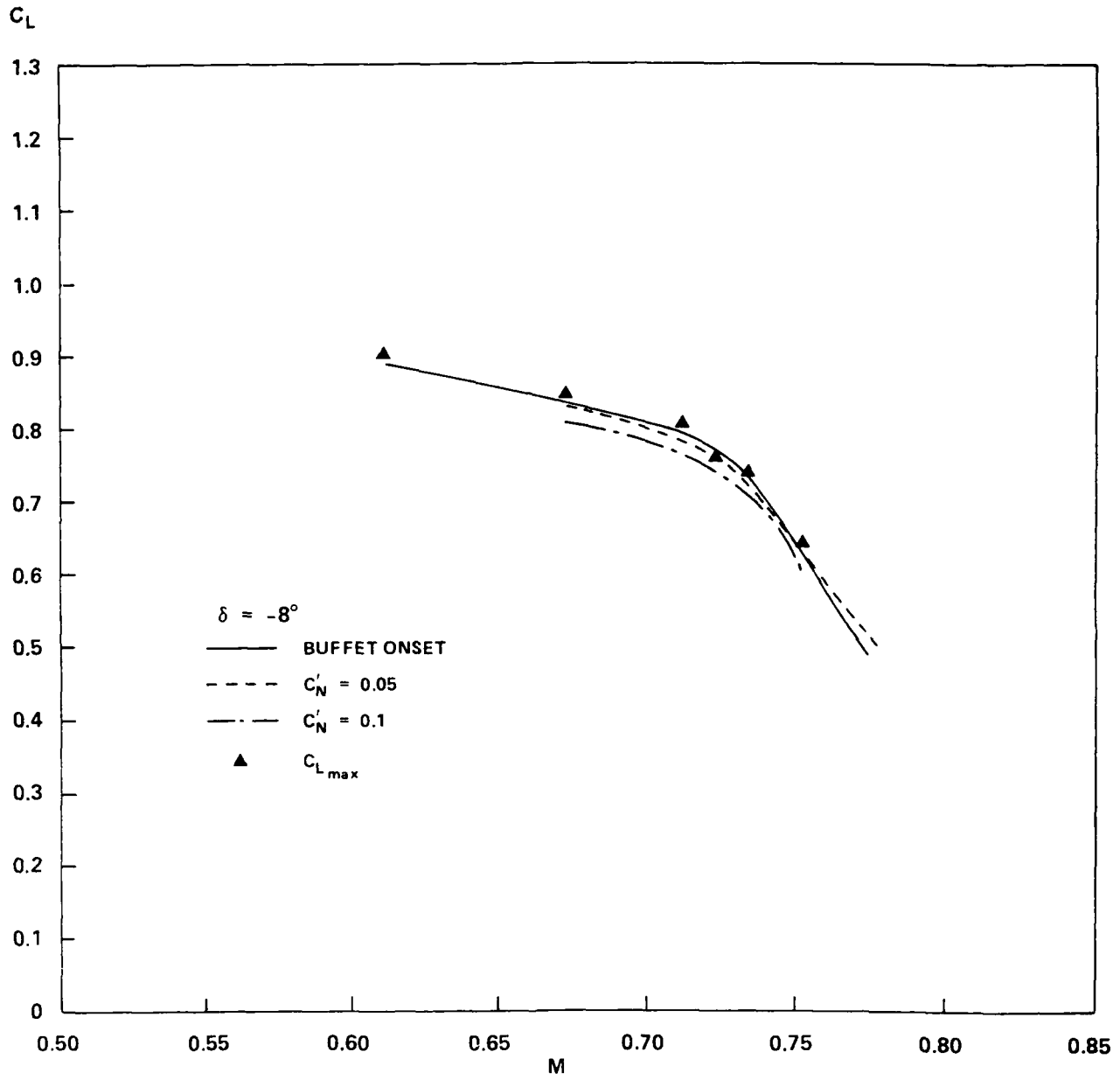

FIG. 17: LIFT VERSUS MACH NUMBER BUFFET BOUNDARIES WITH FLAP ANGLE δ = -8°

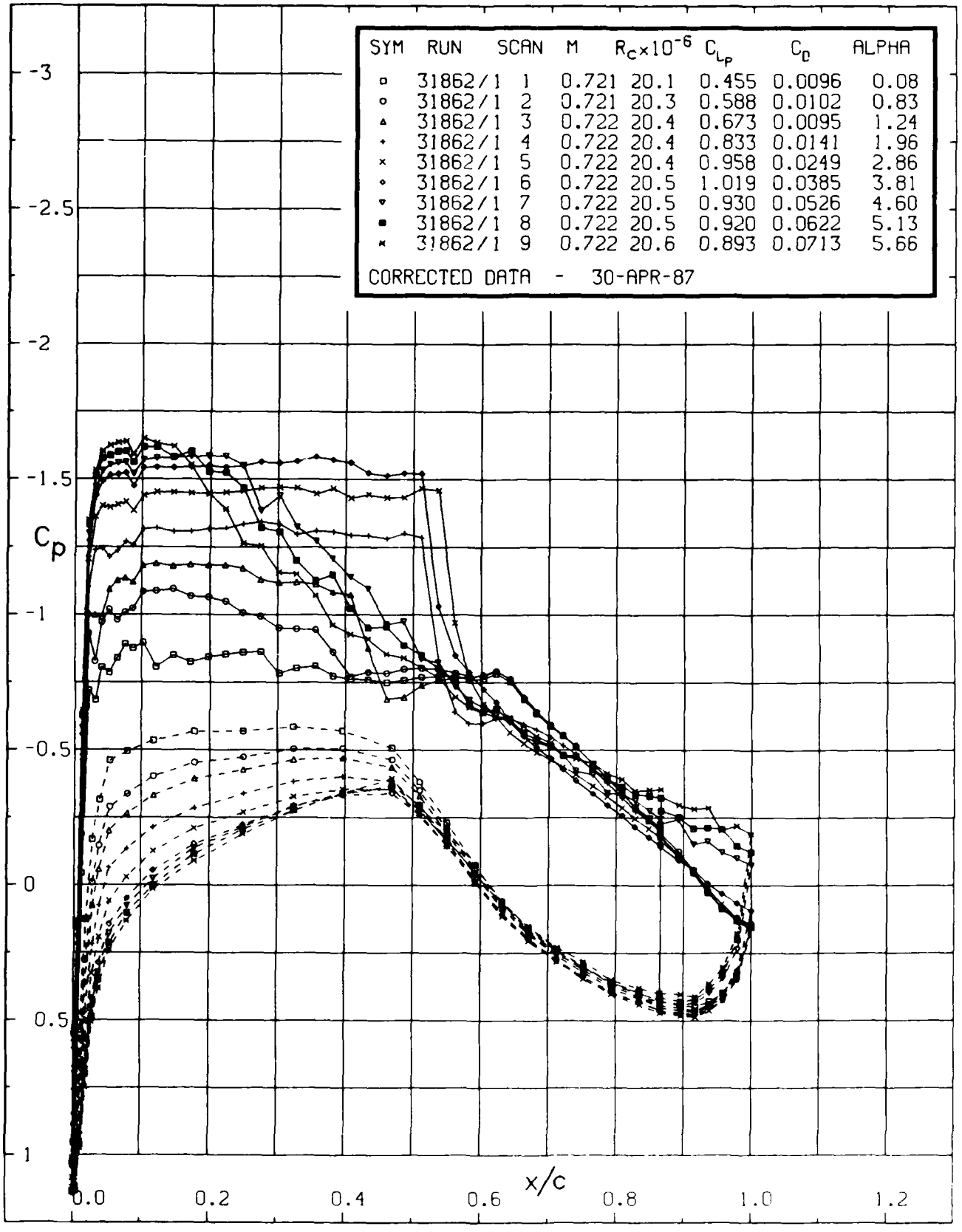

FIG. 18: SURFACE PRESSURE DISTRIBUTIONS AT M ABOUT 0.711 FOR FLAP ANGLE δ = 0°

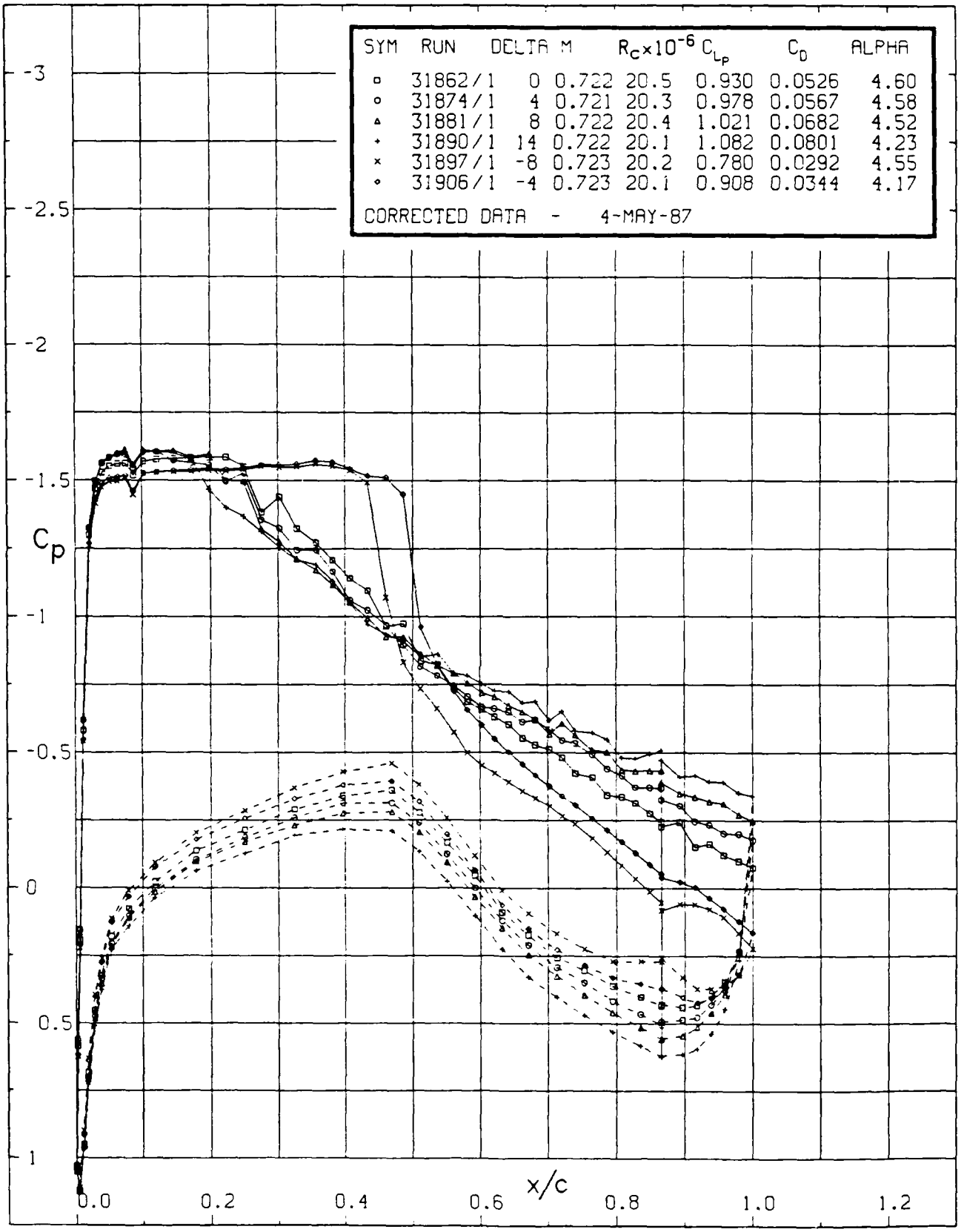

FIG. 19: SURFACE PRESSURE DISTRIBUTIONS AT M ABOUT 0.723 FOR VARIOUS FLAP ANGLES AT α ABOUT 4.5°

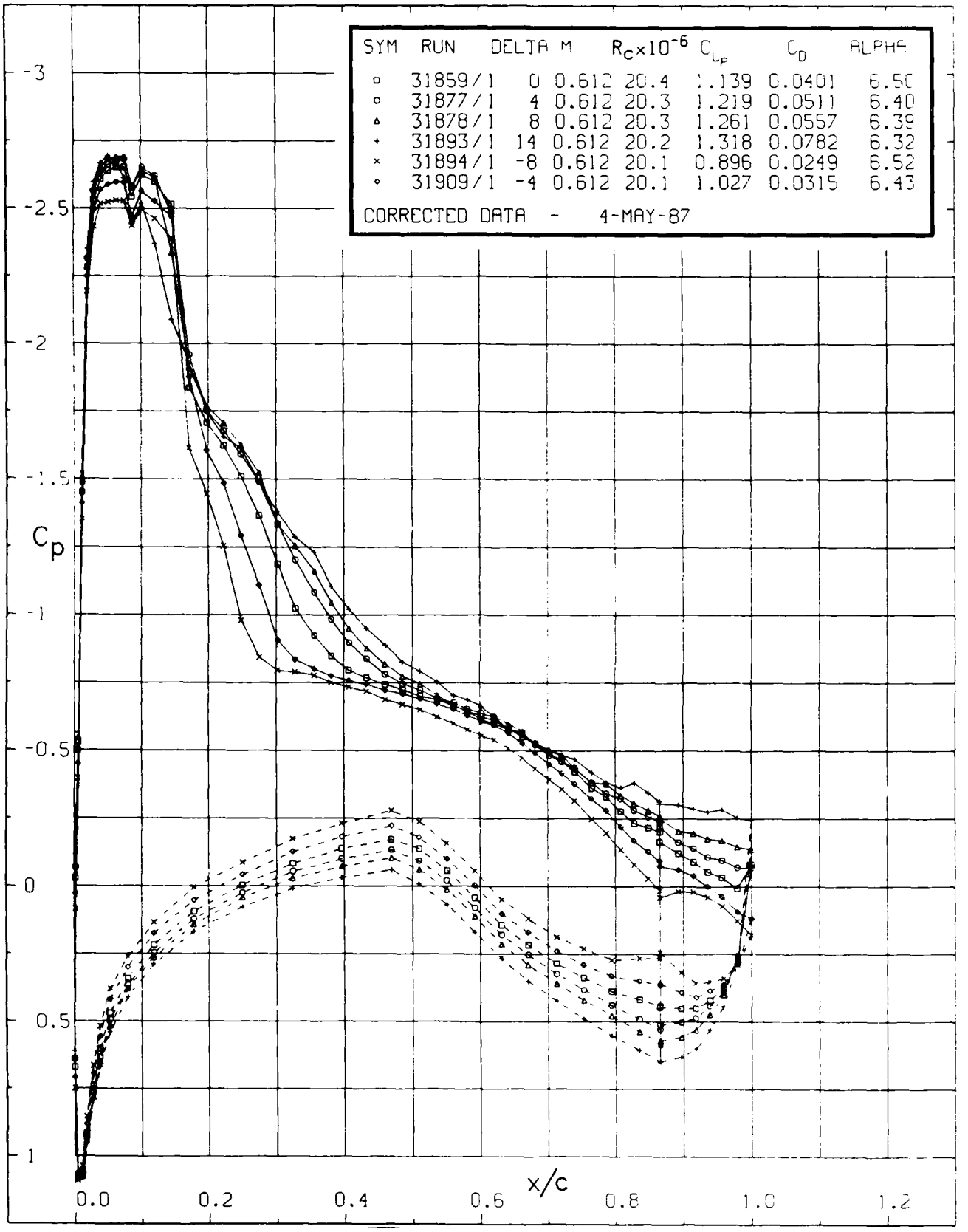

FIG. 20: SURFACE PRESSURE DISTRIBUTIONS AT M ABOUT 0.612 FOR VARIOUS FLAP ANGLES AT α ABOUT 6.5°

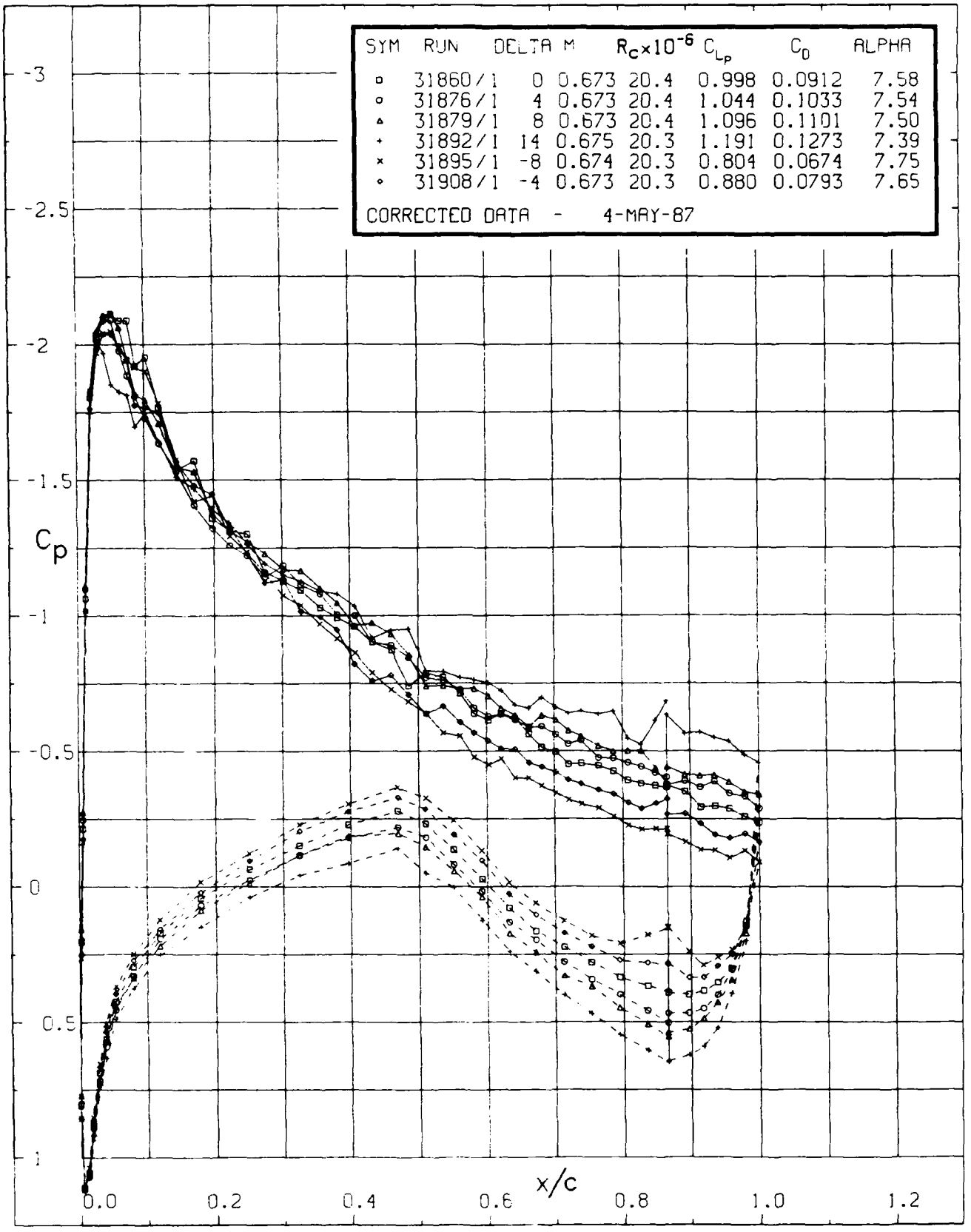

FIG. 21: SURFACE PRESSURE DISTRIBUTIONS AT M ABOUT 0.673 FOR VARIOUS FLAP ANGLES AT α ABOUT 7.5°

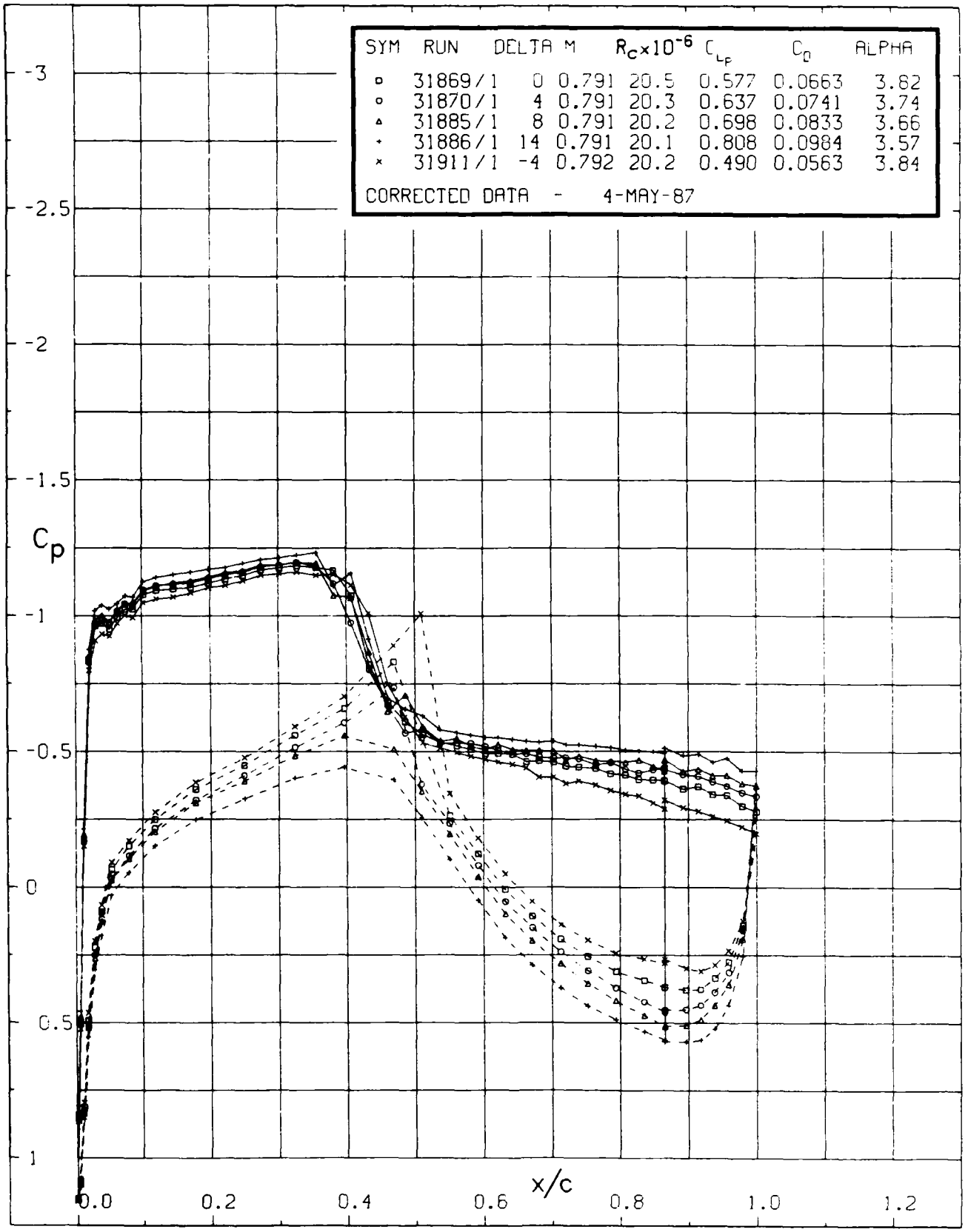

FIG. 22: SURFACE PRESSURE DISTRIBUTIONS AT M ABOUT 0.791 FOR VARIOUS FLAP ANGLES AT α ABOUT 3.75°

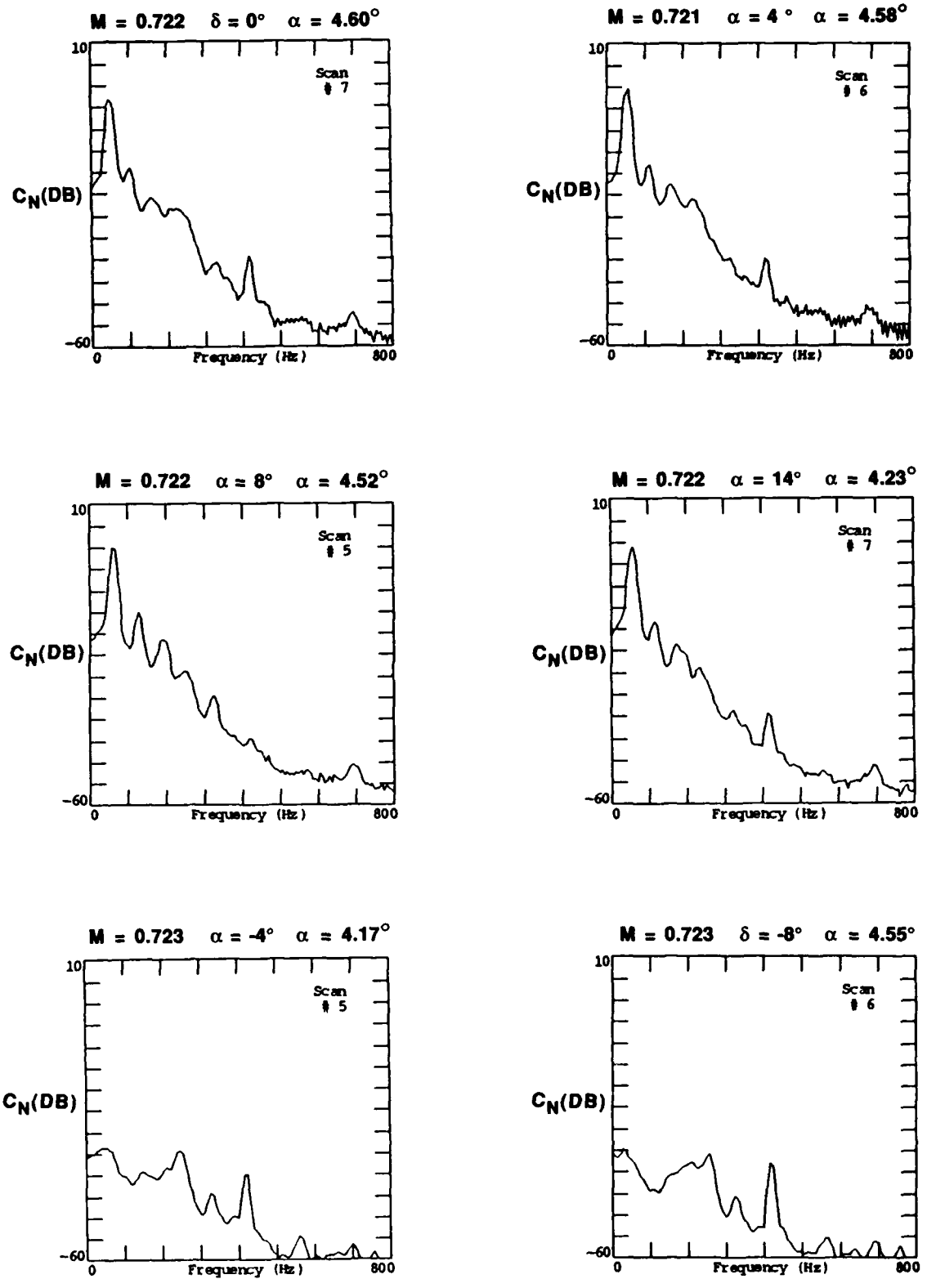

FIG. 23: POWER SPECTRA OF BALANCE NORMAL FORCE AT M ABOUT 0.723 AND α ABOUT 4.5°

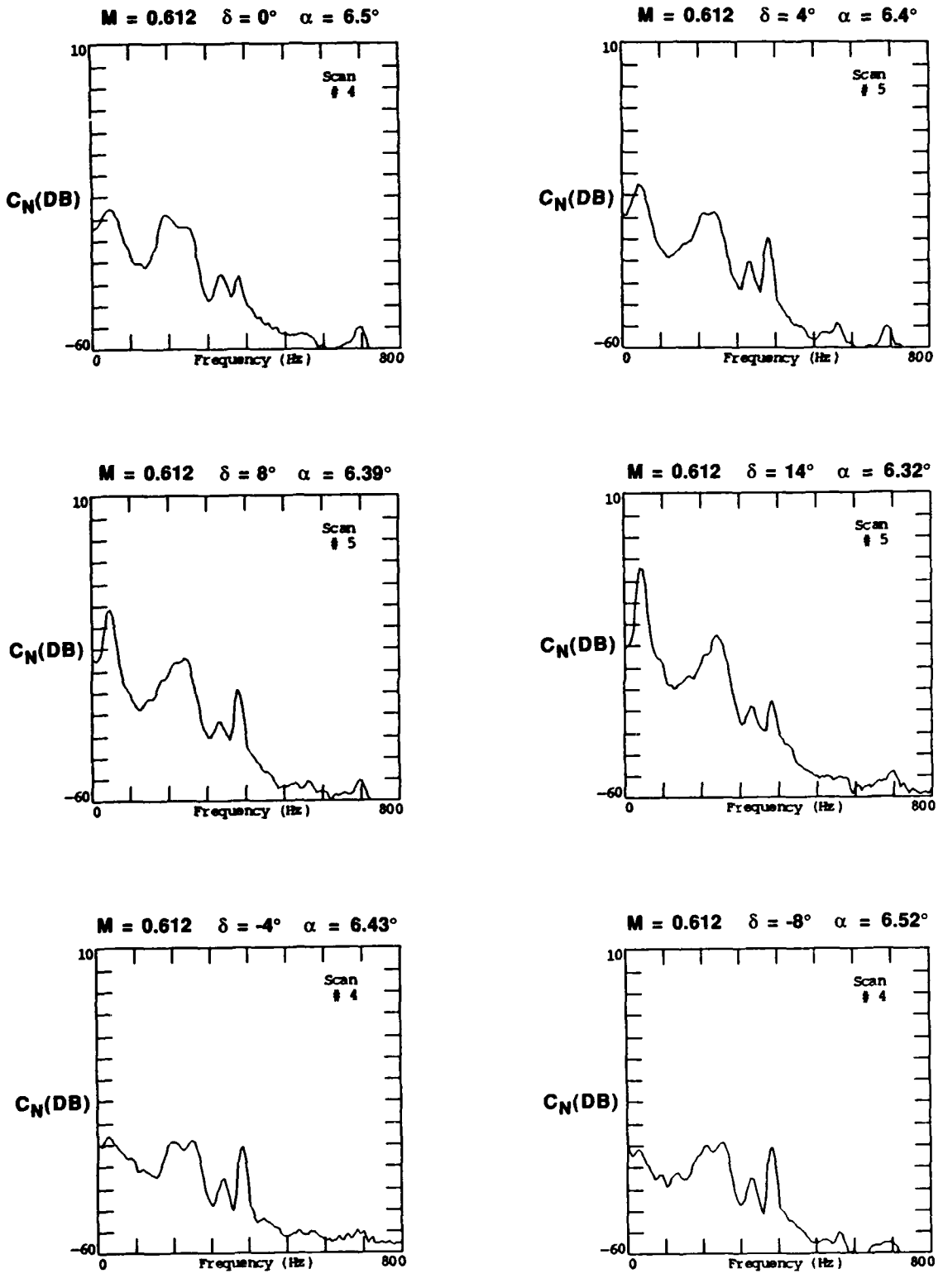

FIG. 24: POWER SPECTRA OF BALANCE NORMAL FORCE AT M ABOUT 0.612 AND α ABOUT 6.5°

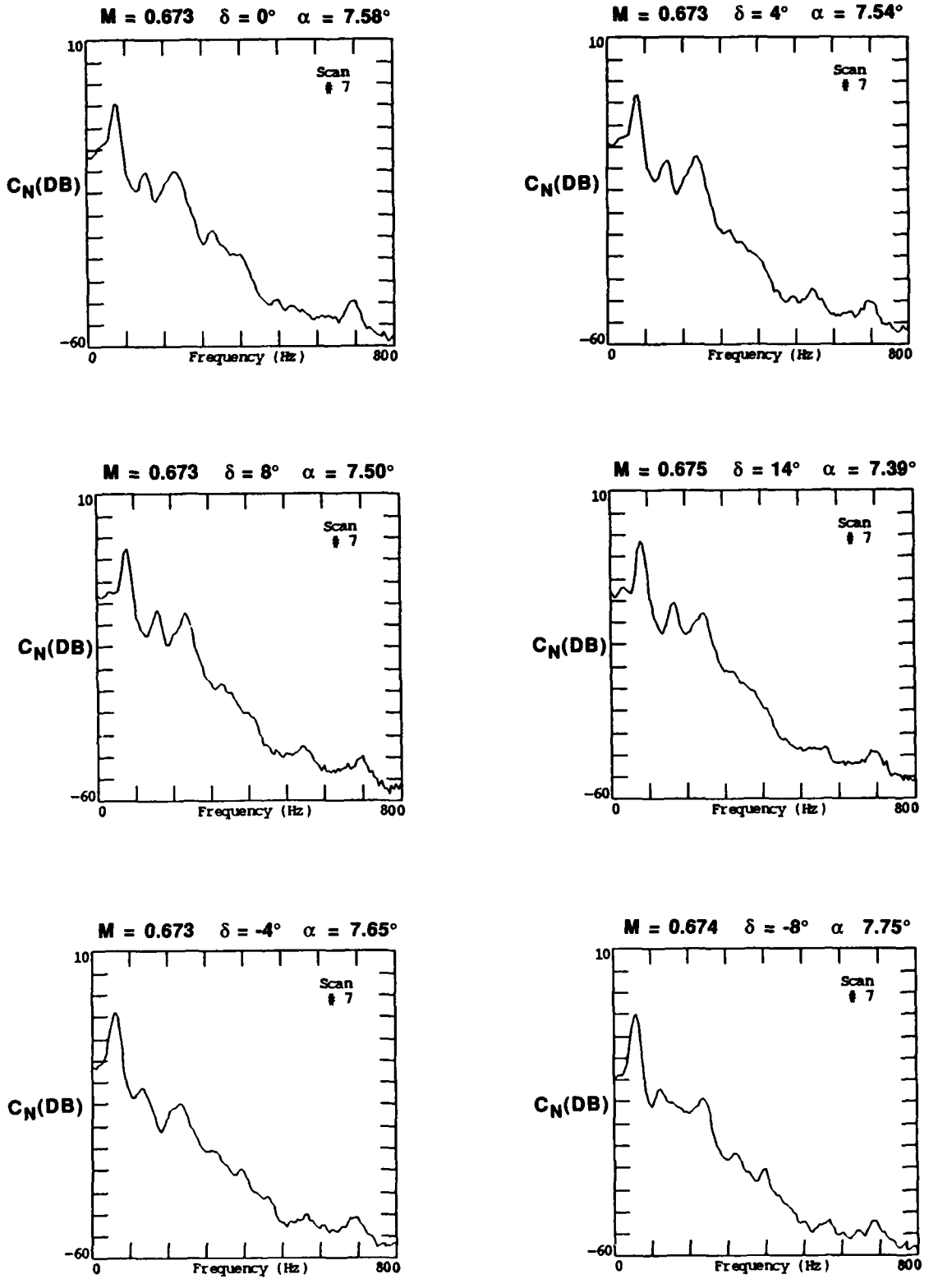

FIG. 25: POWER SPECTRA OF BALANCE NORMAL FORCE AT M ABOUT 0.673 AND α ABOUT 7.5°

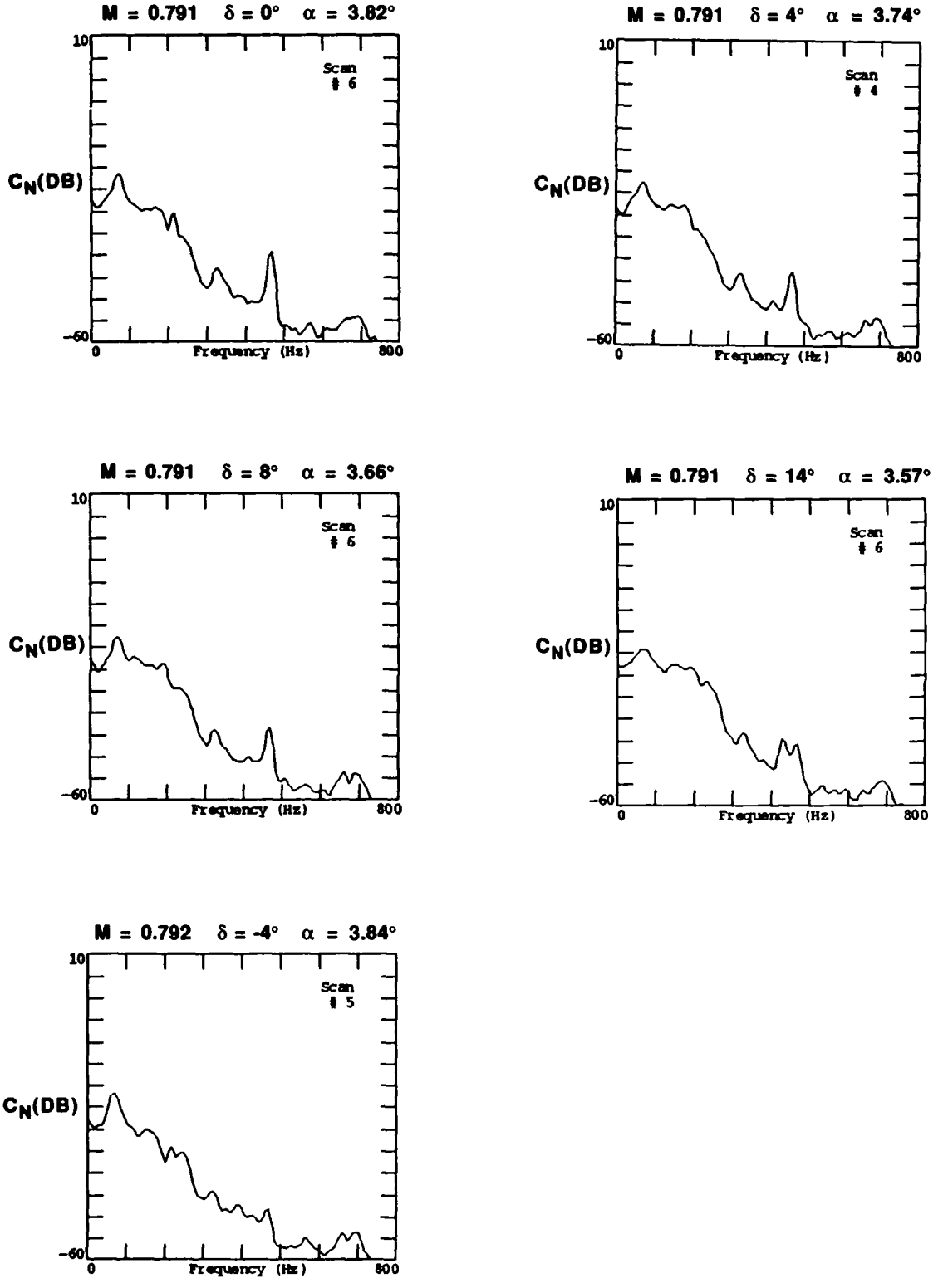

FIG. 26: POWER SPECTRA OF BALANCE NORMAL FORCE AT M ABOUT 0.791 AND α ABOUT 3.75°

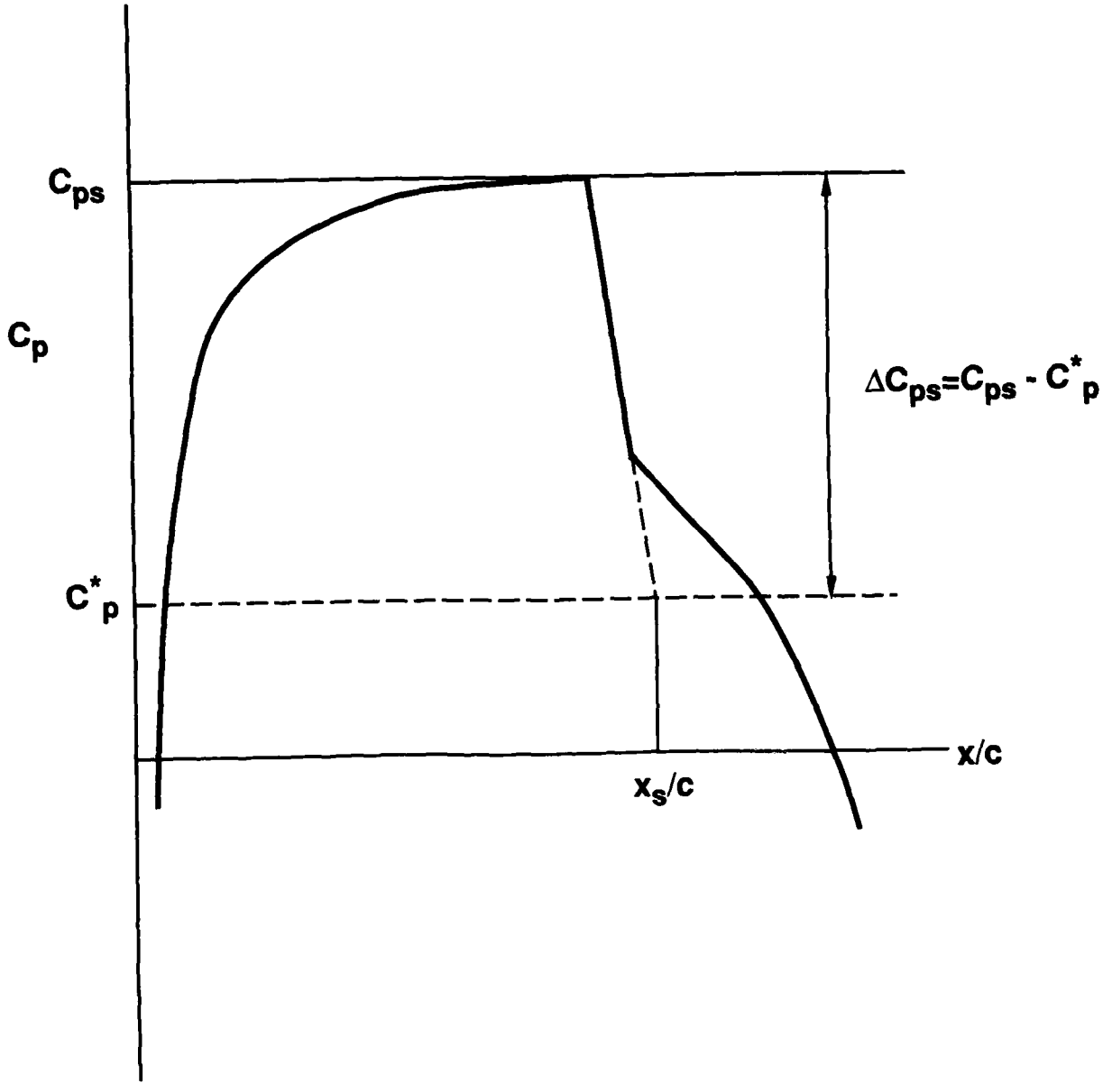

FIG. 27: DEFINITION OF SHOCK LOCATION AND STRENGTH

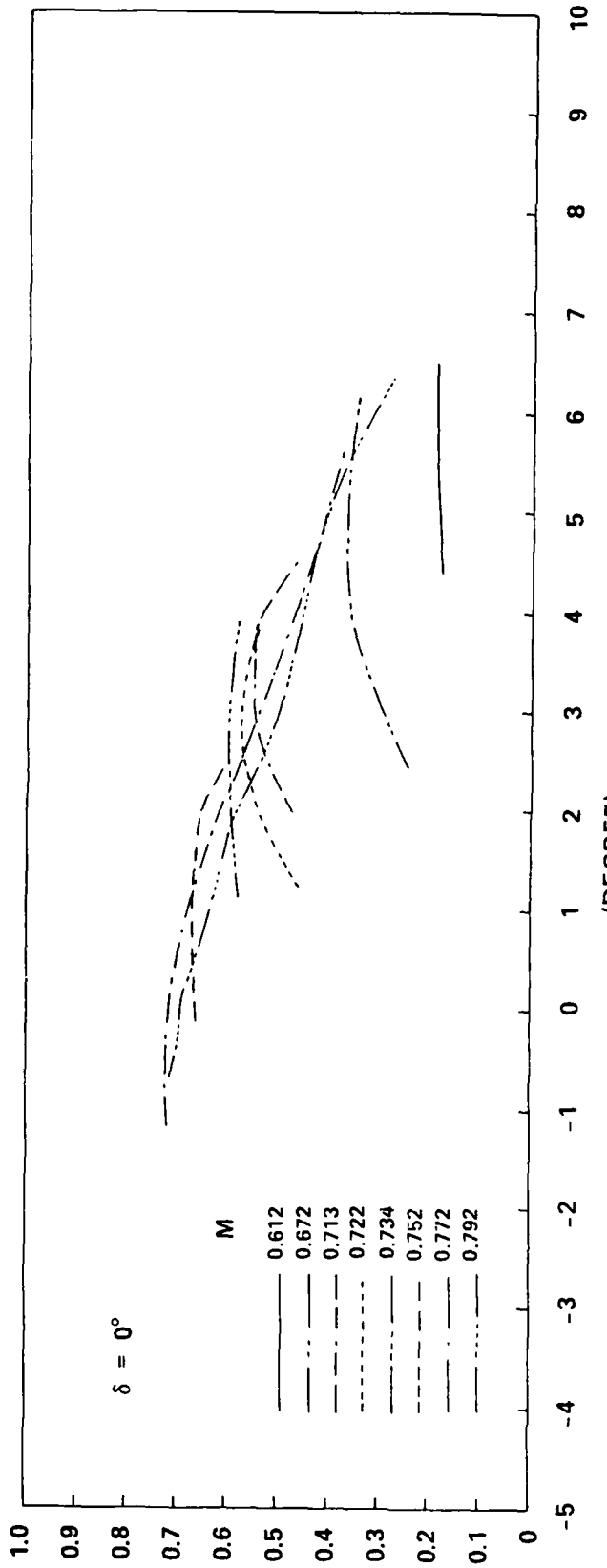

FIG. 28: SHOCK LOCATIONS VERSUS ANGLE OF INCIDENCE AT VARIOUS MACH NUMBERS FOR FLAP ANGLE $\delta = 0°$

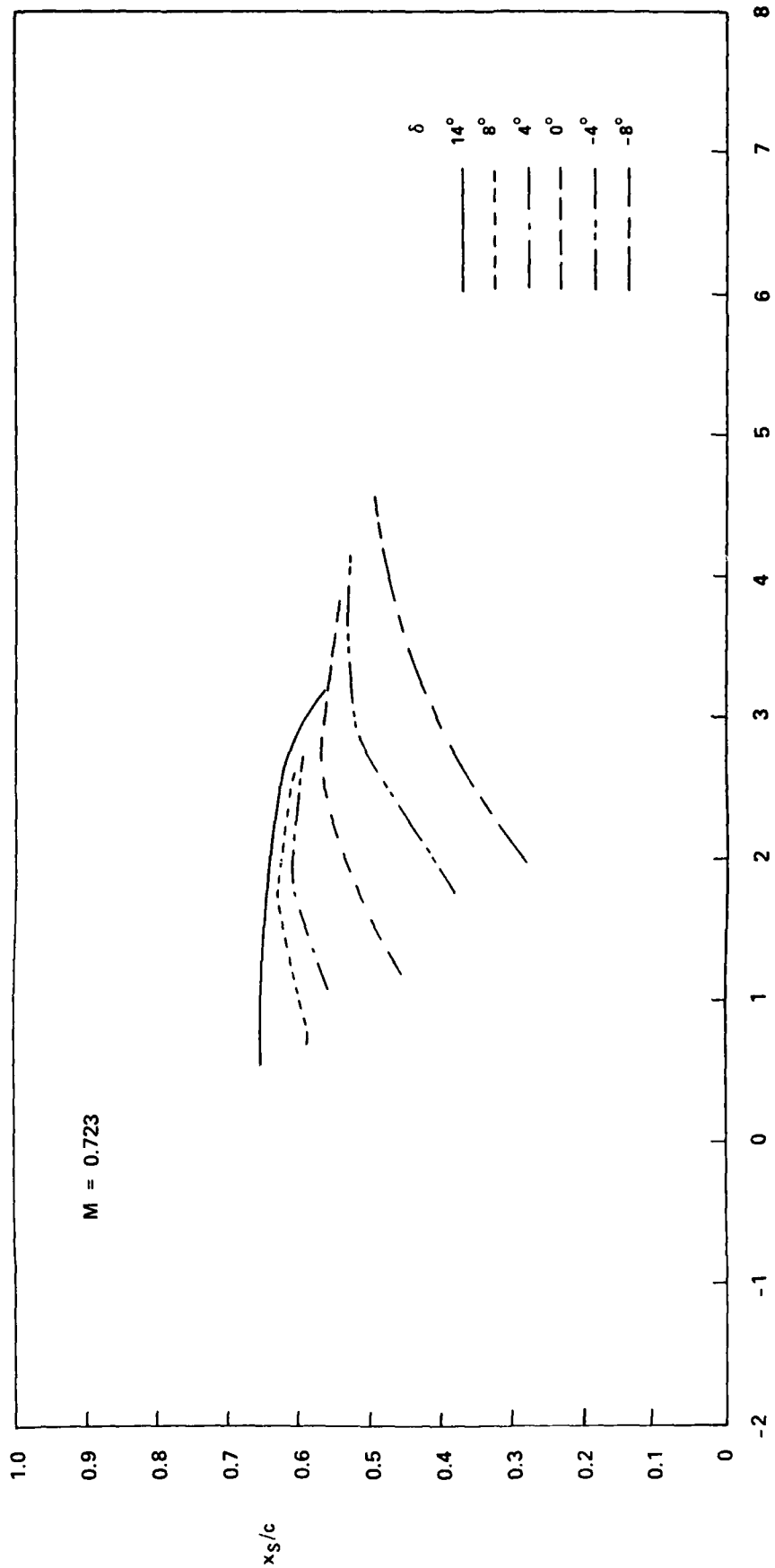

FIG. 29: SHOCK LOCATIONS VERSUS ANGLE OF INCIDENCE AT M = 0.723 FOR VARIOUS FLAP ANGLES

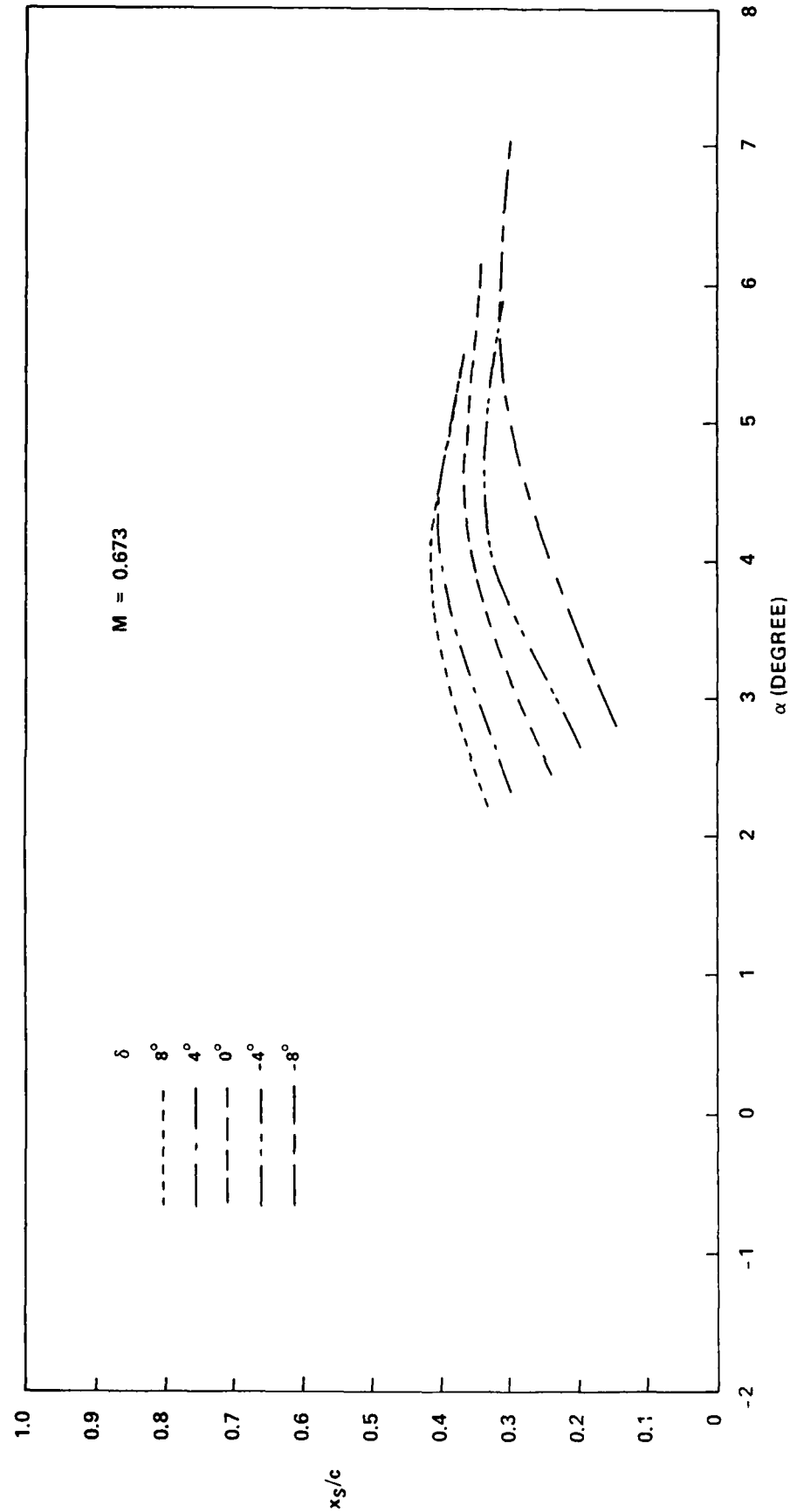

FIG. 30: SHOCK LOCATIONS VERSUS ANGLE OF INCIDENCE AT M = 0.673 FOR VARIOUS FLAP ANGLES

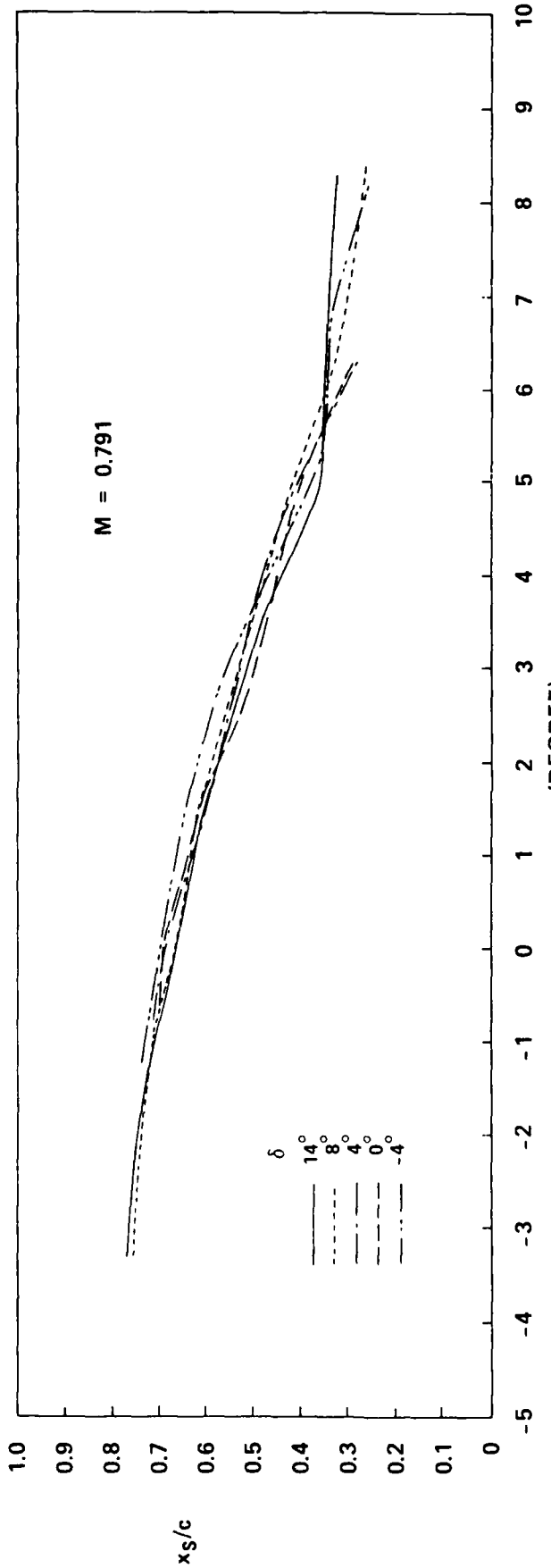

FIG. 31: SHOCK LOCATIONS VERSUS ANGLE OF INCIDENCE AT M = 0.791 FOR VARIOUS FLAP ANGLES

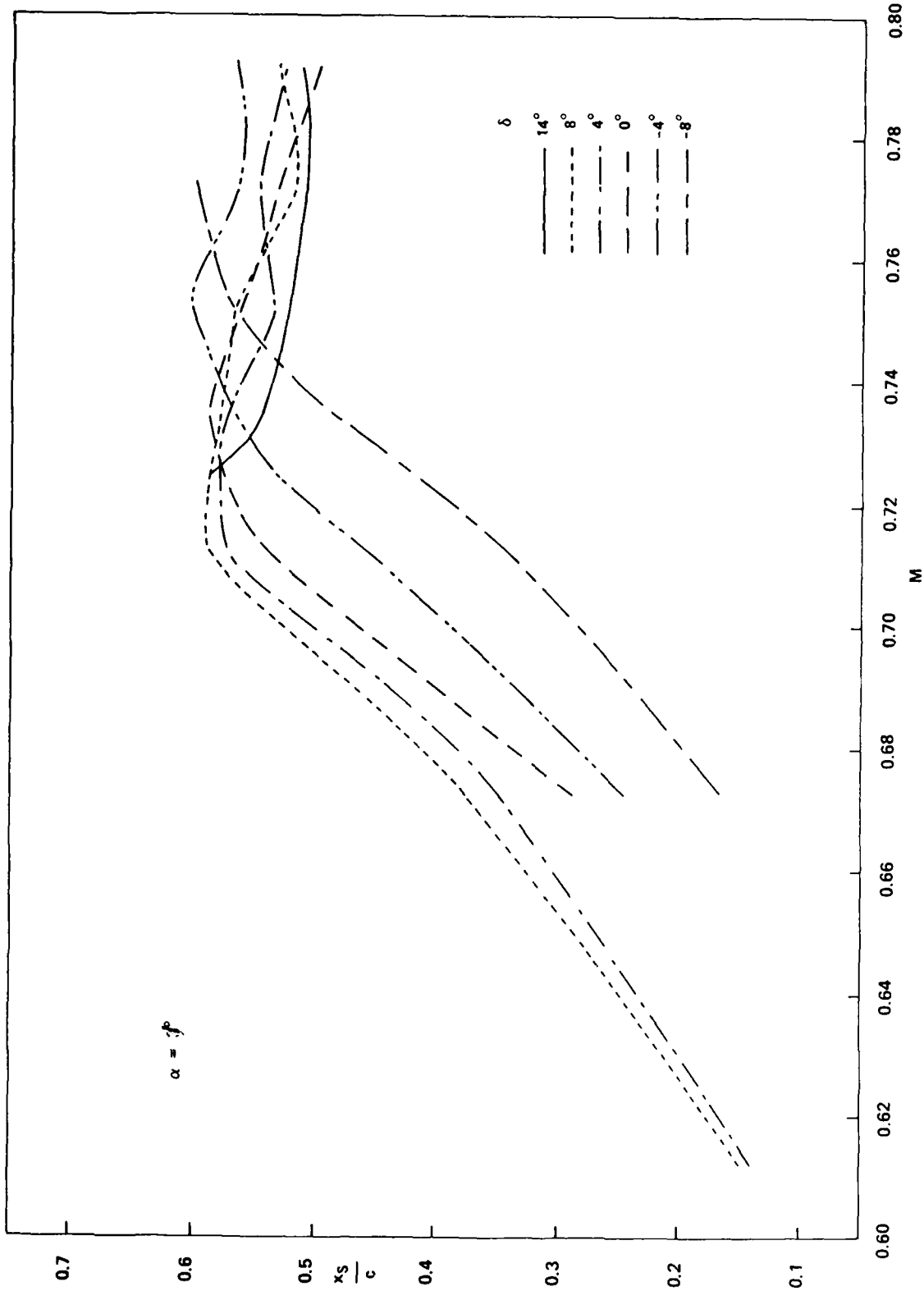

FIG. 32: SHOCK LOCATIONS VERSUS MACH NUMBER AT ANGLE OF INCIDENCE α = 3° FOR VARIOUS FLAP ANGLES

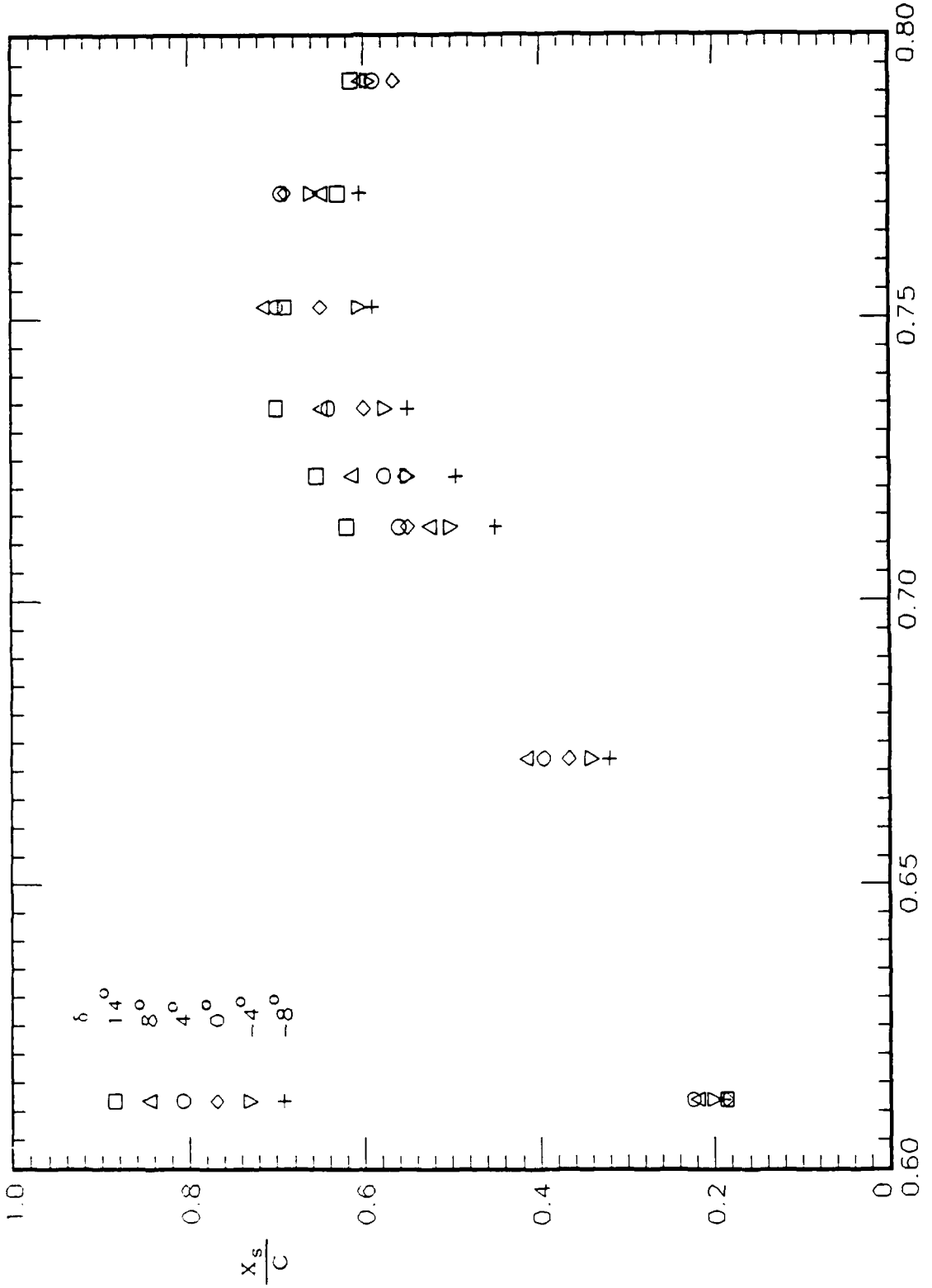

FIG. 33: SHOCK LOCATIONS VERSUS MACH NUMBER AT BUFFET ONSET FOR VARIOUS FLAP ANGLES

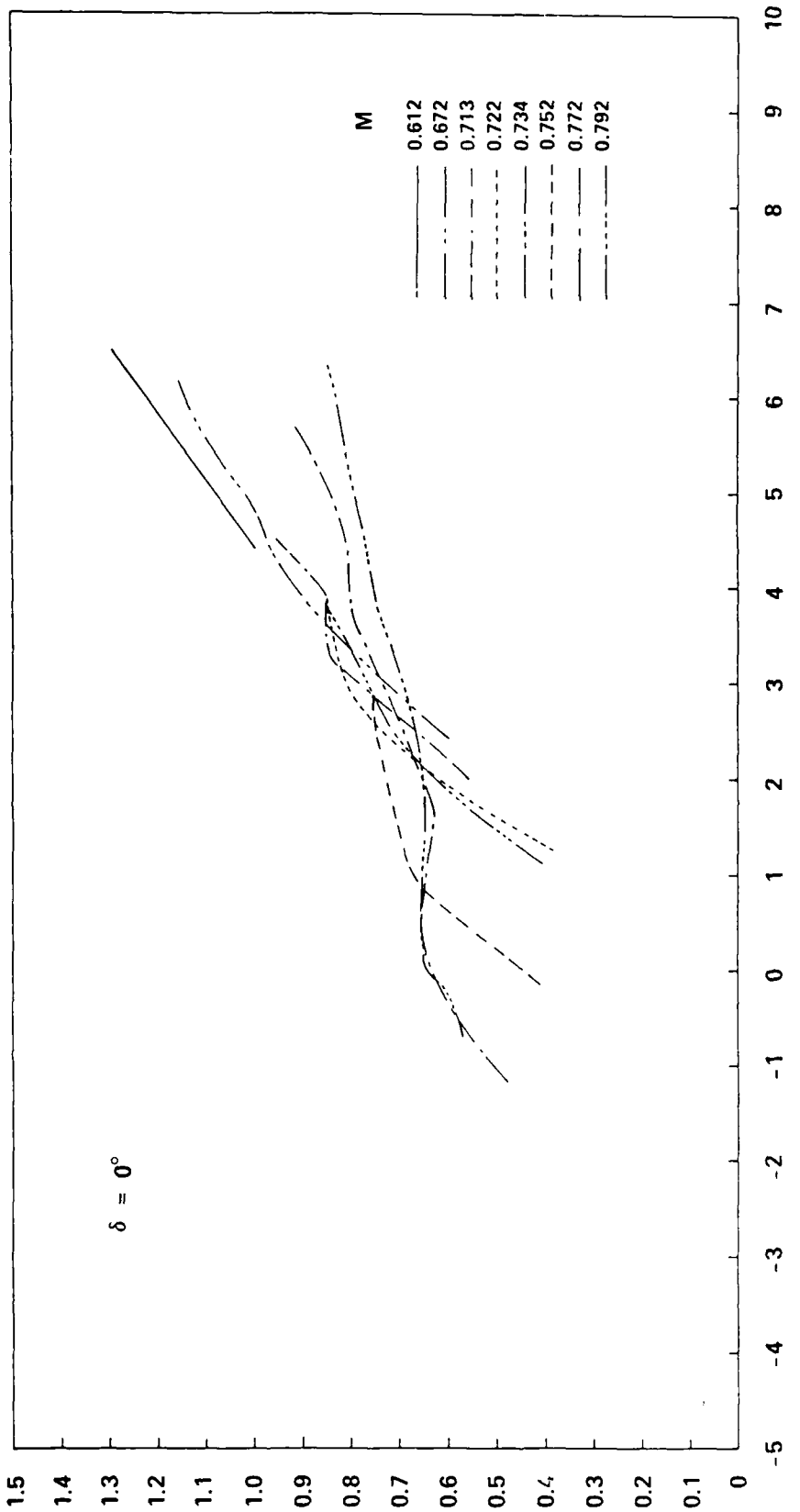

FIG. 34: SHOCK STRENGTHS VERSUS ANGLE OF INCIDENCE AT VARIOUS MACH NUMBERS FOR FLAP ANGLE δ = 0°

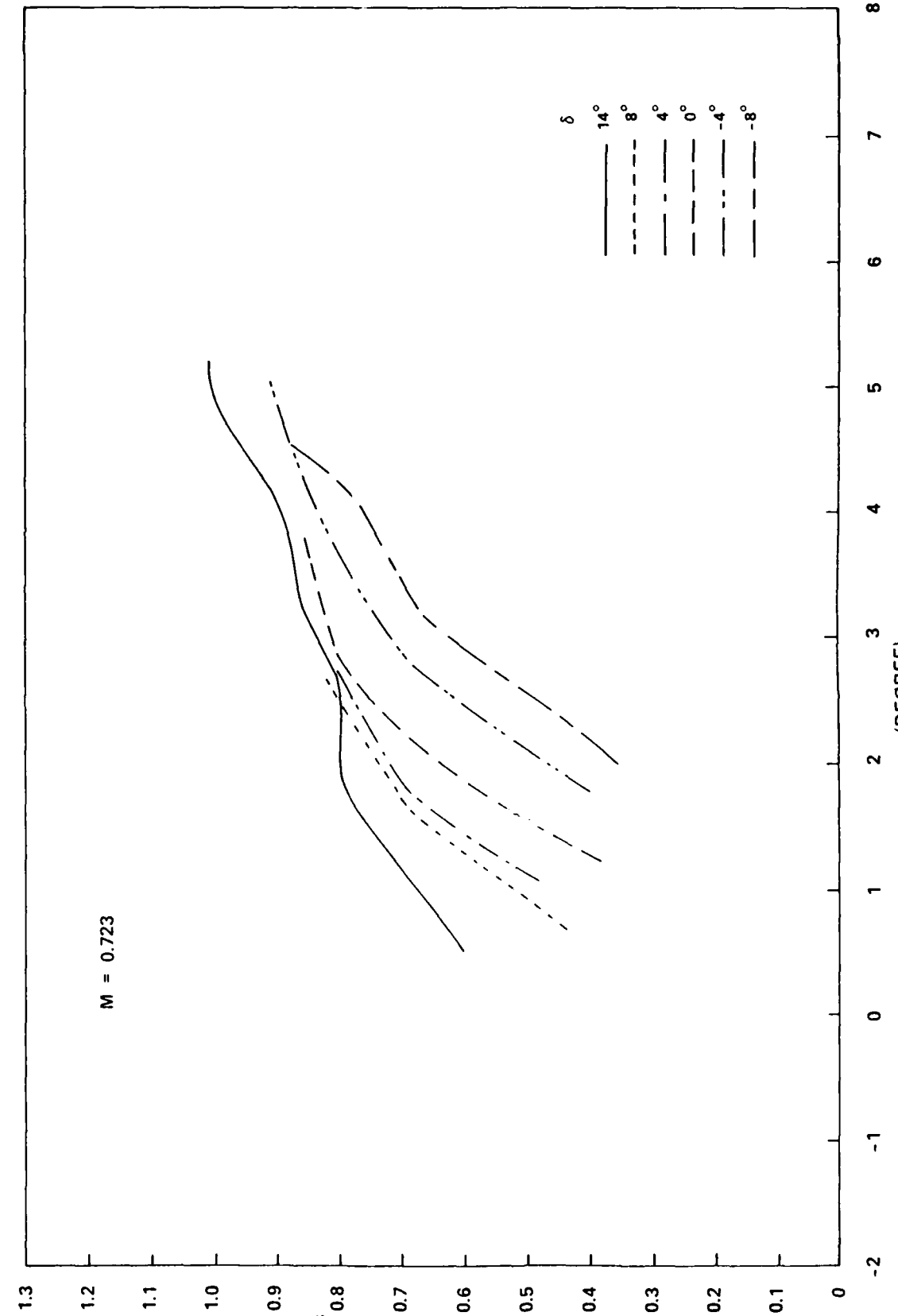

FIG. 35: SHOCK STRENGTHS VERSUS ANGLE OF INCIDENCE AT M = 0.723 FOR VARIOUS FLAP ANGLES

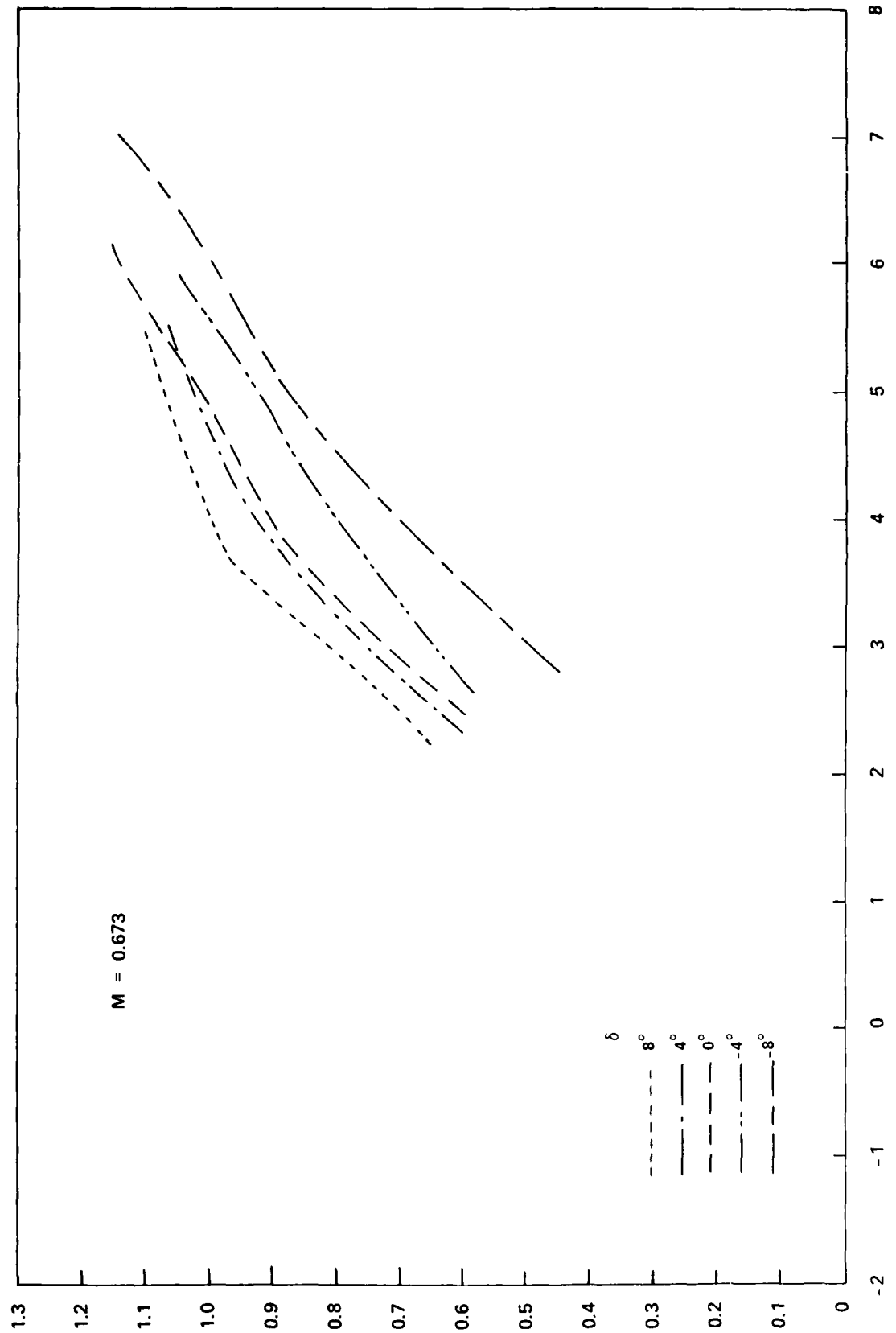

FIG. 36: SHOCK STRENGTHS VERSUS ANGLE OF INCIDENCE AT M = 0.673 FOR VARIOUS FLAP ANGLES

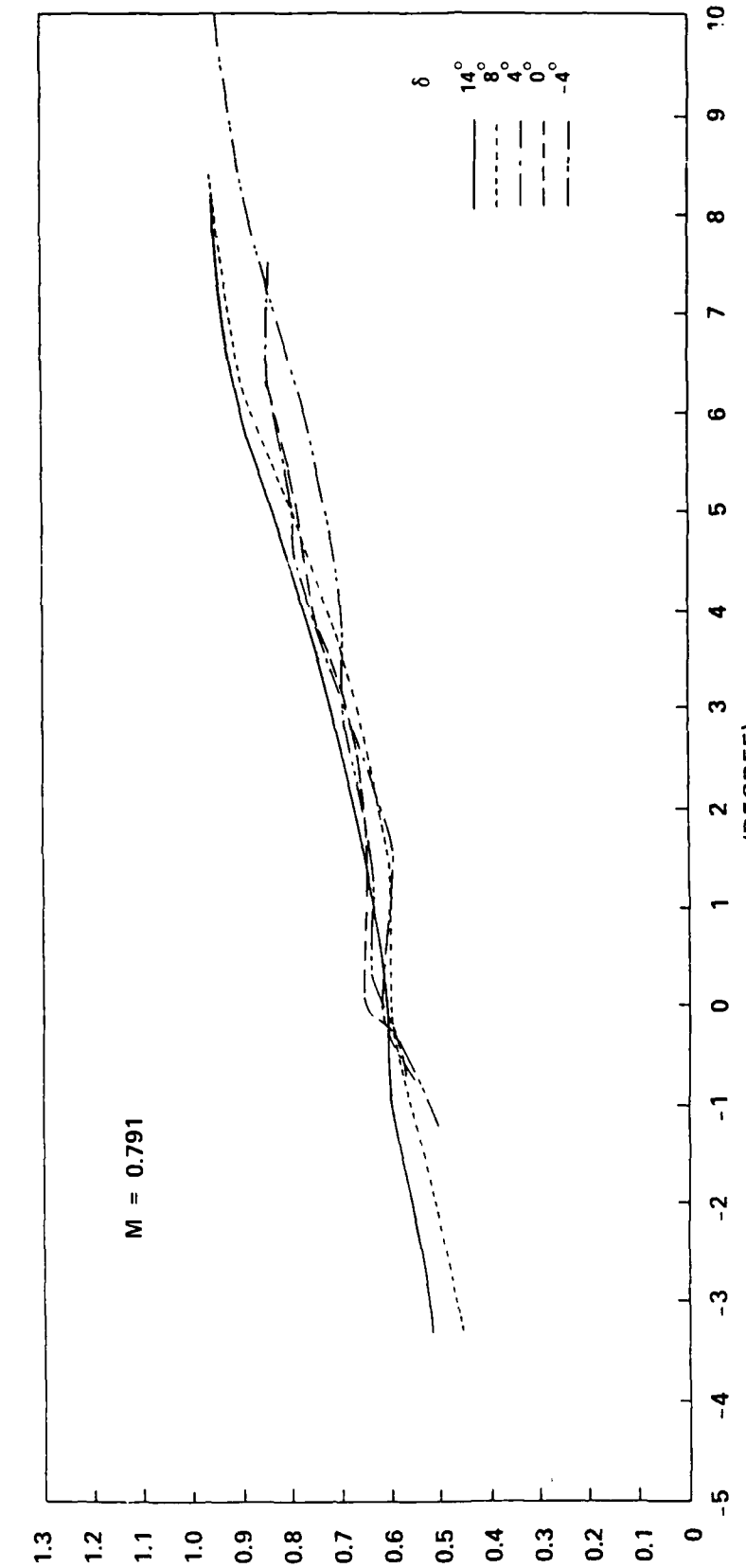

FIG. 37: SHOCK STRENGTHS VERSUS ANGLE OF INCIDENCE AT M = 0.791 FOR VARIOUS FLAP ANGLES

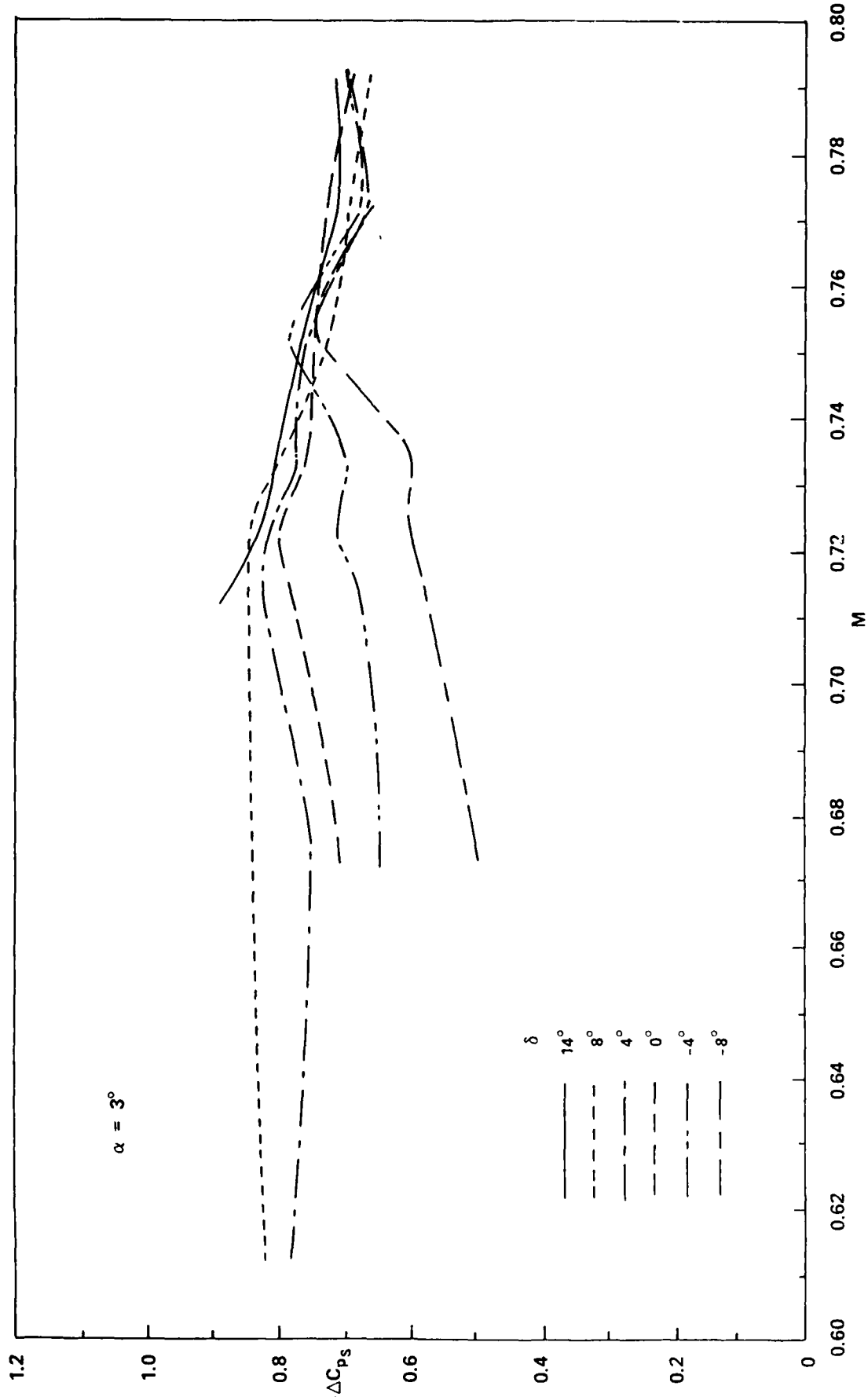

FIG. 38: SHOCK STRENGTHS VERSUS MACH NUMBER AT ANGLE OF INCIDENCE α = 3° FOR VARIOUS FLAP ANGLES

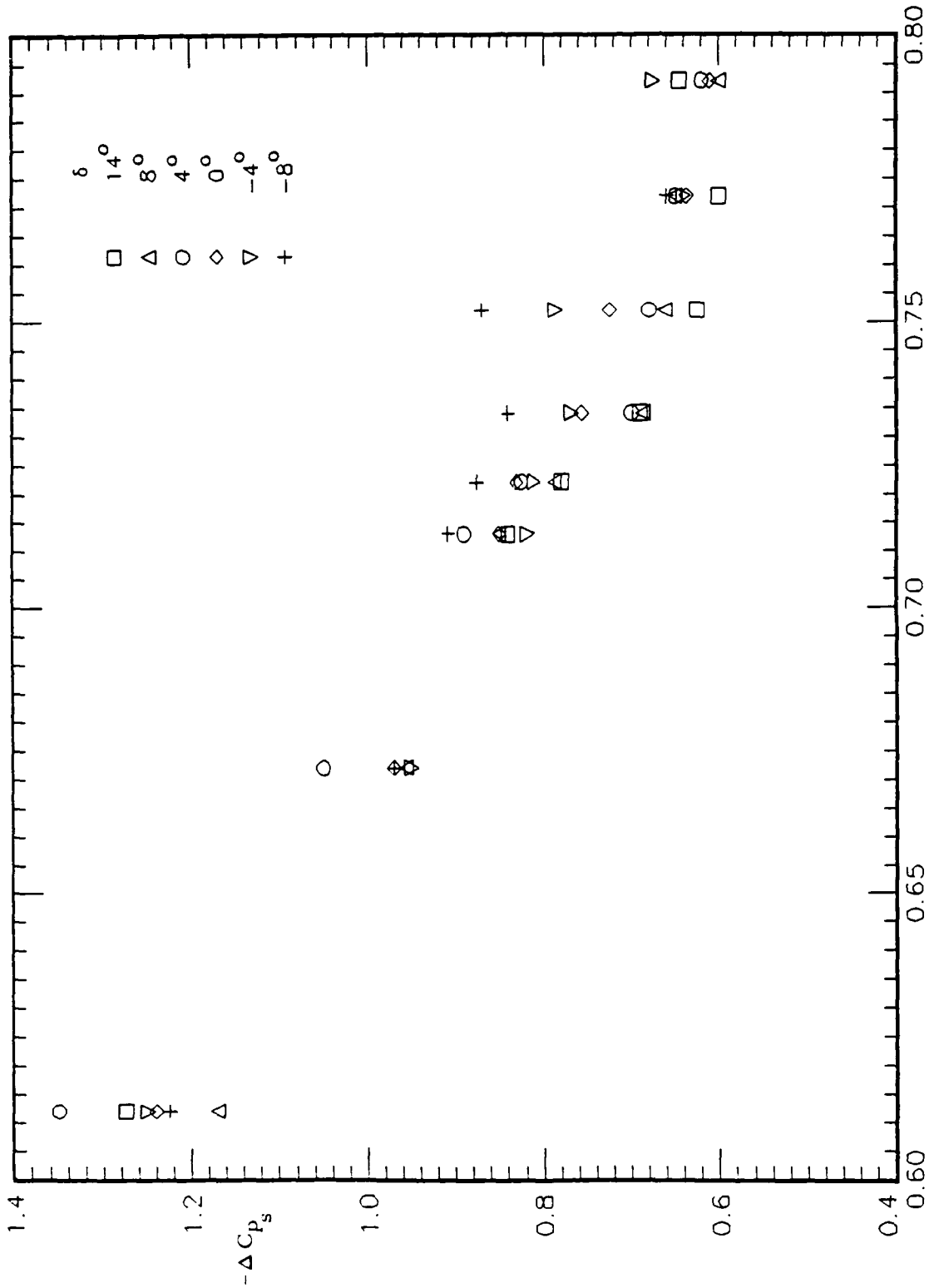

FIG. 39: SHOCK STRENGTHS VERSUS MACH NUMBER AT BUFFET ONSET FOR VARIOUS FLAP ANGLES

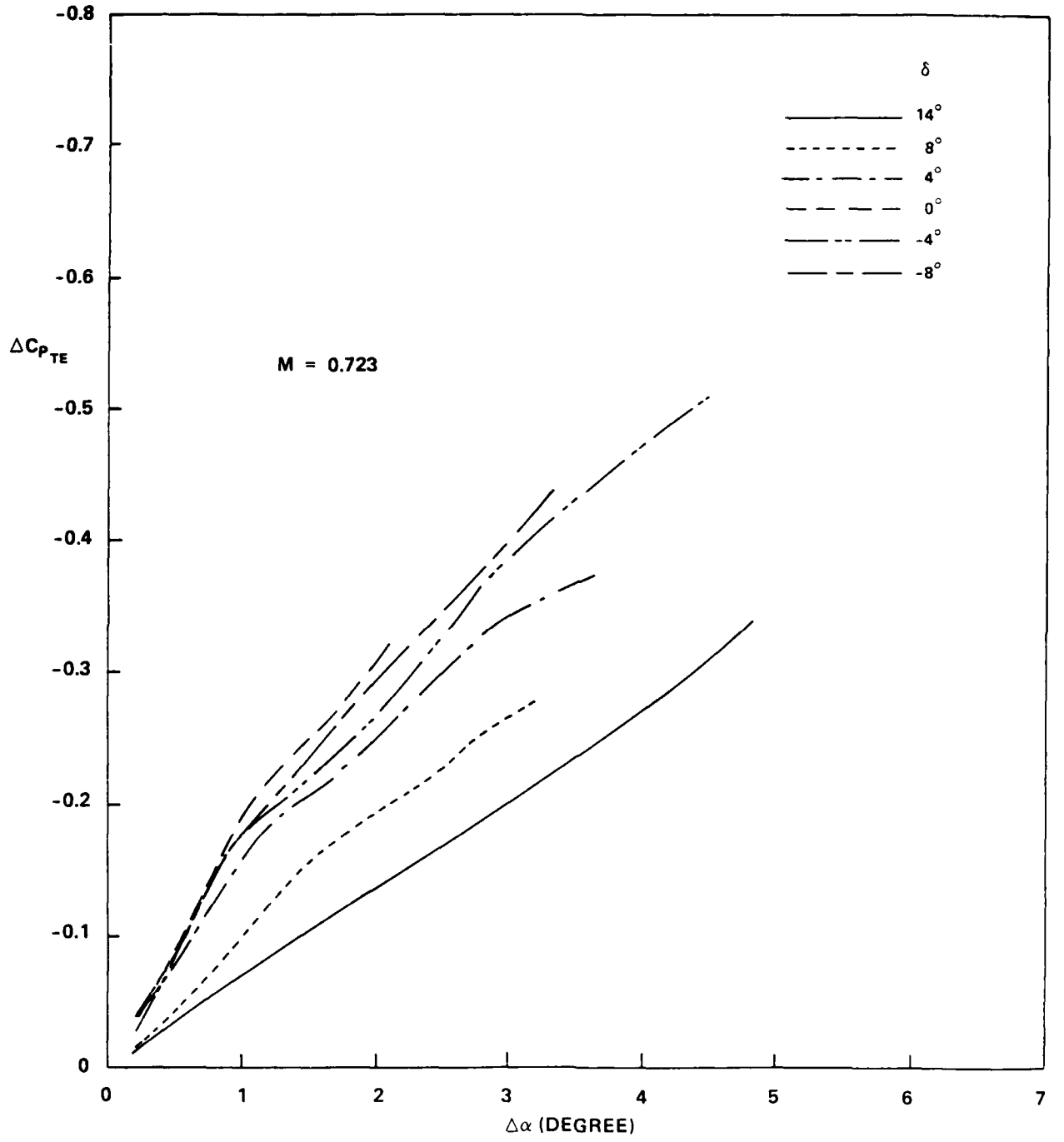

FIG. 40: $\Delta C_{P_{TE}}$ VERSUS $\Delta\alpha$ AT M = 0.723 FOR VARIOUS FLAP ANGLES

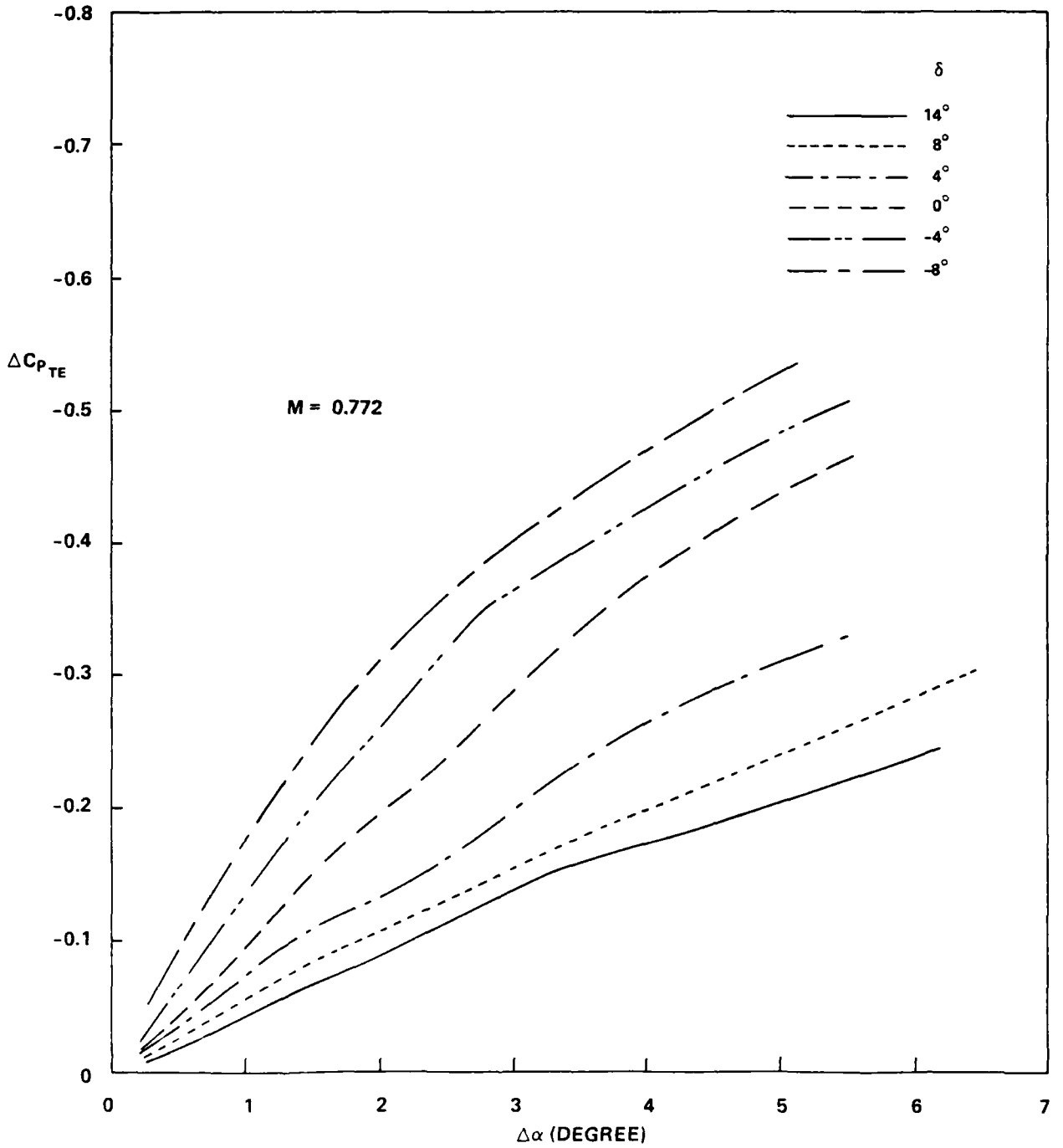

FIG. 41: $\Delta C_{P_{TE}}$ VERSUS $\Delta\alpha$ AT M = 0.772 FOR VARIOUS FLAP ANGLES

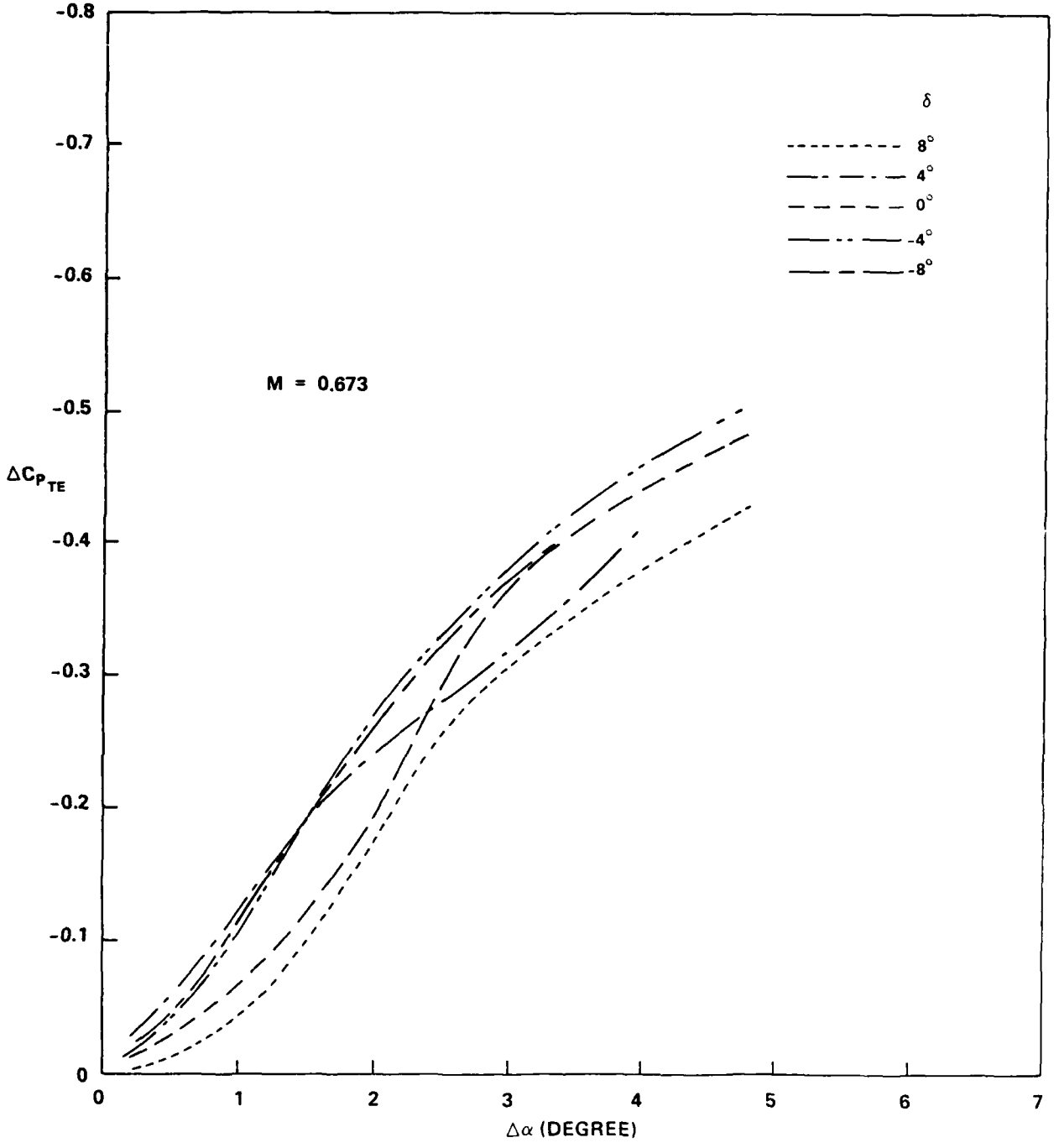

FIG. 42: $\Delta C_{P_{TE}}$ VERSUS $\Delta\alpha$ AT M = 0.673 FOR VARIOUS FLAP ANGLES

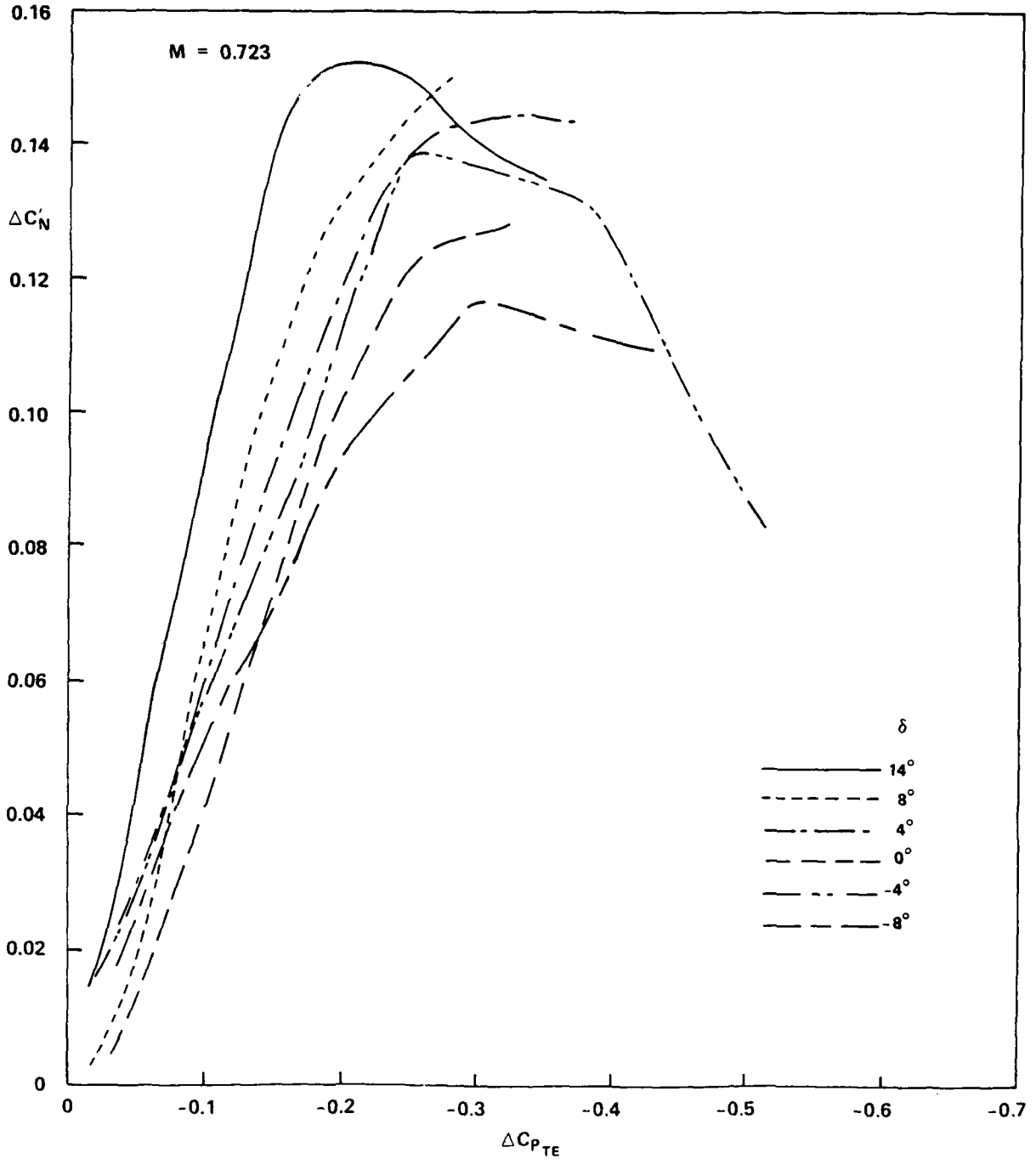

FIG. 43: $\Delta C'_N$ VERSUS $\Delta C_{P_{TE}}$ AT M = 0.723 FOR VARIOUS FLAP ANGLES

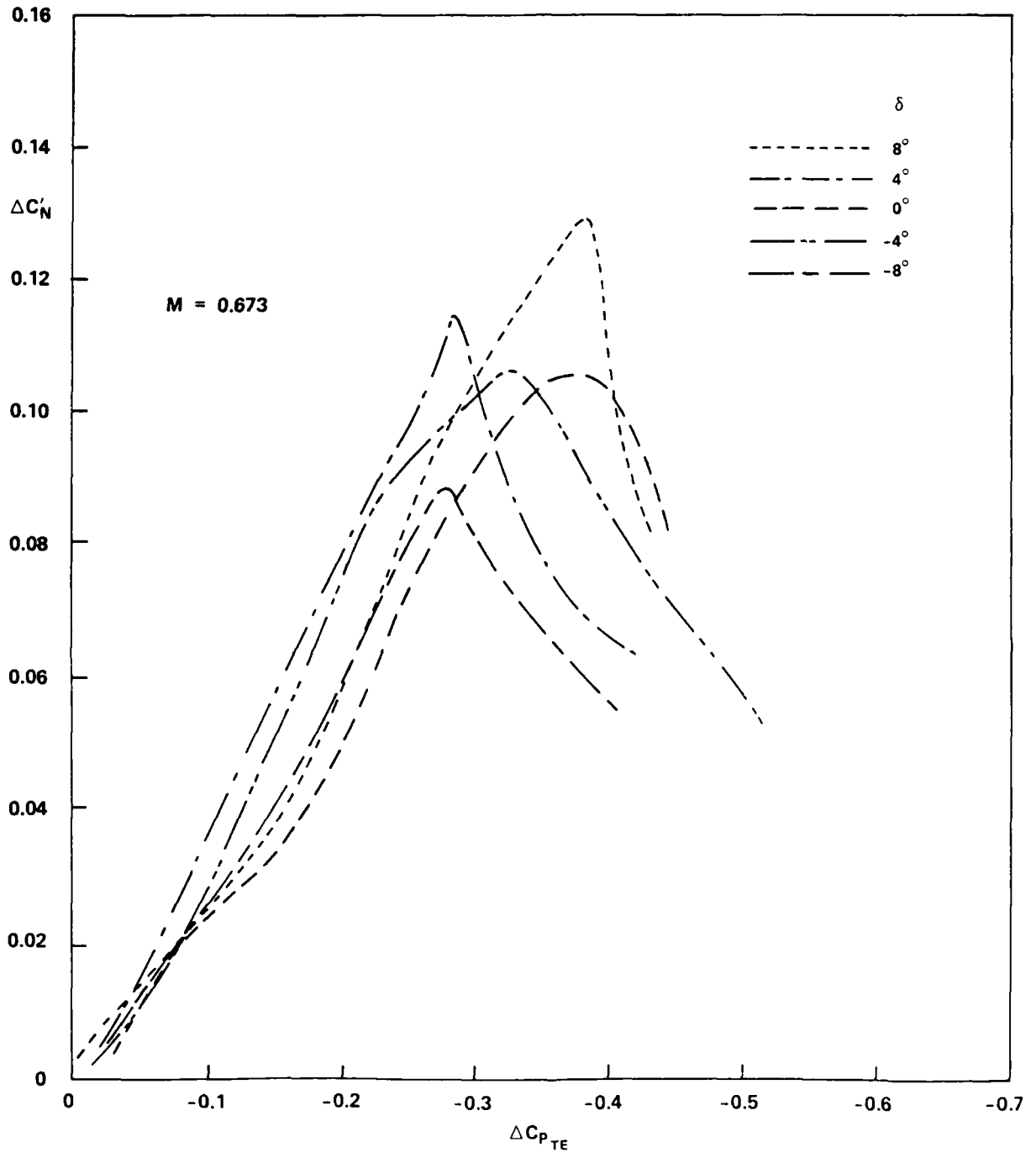

FIG. 44: $\Delta C'_N$ VERSUS $\Delta C_{P_{TE}}$ AT M = 0.673 FOR VARIOUS FLAP ANGLES

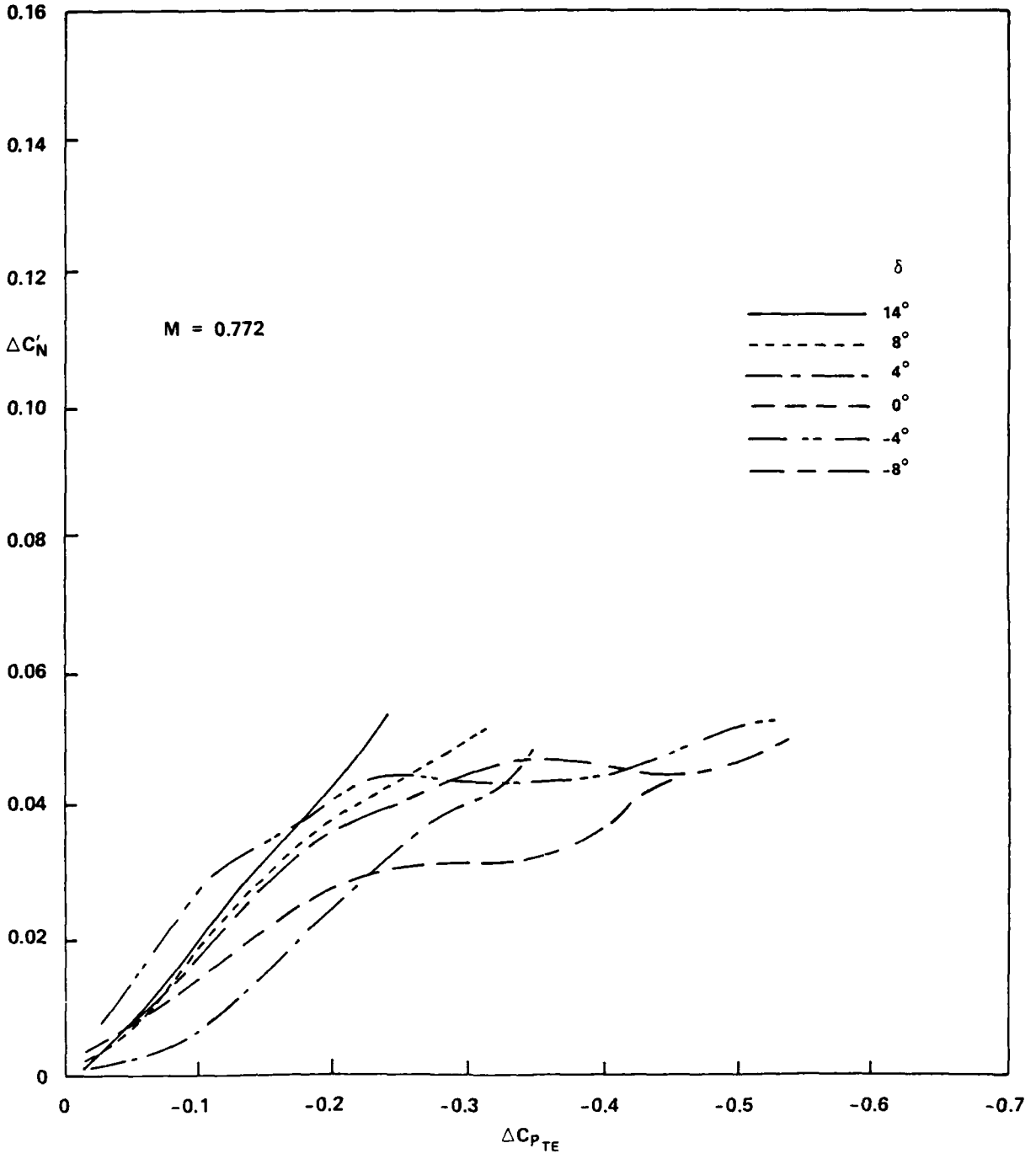

FIG. 45: $\Delta C'_N$ VERSUS $\Delta C_{P_{TE}}$ AT M = 0.772 FOR VARIOUS FLAP ANGLES

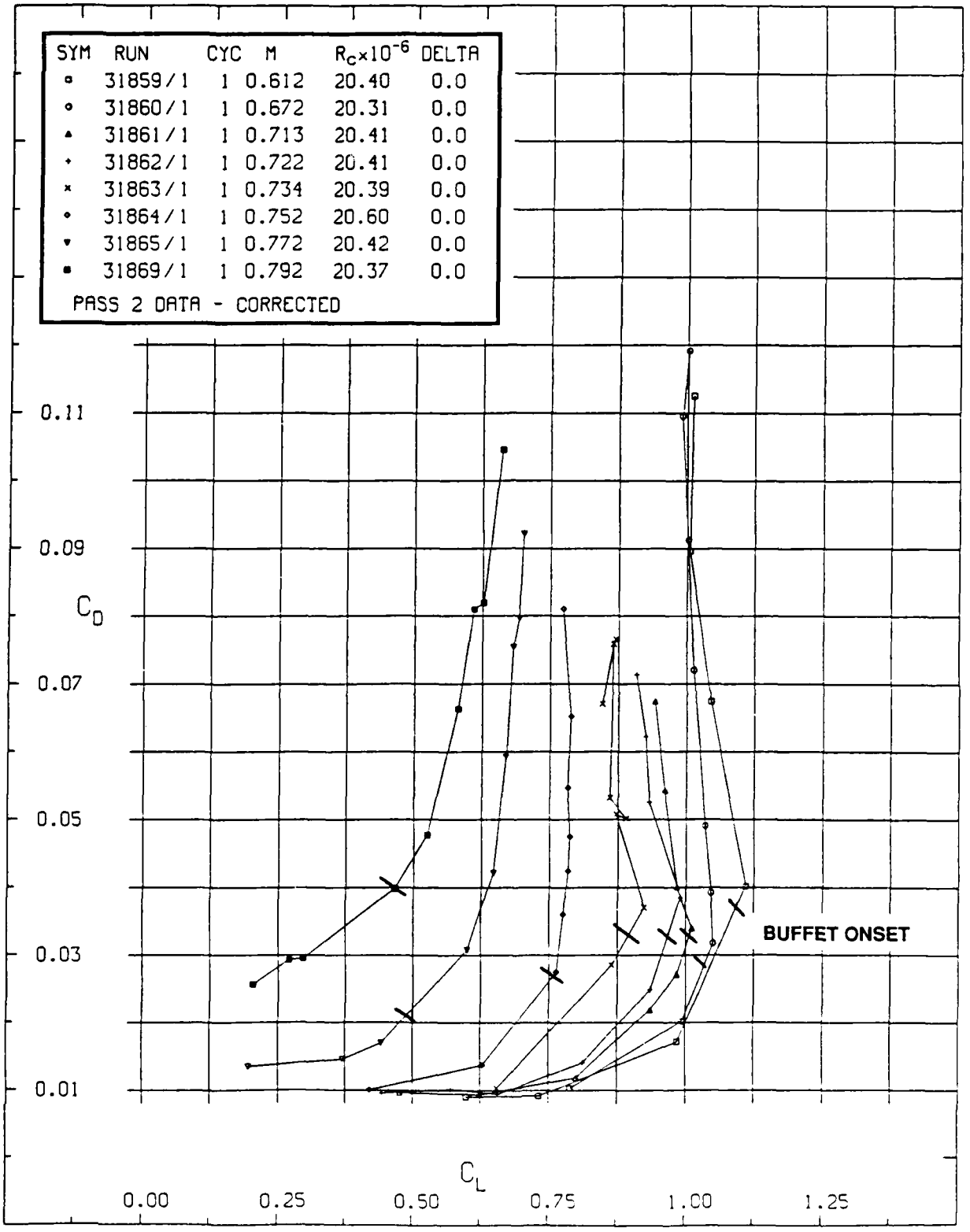

FIG. 46: DRAG VERSUS LIFT AT VARIOUS MACH NUMBERS FOR FLAP ANGLE $\delta = 0°$

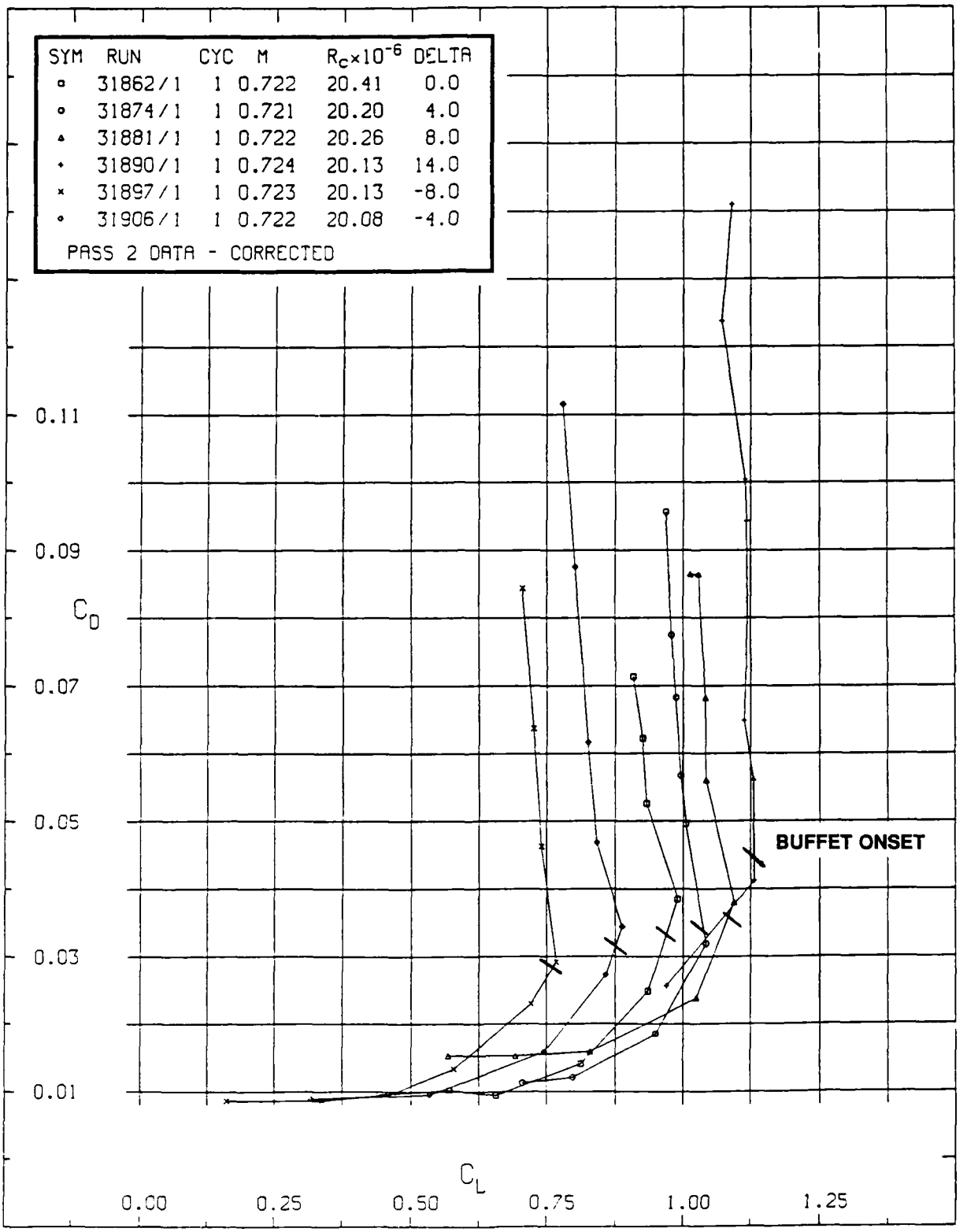

FIG. 47: DRAG VERSUS LIFT AT M ABOUT 0.723 FOR VARIOUS FLAP ANGLES

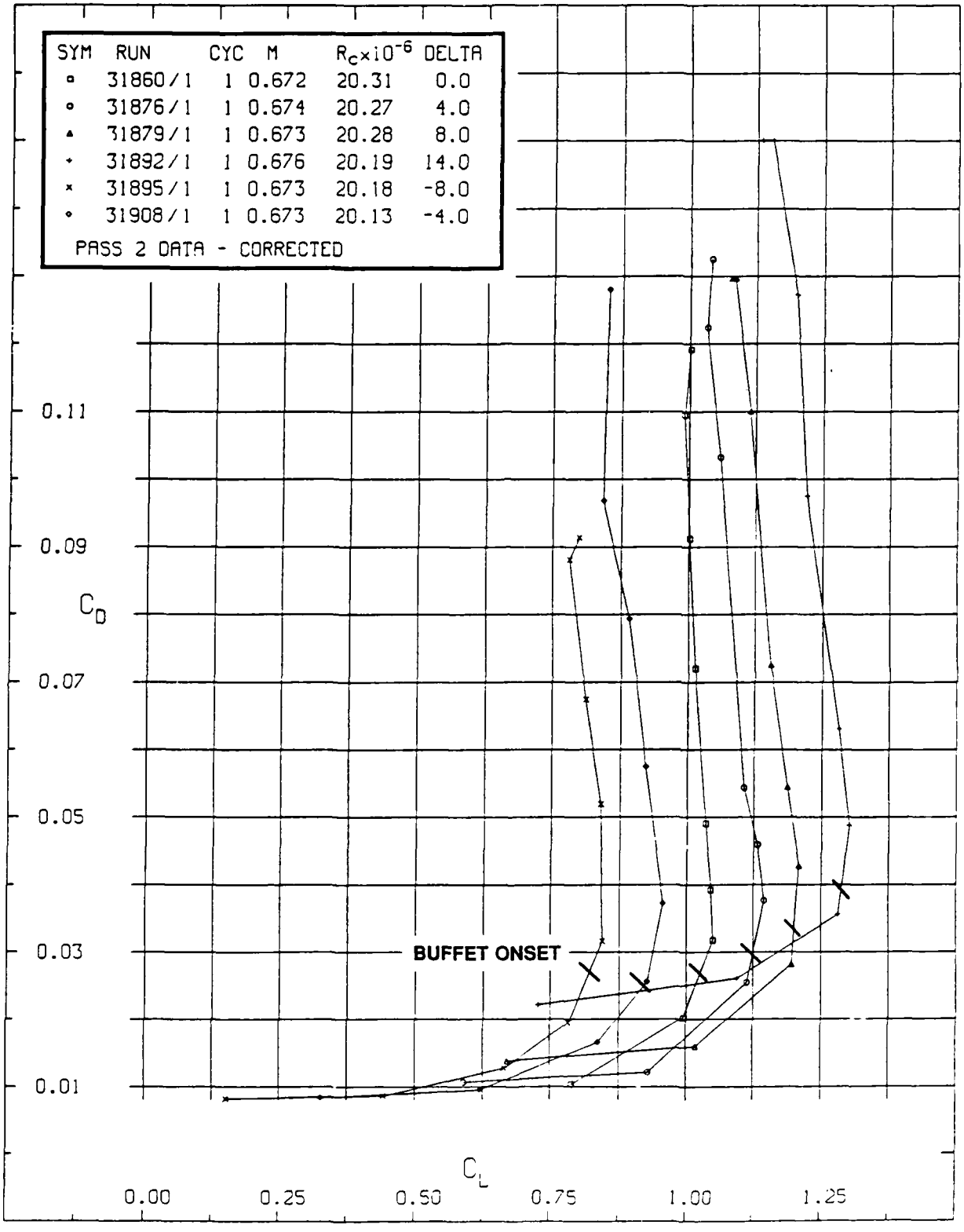

FIG. 48: DRAG VERSUS LIFT AT M ABOUT 0.673 FOR VARIOUS FLAP ANGLES

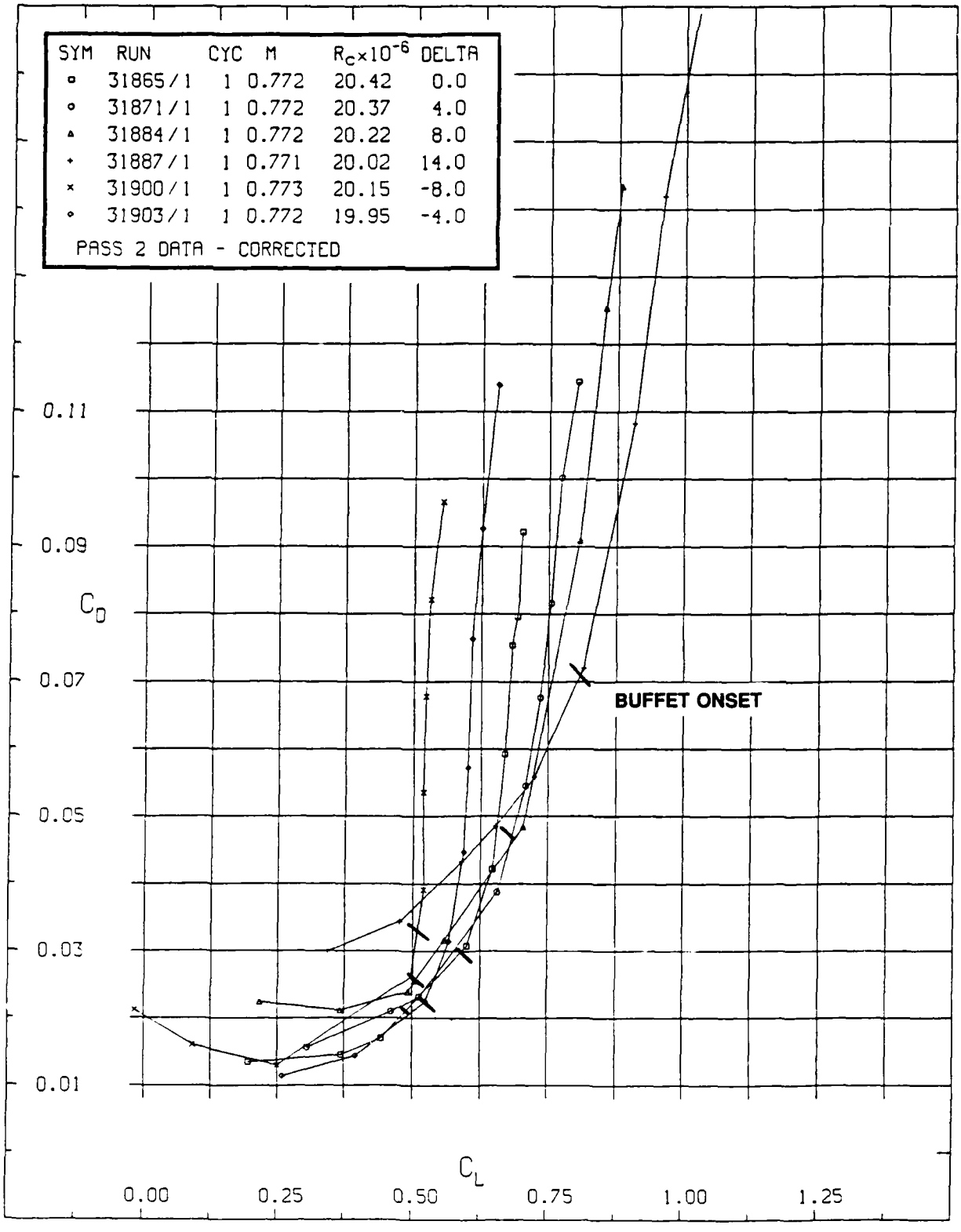

FIG. 49: DRAG VERSUS LIFT AT M ABOUT 0.772 FOR VARIOUS FLAP ANGLES

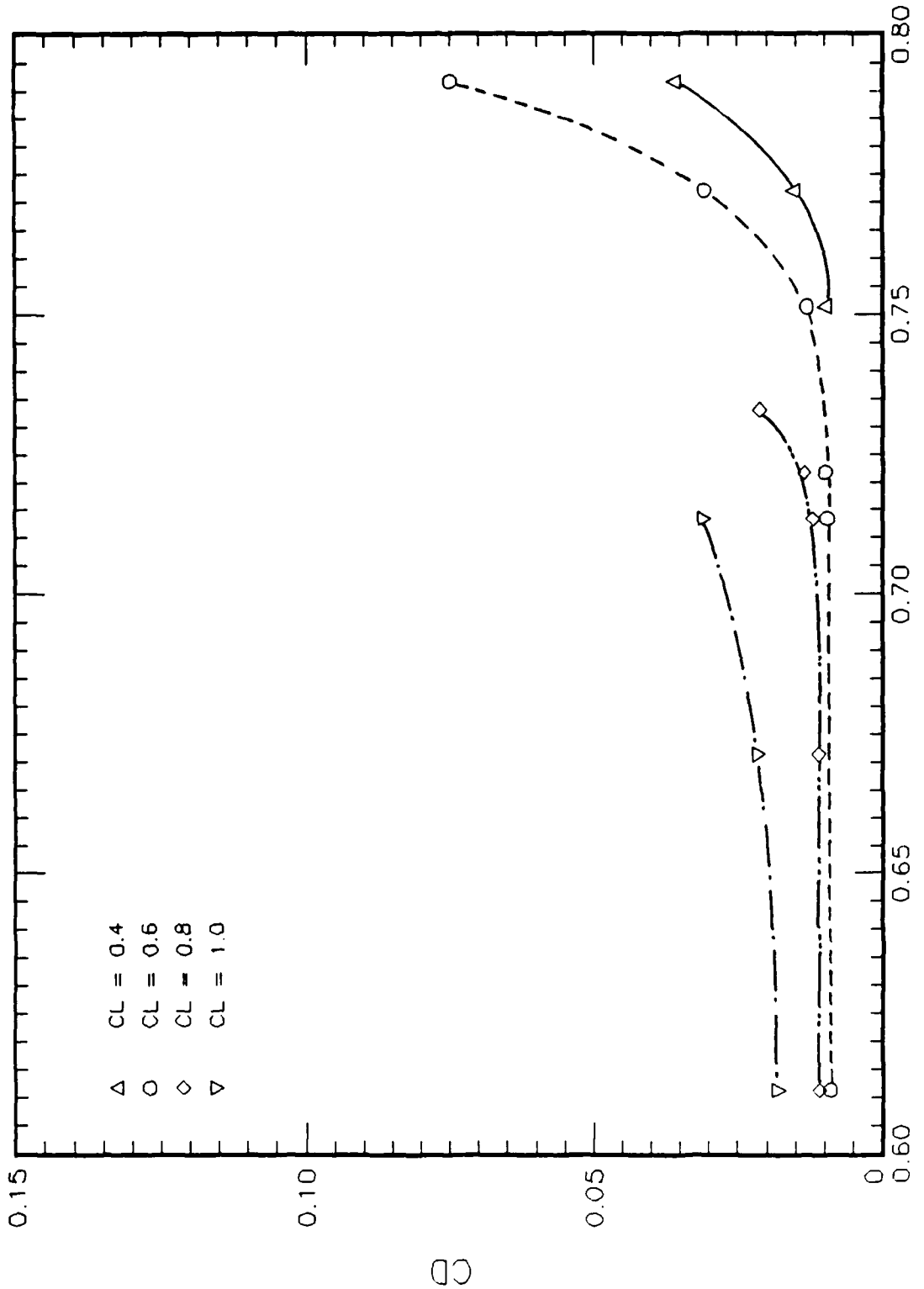

FIG. 50: DRAG VERSUS MACH NUMBER AT VARIOUS LIFT COEFFICIENTS FOR FLAP ANGLE $\delta = 0°$

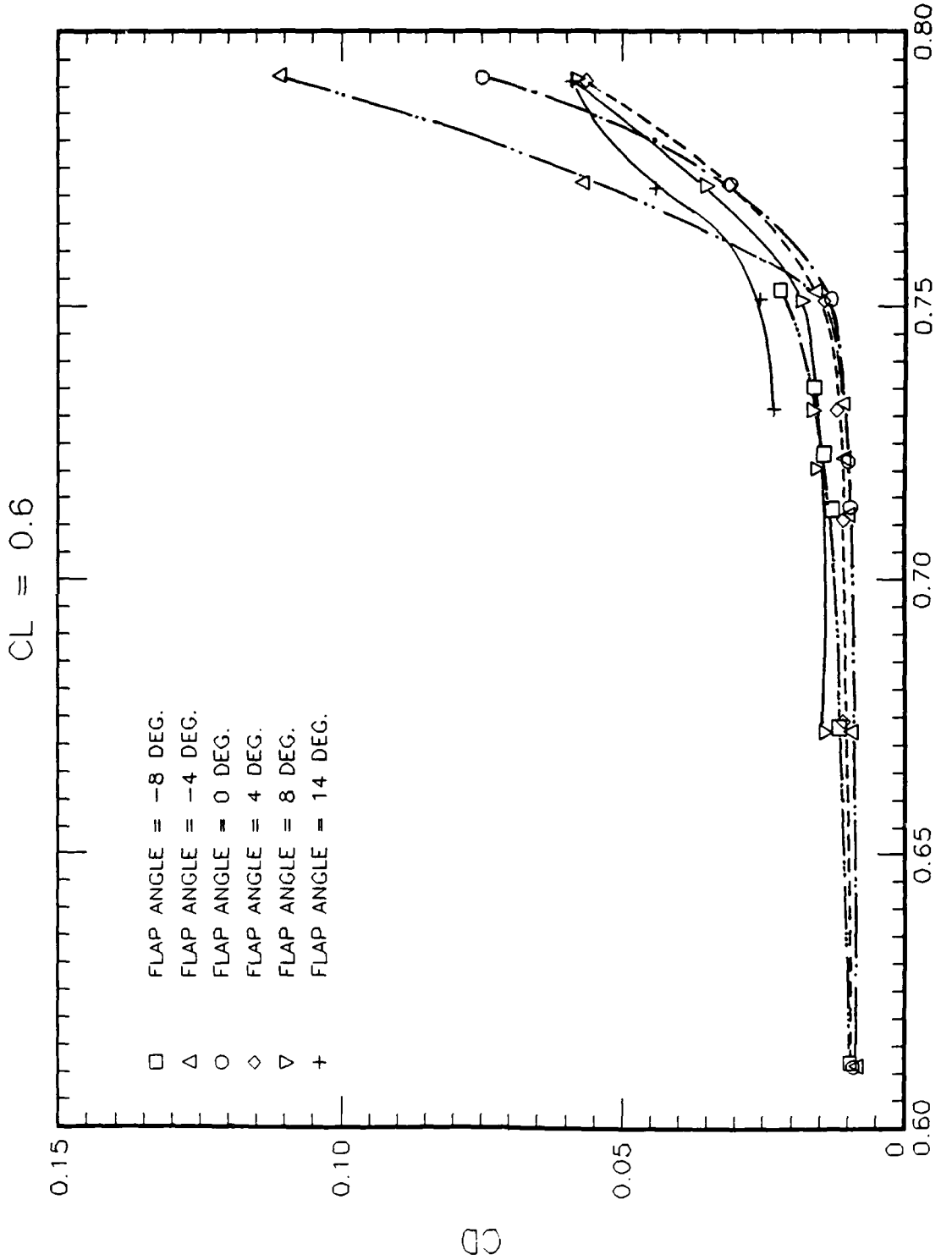

FIG. 51: DRAG VERSUS MACH NUMBER AT $C_L = 0.6$ FOR VARIOUS FLAP ANGLES

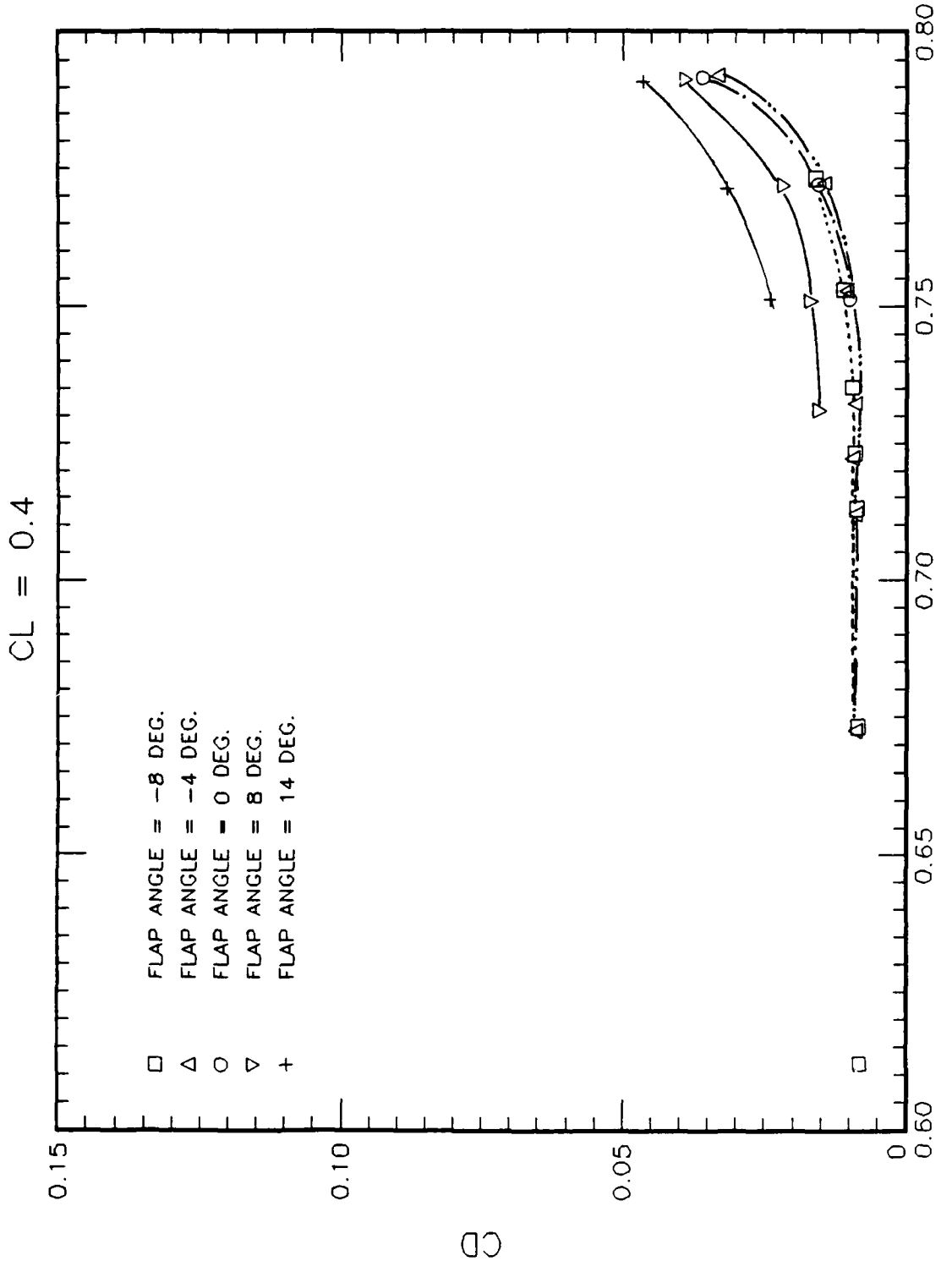

FIG. 52: DRAG VERSUS MACH NUMBER AT C_L = 0.4 FOR VARIOUS FLAP ANGLES

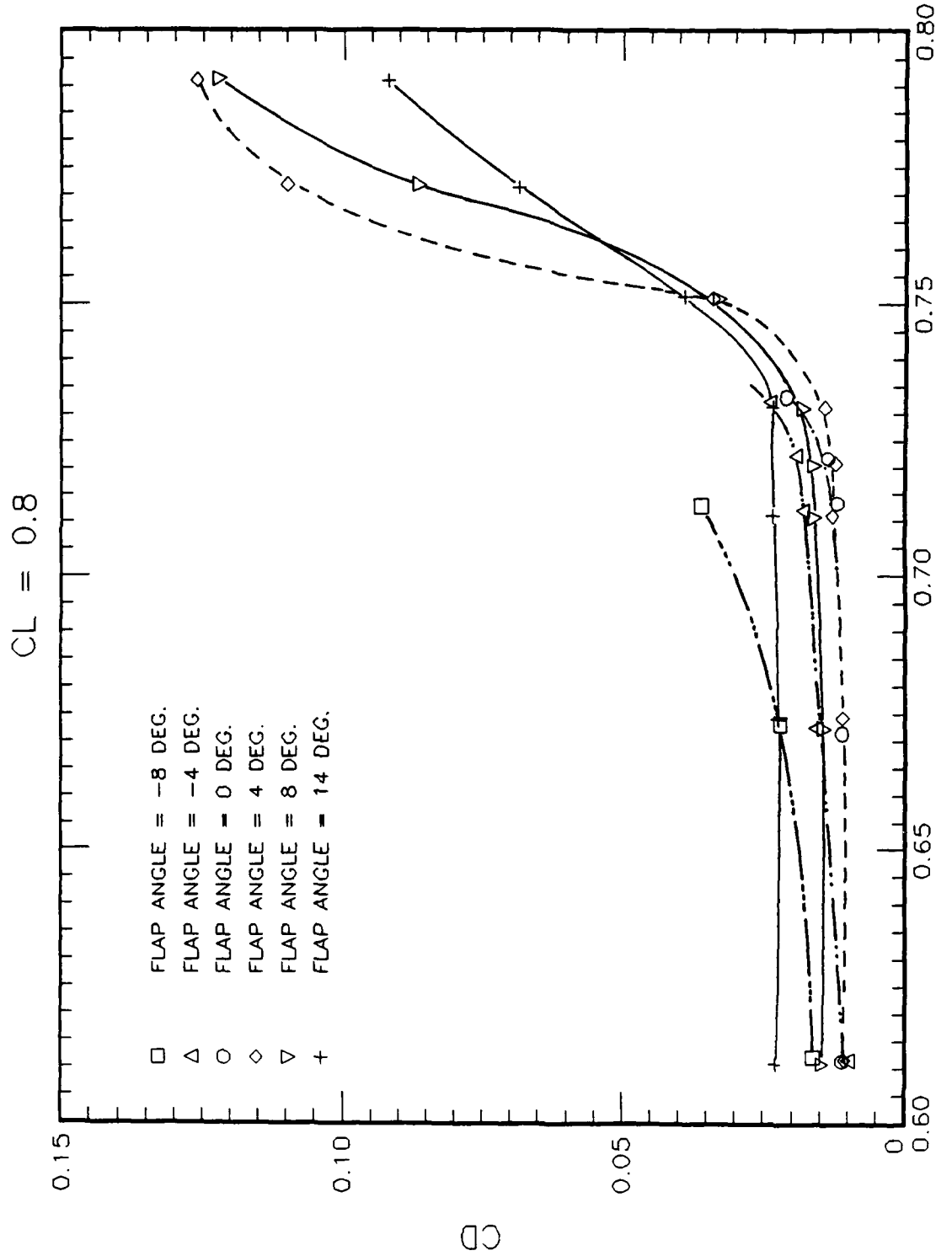

FIG. 53: DRAG VERSUS MACH NUMBER AT C_L = 0.8 FOR VARIOUS FLAP ANGLES

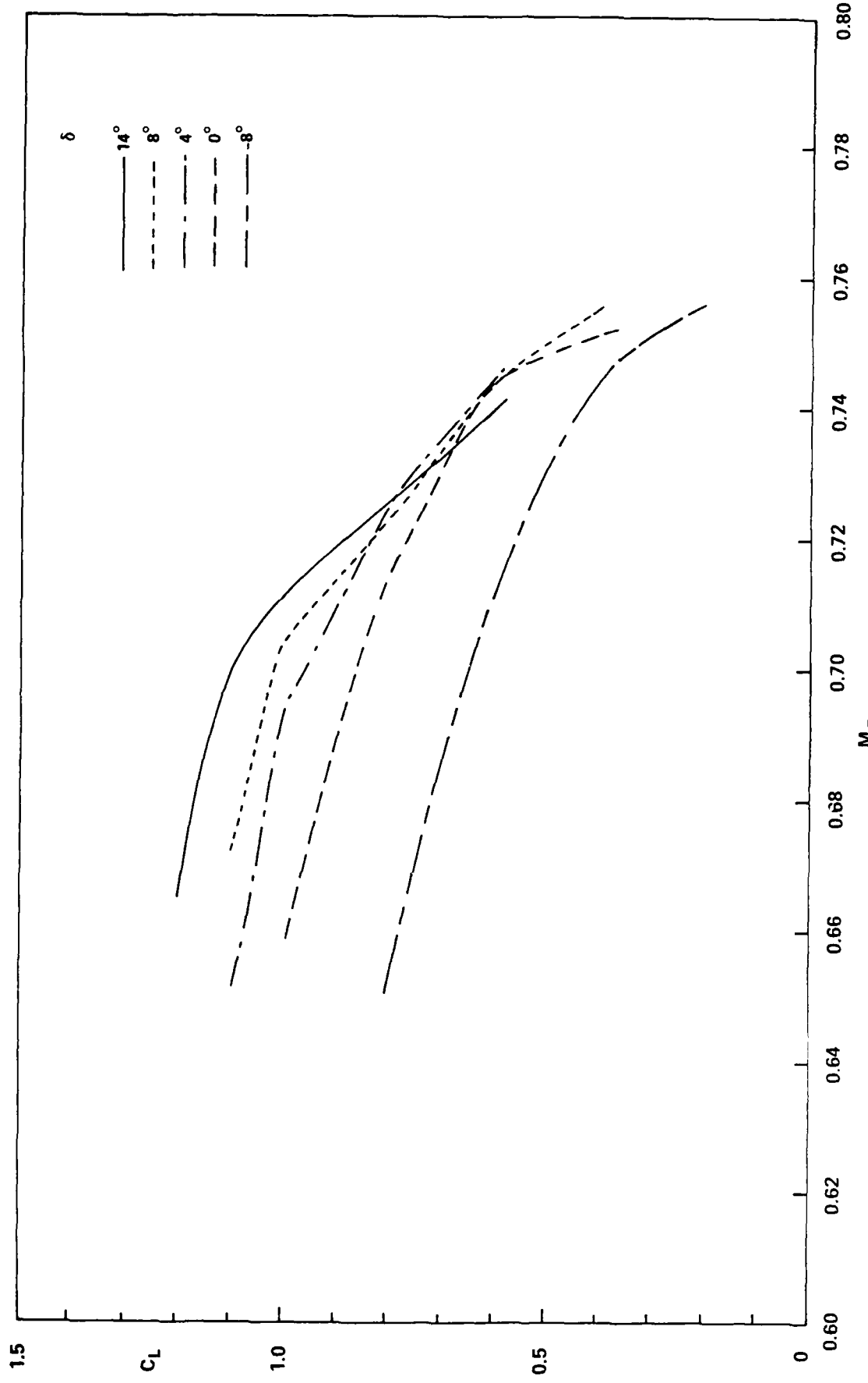

FIG. 54: LIFT VERSUS DRAG RISE MACH NUMBER *FOR VARIOUS FLAP ANGLES*

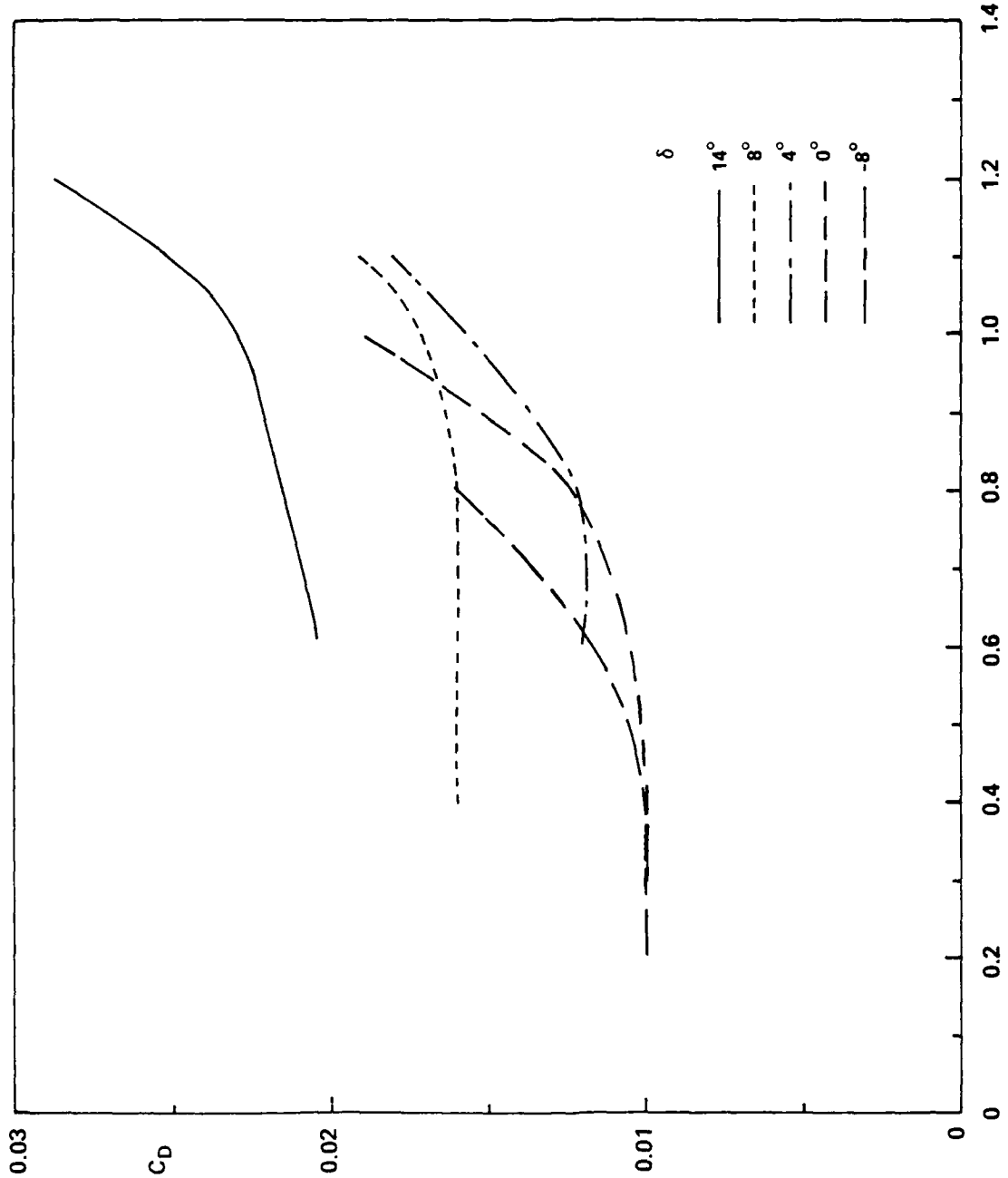

FIG. 55: DRAG VERSUS LIFT AT DRAG RISE MACH NUMBER FOR VARIOUS FLAP ANGLES

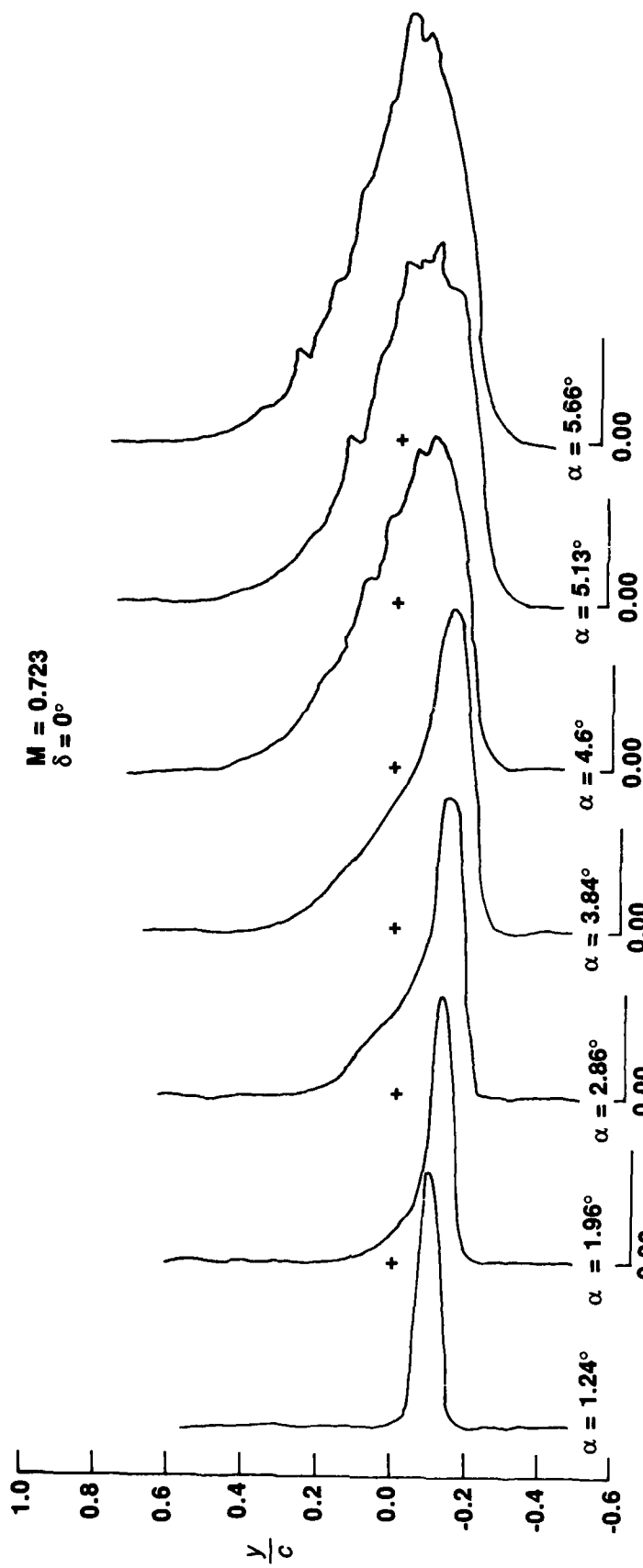

FIG. 56: WAKE PROFILES AT M = 0.723 and δ = 0°
FOR VARIOUS ANGLES OF INCIDENCE

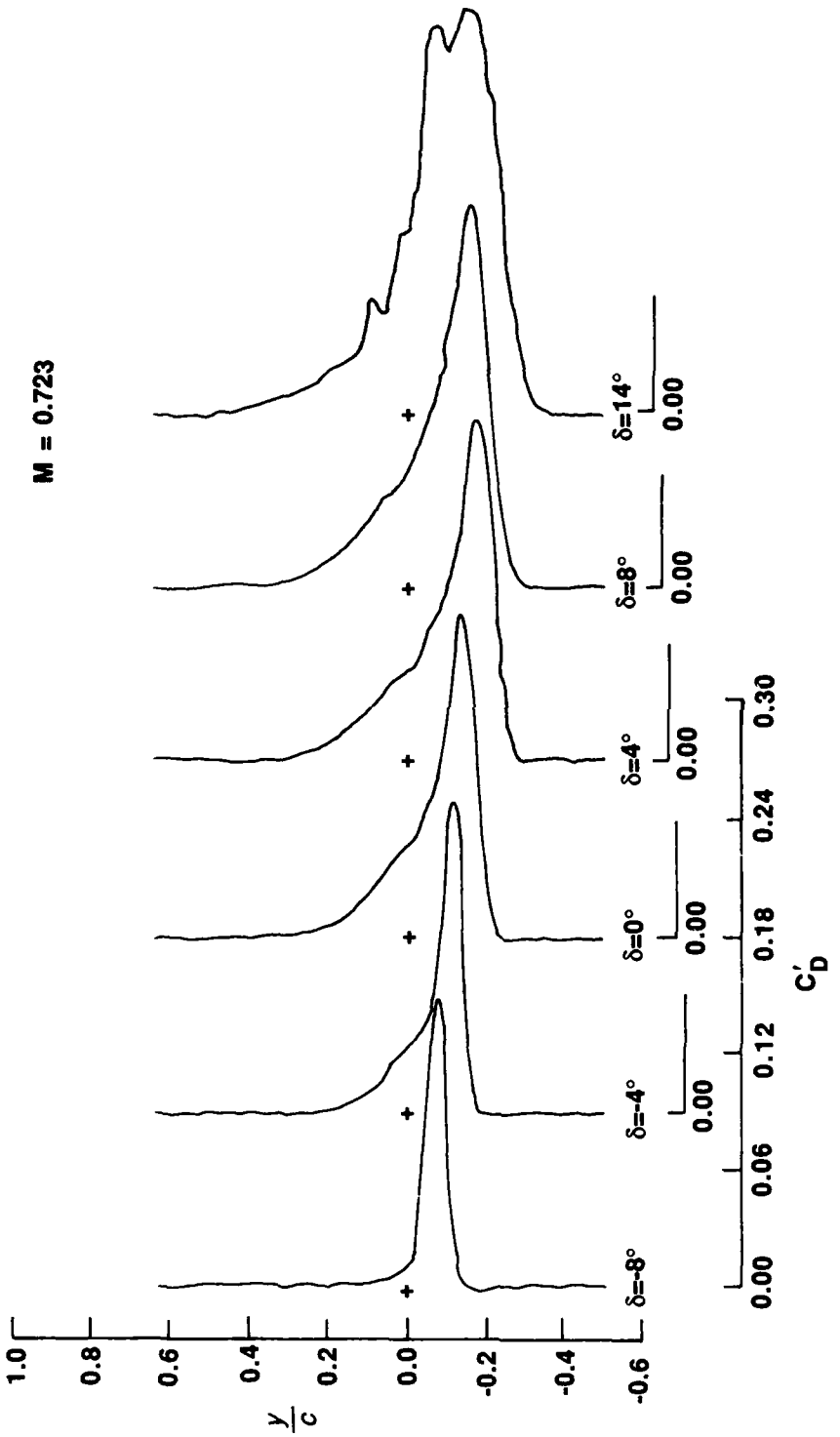

FIG. 57: WAKE PROFILES AT M = 0.723 AND α ABOUT 2.75° FOR VARIOUS FLAP ANGLES

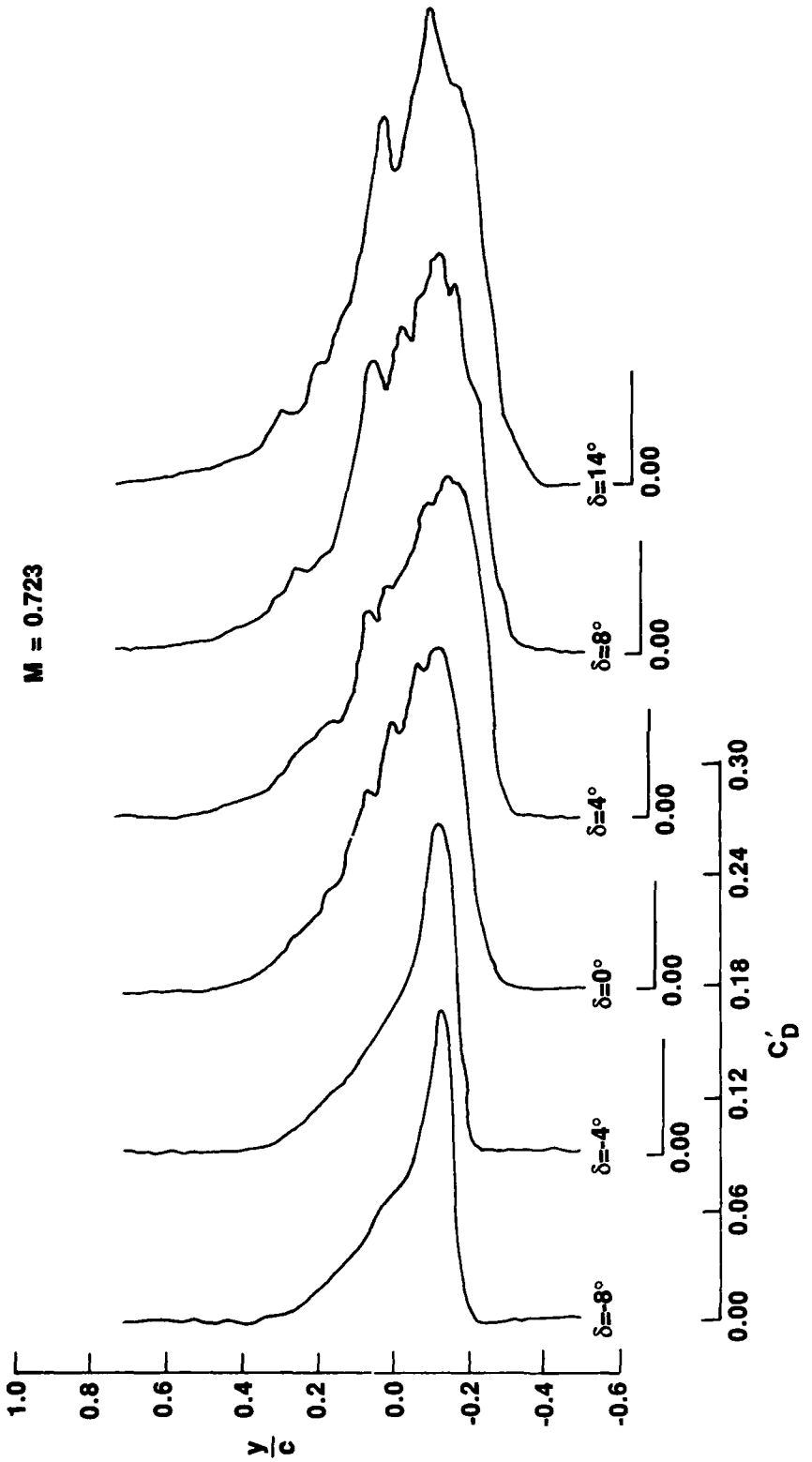

FIG. 58: WAKE PROFILES AT M = 0.723 AND α ABOUT 4.5° FOR VARIOUS FLAP ANGLES

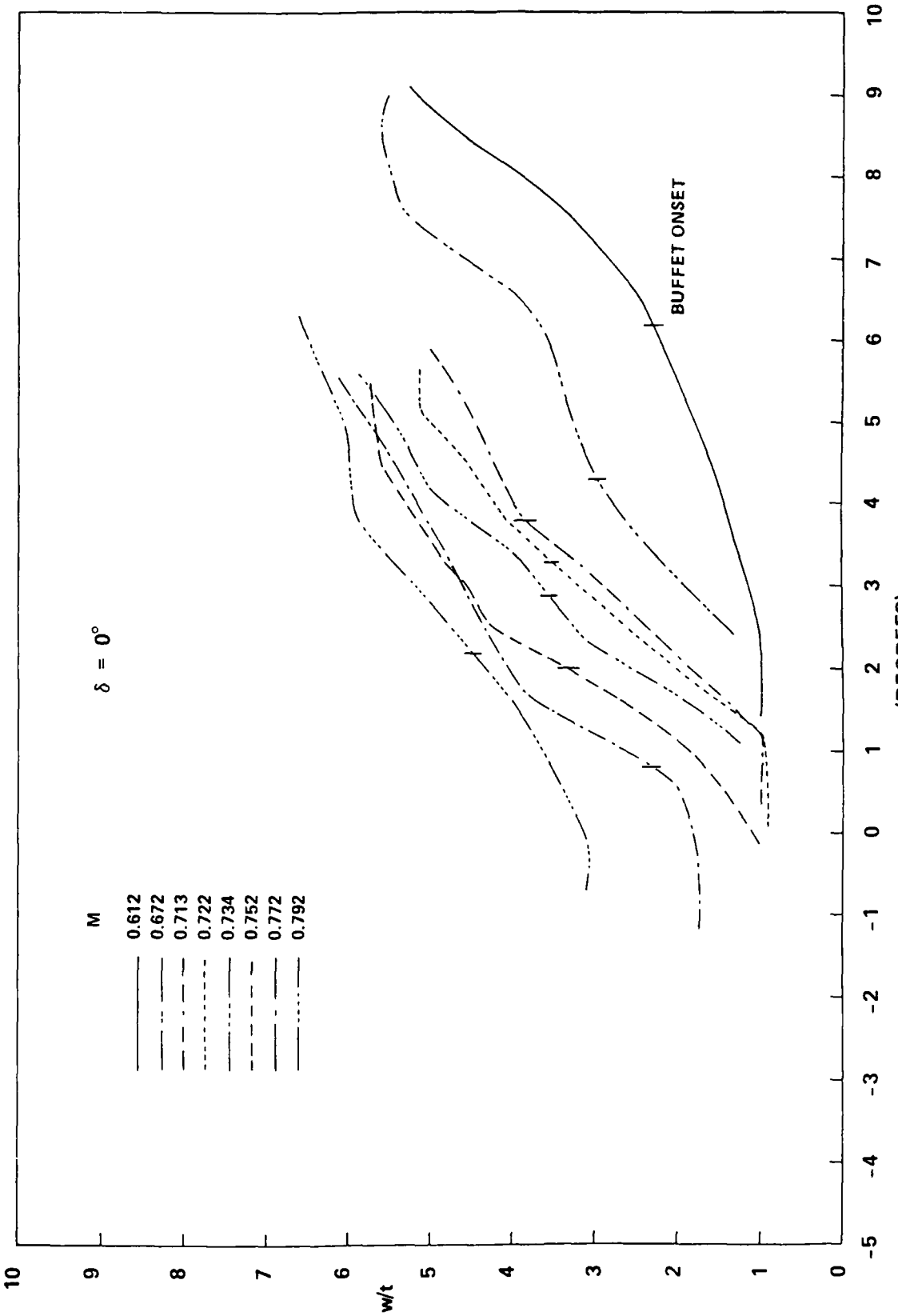

FIG. 59: WAKE WIDTH VERSUS ANGLE OF INCIDENCE FOR VARIOUS MACH NUMBERS AT δ = 0°

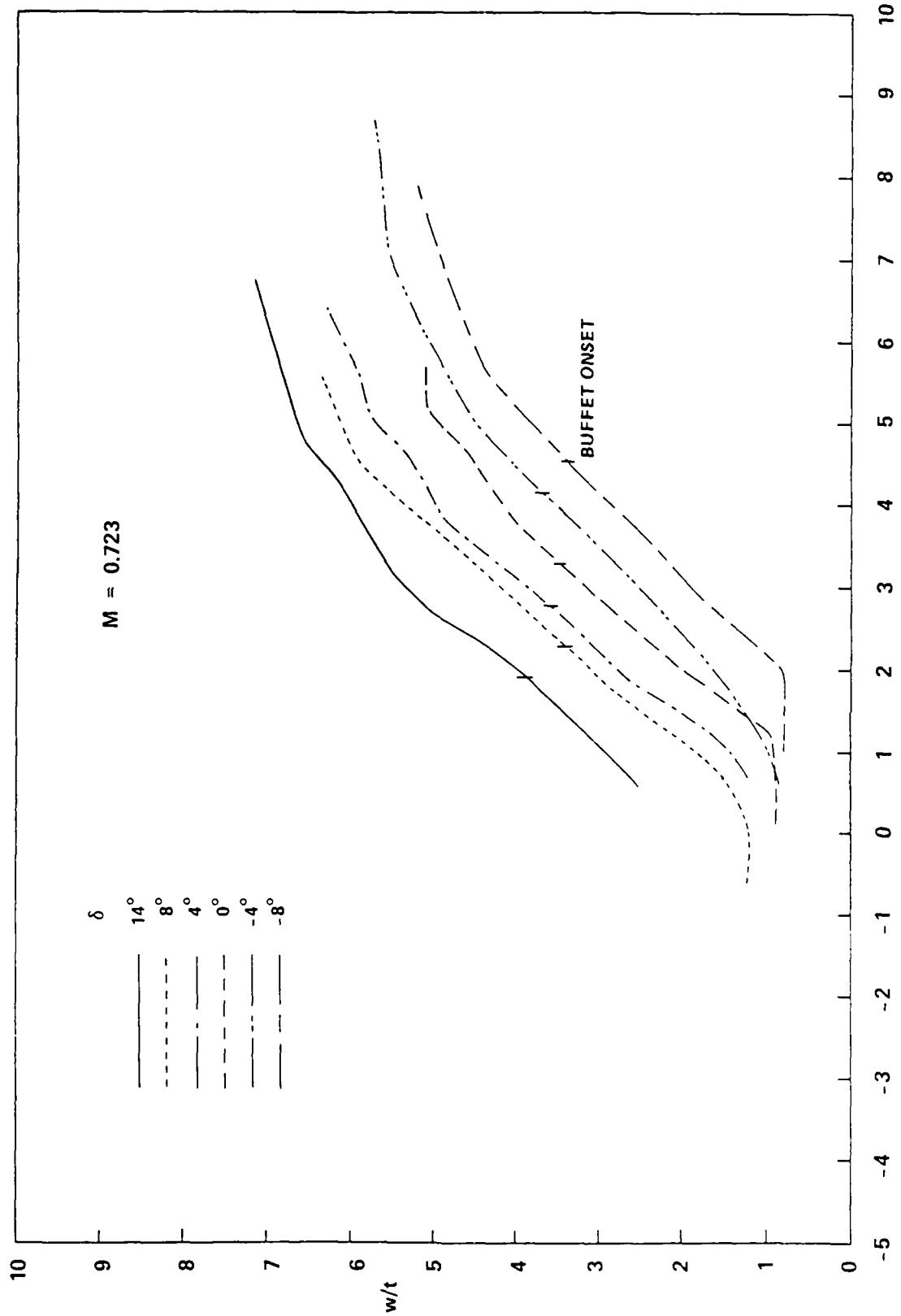

FIG. 60: WAKE WIDTH VERSUS ANGLE OF INCIDENCE AT M = 0.723 FOR VARIOUS FLAP ANGLES

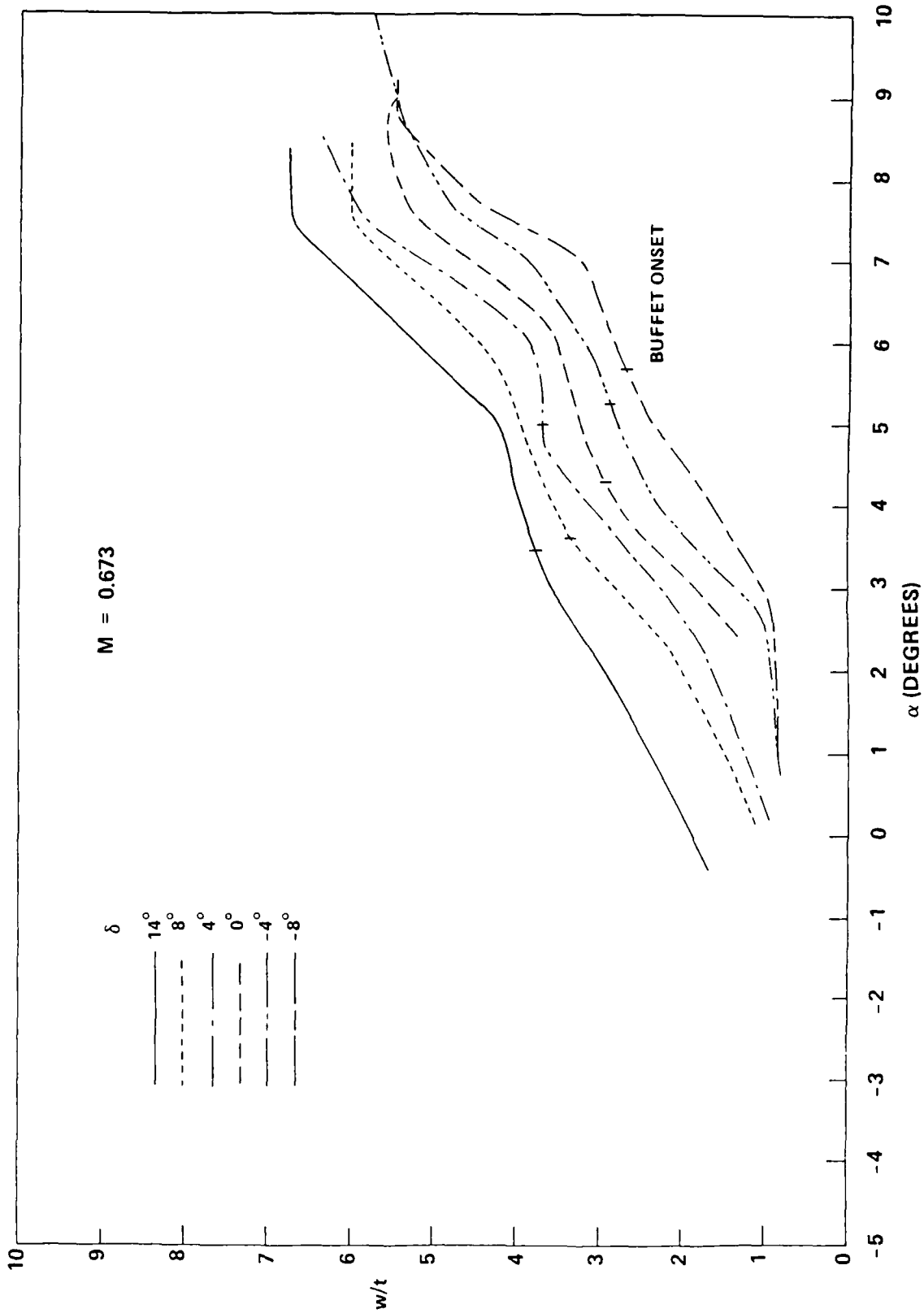

FIG. 61: WAKE WIDTH VERSUS ANGLE OF INCIDENCE AT M = 0.673 FOR VARIOUS FLAP ANGLES

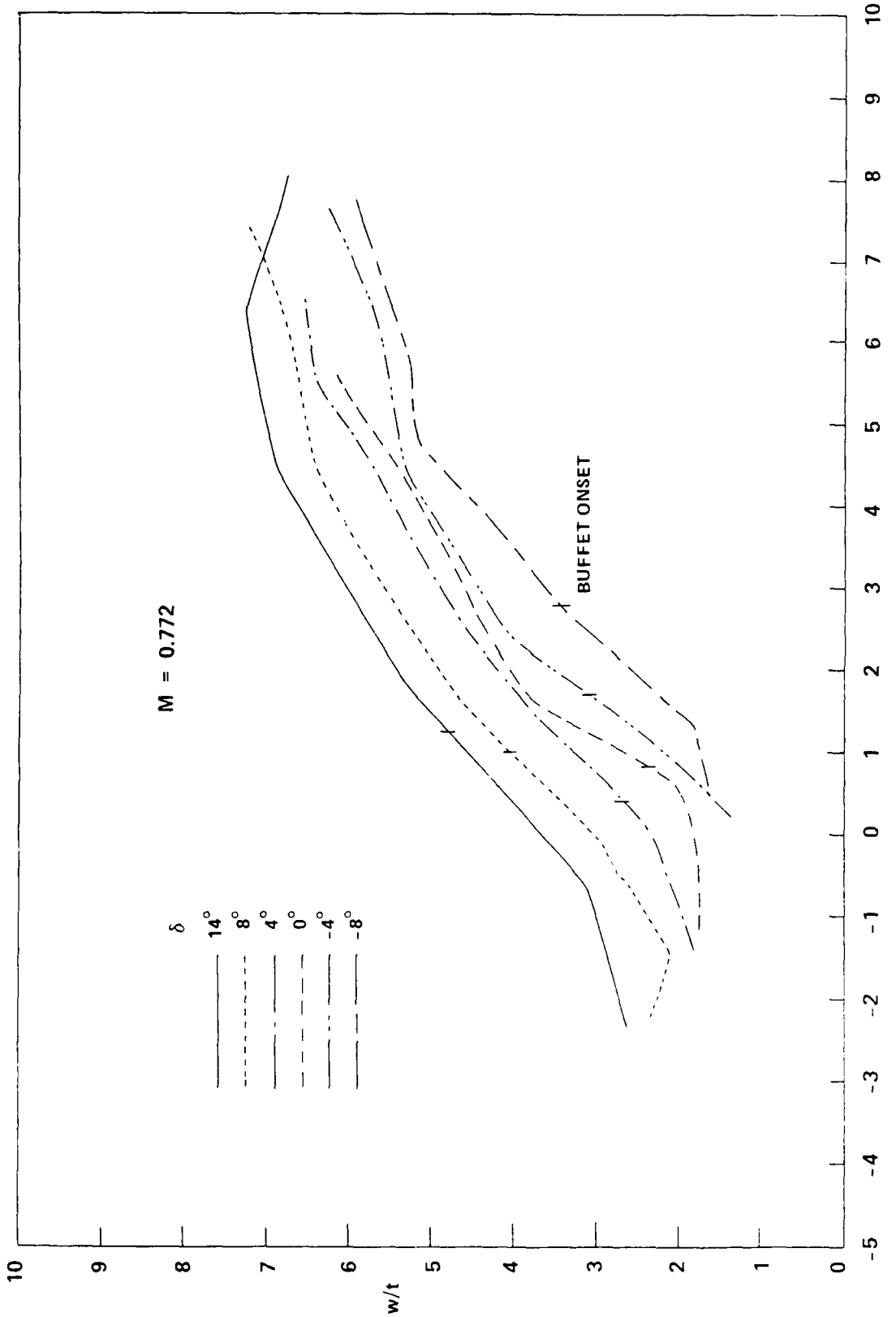

FIG. 62: WAKE WIDTH VERSUS ANGLE OF INCIDENCE AT M = 0.772 FOR VARIOUS FLAP ANGLES

REPORT DOCUMENTATION PAGE / PAGE DE DOCUMENTATION DE RAPPORT

REPORT/RAPPORT	REPORT/RAPPORT
NAE-AN-54 (1a)	NRC No. 29542 (1b)
REPORT SECURITY CLASSIFICATION / CLASSIFICATION DE SÉCURITÉ DE RAPPORT	DISTRIBUTION (LIMITATIONS)
Unclassified (2)	Unlimited (3)

TITLE/SUBTITLE/TITRE/SOUS-TITRE

An Experimental Study of Transonic Buffet of a Supercritical Airfoil with Trailing Edge Flap (4)

AUTHOR(S)/AUTEUR(S)

B.H.K. Lee and F.C. Tang (5)

SERIES/SÉRIE

Aeronautical Note (6)

CORPORATE AUTHOR/PERFORMING AGENCY/AUTEUR D'ENTREPRISE/AGENCE D'EXÉCUTION

National Research Council Canada
National Aeronautical Establishment — High Speed Aerodynamics Laboratory (7)

SPONSORING AGENCY/AGENCE DE SUBVENTION

(8)

DATE	FILE/DOSSIER	LAB. ORDER / COMMANDE DU LAB.	PAGES	FIGS/DIAGRAMMES
88-09			91	62
9	10	11	12a	12b

NOTES

(13)

DESCRIPTORS (KEY WORDS)/MOTS-CLÉS

1. Airfoils — Supercritical
2. Airfoils — Trailing edge flaps
3. Transonic wind tunnels — Testing

(14)

SUMMARY/SOMMAIRE

A supercritical airfoil with a trailing edge flap has been the subject of aerodynamic investigation in the National Aeronautical Establishment's High Reynolds Number 2-D Test Facility. The effects of flap deflection on buffet intensities and delay of buffet onset at transonic speeds were studied. Buffet boundaries for various flap angles were determined from the divergence of the fluctuating balance normal force measurements (C_N'). The onset of buffet was obtained from plots of C_N' versus C_L at values of C_L where the slope was 0.1. This value for the slope was arbitrarily chosen, but was found to give consistent results which agreed well with values computed from the criterion using the trailing edge pressure divergence for those cases where buffet onset is primarily due to trailing edge separation.

For given flow conditions the deflection of the trailing edge flap altered the circulation and hence the position of the shock wave and its strength. The variations of these two quantities with flap angles were determined from pressure measurements carried out on the airfoil surface. The test was performed quite deep inside the buffet régime and shock wave oscillations were investigated from spectral analyses of the balance output. Fluctuations in the shock motion of approximately 70 Hz were detected.

The drag of the airfoil was computed from the wake stagnation pressure deficit and the drag penalties for large flap angles were quite significant. Analysis of the wake profiles with flap settings was carried out to study the changes in wake characteristics.

(15)